Hydraulic Tomography:
A New Approach Coupling
Hydraulic Travel Time, Attenuation and Steady Shape Inversions
for High-Spatial Resolution Aquifer Characterization

Dissertation
zur Erlangung des Doktorgrades
der Mathematisch-Naturwissenschaftlichen Fakultäten
der Georg-August-Universität zu Göttingen

vorgelegt von

Rui Hu

Aus Jiangsu, China

Göttingen 2011

D 7

ABSTRACT

Hydraulic travel time, attenuation, and steady shape inversions are complementary methods for tomographic aquifer characterization. In this work, a coupled procedure is presented that facilitates the determination of the spatial distribution of hydraulic conductivity, diffusivity, and specific storage in heterogeneous groundwater systems. The procedure is first applied to a highly heterogeneous sedimentary aquifer analogue that is implemented as a two- and three-dimensional case study in a numerical flow model. By interpreting the observations from multiple simulated short-term pumping tests, the analogue is successively reconstructed in two and three dimensions. Final results demonstrate the high potential of the coupled procedure for identifying the dominant structural elements and the composition of the sedimentary deposit.

Consequently, the coupled inversion scheme is assessed at a field test site. As in the numerical study, the data set for the inversion is derived from a series of short-term pumping tests. The successful two-dimensional high-resolution aquifer reconstruction, as well as the substantial agreement between the individual inversion results, strongly proves the reliability of this coupled inversion scheme for spatial aquifer characterization. As well as the hydraulic tomography approach, numerous traditional methods are also used for the aquifer characterization at this test site. The results from the analyses of 103 grain size distributions, 57 pumping test response curves, 241 slug test response curves and 9 tracer test breakthrough curves are consistent with the inversion results as well. Finally, the two-dimensional inversion results are compared with the three-dimensional inversion results based on cross-well slug tests. The agreement between the inversion results strongly proves the potential of hydraulic tomography for spatial aquifer reconstruction.

This coupled approach also shows the limits which are imposed by the resolution of hydraulic travel time tomography. Small scale variability of hydraulic conductivity with high discrepancies can hardly be resolved. Still, the new coupled scheme is very attractive for an upscaled reconstruction on the sub-meter scale. For the exigent case study, representative parameter values may be estimated in a computationally efficient way and the zonations derived from the performed inversions can serve as a starting model for further investigations with the goal to resolve the multi scale heterogeneity.

KURZFASSUNG

Hydraulische Laufzeit-, Dämpfungs- und „steady shape"-Inversionen sind komplementäre Methoden zur tomographischen Charakterisierung des Grundwasserleiters. In dieser Arbeit wird eine kombinierte Methode vorgestellt, die die Bestimmung der räumlichen Verteilung von hydraulischer Leitfähigkeit, Diffusivität und Speicherkoeffizient in heterogenen Grundwassersystemen erleichtert. Deren Anwendung erfolgt zunächst auf einen stark heterogenen fluvio-klastischen Aquifer-Analog, welcher als zwei- und dreidimensionale Fallstudie in einem numerischen Strömungsmodell implementiert wurde. Durch Interpretation der Beobachtungen von mehreren simulierten Kurzzeitpumpversuchen ist es möglich, das Aquifer-Analog sukzessiv in zwei und drei Dimensionen zu rekonstruieren. Endgültige Ergebnisse zeigen das hohe Potenzial des kombinierten Verfahrens zur Ermittlung der dominanten strukturellen Elemente sowie der Zusammensetzung der fluvio-klastischen Ablagerung.

Anschließend wird dieser tomographische Auswerteansatz in einem Naturtestfeld angewendet und beurteilt. Als Datenbasis dienen, wie schon bei der numerischen Fallstudie, Kurzzeitpumpversuche. Die erfolgreiche zweidimensionale hochaufgelöste Aquiferrekonstruktion, sowie die gute Übereinstimmung zwischen den einzelnen Inversionsergebnissen, beweist die Zuverlässigkeit dieses gekoppelten Inversionsschemas für die räumliche Charakterisierung eines Grundwasserleiters. Neben dem hydraulisch-tomographischen Ansatz sind auch zahlreiche traditionelle Methoden für die Charakterisierung des Grundwasserleiters in diesem Testfeld angewendet worden. Die Ergebnisse, die aus 103 Korngrößenanalysen, 57 analytischen Auswertungen von Pumpversuchen, 241 analytischen Auswertungen von Slug-Tests und 9 Durchbruchskurvenanalysen von Markierungsversuchen abgeleitet wurden, stimmen mit den Inversionsergebnissen überein. Schließlich sind die zweidimensionalen Inversionsergebnisse mit den Ergebnissen der dreidimensionalen Inversion, welche auf Cross-well Slugtests basieren, verglichen worden. Die hohe Übereinstimmung zwischen den Ergebnissen der verschiedenen Inversionen unterstreicht das Potential der hydraulischen Tomographie zur Aquiferrekonstruktion.

Dennoch weist dieser kombinierte Ansatz Einschränkungen auf, die sich aus der Auflösung der hydraulischen Laufzeittomographie ergeben. Kleinmaßstäbliche Schwankungen der hydraulischen Leitfähigkeit sind kaum bei hoher Diskrepanz aufzulösen. Für eine hochskalierte Rekonstruktion im Sub-Meter Umfang ist die neue gekoppelte Methode jedoch sehr attraktiv. Repräsentative Parameterwerte können in solch einer anspruchsvollen Studie auf rechnerisch effiziente Weise abgeschätzt werden. Des Weiteren können die Parameterzonierungen, die aus den durchgeführten Inversionen abgeleitet wurden, als Ausgangsmodell für weitere Untersuchungen dienen, mit dem Ziel, die Heterogenität mehrskalig aufzulösen.

ACKNOWLEDGEMENTS

LIST OF FIGURES

LIST OF TABLES

1   INTRODUCTION

Exact, precise, and highly resolved hydrogeological maps are highly sought after and beneficial tools for geoengineering, geotechnical, and hydrogeological projects as well as environmental engineering problems within the context of water resources management (Rubin and Hubbard, 2005). With increased concern regarding groundwater contamination, environmental projects such as groundwater remediation are often carried out. Most of these projects require the predictive results of groundwater transport models (Liedl and Ptak, 2003), which depend strongly on the accuracy of hydraulic investigations (Dietrich et al., 2005; Zheng and Gorelick, 2003) and especially the determination of the continuity of preferential flow paths or hydraulic barriers (Poeter and Mckenna, 1995). For these investigations, the mapping of hydraulic subsurface features, their process monitoring, as well as the evaluations of spatial distribution of individual hydraulic properties of heterogeneous aquifers are required. However, it has been proven that even at well-instrumented groundwater research test sites, it is a difficult task to predict the detailed transport process (e.g. Sauty, 1980; Gelhar and Axness, 1983; Freyberg, 1986; Sudicky, 1986; Farrell et al., 1994; Butler, 1994; Teutsch et al., 1998; Béland-Pelletier et al., 2010).

1.1   Traditional aquifer characterization methods

In the past years, extensive research has been focused on the characterization of the ground subsurface. *Soil sampling and laboratory-based methods*, such as *particle size statistics* and *permeameter analysis*, can provide information at very small scales. Unfortunately, undisturbed cores rarely can be obtained in unconsolidated formations. Even with the obtainment of undisturbed cores, one may not easily draw significant conclusions on the geometry and properties of complex underground geological structures, using the information obtained from these methods, since these explorations are only representative of single points in the subsurface where samples have been taken from. Also, due to the empirically derived and indirect nature of estimation used to determine hydraulic properties via this approach, confidence may be low and therefore these limitations often may lead to inadequate aquifer characterization, as is needed for detailed contaminant transport modelling (Burger and Belitz, 1997; Klute and Dirksen, 1986; Rovey, 1998; Gee and Bauder, 1986; Danielson and Sutherland, 1986; Taylor et al., 1990). Alternatively, borehole/well measurement

techniques with a slightly larger radius of investigation, such as *dipole-flow tests* (Kabala, 1993; Kabala and Xiang, 1992; Zlotnik and Zurbuchen, 1998; Zlotnik and Ledder, 1996; Butler et al., 1998; Peursem et al., 1999), *borehole flow meter tests* (Molz et al., 1989; Molz and Young, 1993; Young and Pearson, 1995; Boman et al., 1997), and *multilevel slug tests* (Melville et al, 1991; Butler et al., 1994; Butler et al., 1996; Butler 1998; Brauchler et al., 2010; Diem et al., 2010) can directly provide detailed information about vertical variations in horizontal hydraulic conductivity (K). However, the radius of investigation is not likely to exceed that of several times the well radius (Taylor et al., 1990). Also, problems often occur due to well design, installation and development procedures, which surely have a significant influence on the quality of information obtained with these techniques, especially when straddle packers are used during tests. Small test intervals for the purpose of higher resolution hydraulic parameter evaluation may bring problems such as significant vertical flow components or inaccuracy introduced by disturbed zones within the radius of investigation , which should not be ignored during the analysis. A further more advanced alternative, is the *single-well electrical tracer test* (Taylor et al., 1988), which has a larger radius of representative formation (3~4 meters) and can thus avoid some of the problems associated with the other techniques. In contrast to the tests which employ the straddle packer system, where only a section of the well is pressurized, in the single-well electrical tracer test, the well is subjected to an even hydraulic head throughout. This eliminates errors associated with packers such as those involving leakage around the packer. However, single-well electrical tracer tests are quite time-consuming, being based on steady-state conditions, and also require injection of large amounts of salt water into the underground.

With the establishment of Direct-Push technology, geophysical methods such as *electric conductivity (EC) logging* are now often applied for small-scale hydraulic parametrization of aquifers. This method, however, is often not reliable. Unfortunately, even for a geologically homogeneous aquifer, accurate hydraulic parameters like porosity or hydraulic conductivity are not likely to be obtained directly from this method, since the determination of porosity is limited for clay-free formations and in general, there is no unique relationship between electrical and hydraulic conductivity. Numerous empirical relationships developed between electrical and hydraulic conductivity (Urish, 1981; Mazac et al., 1985; Kwader, 1985; Huntley, 1986) are only applicable to limited matrix types i.e. of specific formations. Therefore, this efficient and rapid data

collecting method is rather an exploration for geological texture than an aquifer characterization method. Recently developed *Direct-Push injection loggings* can obtain feasible information of hydraulic conductivities in the absence of well, in smaller scale (Butler and Dietrich, 2004; Butler, 2005; Butler et al., 2007; Dietrich et al., 2008; Liu et al., 2009; Lessoff et al., 2010), directly and rapidly. Despite limitations, this tool is promising for characterization of shallow unconsolidated aquifers, and can especially provide supplementary information to hydraulic tomographical approaches (Bohling, 2007). However, unfortunate shortcomings of this method are common with the other methods mentioned above: all data obtained are from point measurements and are therefore insufficient in identifying heterogeneities over a large area which have a strong affect on groundwater flow and which are important to include in a groundwater transport model (Bohling et al., 2007).

Conventional aquifer investigation methods like *pumping tests* can provide estimations of hydraulic conductivity and specific storage, which are representative of a larger area. However, these methods provide estimates of parameters which are spatially intergrated and thus have a low spatial resolution, i.e. the exact affect of known and unknown heterogeneities are not registered (Butler, 2005; Bohling, 2009). Resolving this issue in part can be done by the use of *multiple pumping/observation well configurations*. In this case vertical variance of horizontal hydraulic conductivity may be resolved (K values). K values from multiple well configurations are only representative for the bulk average aquifer matrix in a fairly limited region around the pumping intervals (screened and packer-separated vertical intervals of well) or in the immediate vicinity of the observation wells (Clemo et al., 2003; Bohling, 2009). *Multilevel/multi-well tracer tests* can provide useful information on spatial K variations between wells (Ptak et al., 2004). However, logistical, cost, and regulatory constraints significantly restrict their use for site characterization activities (Butler et al., 2007). All of these different variations of test have the same disadvantages in common: they are quite time consuming and have limitations at sites with a sparse well network.

Despite the restrictions that problems of scale impose on estimated flow parameters by the above-mentioned tests (Wu et al., 2005), one may be able to use these techniques over a dense network of wells over a large area in order to achieve a large investigation area with a good enough resolution for conceptual aquifer reconstruction. However, this is an extremely time consuming and work-intensive task not to mention cost and the destruction of the subsurface. Problems often also arise

from statistical uncertainty, i.e. whether the results of the geostatistical analysis based on data collected through the individual small-scale measurements is undoubtedly representative of the aquifer properties over a much larger area (Illman et al., 2008; Wu et al., 2005). Further alternatives and new methods are therefore desired to resolve these shortcomings.

Tomographic geophysical methods based on inverse techniques are often applied to address the problems presented by a sparse well network. Unlike the former hydrological techniques, which normally require the instalment of wells, the tomographic geophysical methods avoid the change of the natural flow processes in the vicinity of installed wells and can hence represent the unsampled areas non-destructively (Hubbard et al., 1999). The method of tomography was first developed for medical use. Although largely obsolete, conventional tomography is still used in specific situations such as dental imaging (orthopantomography) or in intravenous urography based on the Roentgen radiation attenuation. Besides that, the application of geophysical tomography for reconstructing two- or three-dimensional images of the physical properties of a subsurface has also been well established for years. It has to be noted, however, that geophysical methods such as *radar tomography* (e.g. Davis and Annan; 1989; Becht et al., 2004), *seismic tomography* (e.g. Bois et al., 1972; Gelbke, 1988; Harris et al., 1990; Hyndman et al., 1993) or *electrical impedance tomography* (e.g. Yorkey et al., 1987; Kohn and Vogelius, 1984, Kohn et al., 2008, Ramirez et al., 1999) yield a geophysical parameter distribution that does not necessarily have to be in accordance with hydraulic properties of the subsurface (Brauchler, 2003). The relationships between geophysical and hydraulic parameters are yet to be successfully quantified and established (e.g. Han et al., 1986; Marion et al., 1992; Dietrich et al., 1995, 1998, 1999; Hyndman and Tronicke, 2005). New tomographic methods which directly lead to the three dimensional distribution of hydraulic properties with high resolution are therefore desired.

1.2 Hydraulic tomography

Evolved from the medical and geophysical tomography concept, a new approach, *hydraulic tomography* has been developed, which enables the reconstruction of detailed spatial distributions of hydraulic parameters between wells (e.g. Bohling, 1993; Gottlieb and Dietrich, 1995; Butler et al., 1999; Yeh and Liu, 2000). In contrast to geophysical methods, hydraulic tomography enables the direct determination of hy-

draulic properties of the aquifer. The great advantage of hydraulic tomography, com-
pared with analytically based evaluations of traditional hydraulic tests, is its high-
spatial resolution characterization of the aquifer. Hydraulic tomography normally con-
sists of a series of cross-well interference tests, during which the wells are separated
into many vertical intervals using packers or a multi-chamber design. Through each
test, the water is pumped from or injected into the aquifer only through a certain in-
terval (length of well screen hydraulically separated from rest of well) of the well and
meanwhile the hydraulic head responses of the aquifer are recorded at observation
intervals. By varying the pumping (or injecting) and observation intervals through a
series of tests in a tomographical array, a large amount of aquifer responses can be
recorded. Based on such a vast amount of relevant information, an appropriate in-
verse model can thus capture the detailed three-dimensional hydraulic heterogeneity
of the subsurface with a reduction of the non-uniqueness issue through common in-
verse problems (Yeh and Liu, 2000).

Some of the hydraulic tomographic approaches are based on a numerical
groundwater flow model and a parameter estimator. The response data can be calcu-
lated forward using a numerical model which solves the groundwater flow equation.
Subsequently, with the help of a parameter estimator employing inverse modeling,
the hydraulic parameters can be estimated by fitting the calculated response data di-
rectly to the observed data (e.g. Gottlieb and Dietrich, 1995; Snodgrass and Kitanidis,
1998; Yeh and Liu, 2000; Liu et al., 2000; Vesselinov et al. 2001a; b; Fienen et al.,
2008;). Large amounts of response data can help reduce the problem of non-
uniqueness through inversions. However, the information from the data can also be
an overload, which may cause substantial computational burdens and numerical in-
stabilities (Hughson and Yeh, 2000).

In order to overcome these difficulties, a great amount of research has been done.
Yeh and his colleagues developed and assessed a *sequential successive linear es-
timator technique* to overcome this shortcoming (e.g. Yeh and Liu, 2000; Zhu and
Yeh, 2005; Illman et al., 2008; Hao et al., 2008). With this approach, computational
burdens can be substantially reduced by sequentially including information obtained
from different pumping tests. The non-uniqueness issue is also resolved by providing
the best unbiased conditional mean estimates. Another method, which can help ease
the computational burden and shorten the time-consuming analysis, is based on
moment analysis (e.g. Li et al., 2005; Zhu and Yeh, 2006; Yin and Illman, 2009). With

this method, only the selected temporal moments of drawdown are fitted to the model instead of the whole transient response data. In addition to these two methods, Bohling et al. (2002) developed an inversion approach based on a *steady shape flow regime*. At steady shape conditions, drawdown varies with time but the hydraulic gradient does not, which means the head difference between two observation points does not vary. The head difference is characteristic for the hydraulic conductivity and not sensitive to the specific storage. Jacob (1963) and Krusemann and de Ridder (1990) describe the steady shape flow regime as steady radial flow and transient steady-state flow, respectively. Steady shape conditions are established very rapidly in many field settings, even before the boundary effects take place. Therefore, this method is well suited for the evaluation of a large number of hydraulic cross-well tests in a short time. The transient data can be analyzed with the computational efficiency of a steady-state model to estimate hydraulic conductivity even though the flow system may be far from true steady-state conditions. Application of a steady-state model reduces the calculation time by several orders of magnitude in comparison to a standard inversion of transient data. All of these above-introduced inverse modelling-based hydraulic tomography approaches have been tested through numerical models. Some of them have been tested through laboratory experiments (e.g. Liu et al., 2002; McDermott et al., 2003; Liu et. al., 2007; Illman et al., 2007; 2008; 2010a; 2010b; Liu and Kitanidis, 2011) as well as field assessments (e.g. Bohling et al., 2007; Li et al., 2007; 2008; Straface et al., 2007, Illman et al., 2009; Cardiff et al., 2009;).

Alternative hydraulic tomographic approach is based on the inversion of travel times of hydraulic pressure pulse and follows the procedure of seismic tomography. The main feature of this procedure is a travel time integral relating the square root of the peak travel time of transient pressure pulse to the inverse square root of the hydraulic diffusivity for a Dirac point source at the origin (Vasco et al., 2000; Kulkarni et al., 2001; Datta-Gupta et al., 2001). Diffusivity is the quotient of hydraulic conductivity to specific storage ($D = K / S_s$). It provides a quantitative measure of response rate of the groundwater heads during transient flow and is a key consideration for the predictive simulations of the groundwater contaminant transport models (Shepley and Taylor, 2003). The derivation of the travel time integral is based on the transformation of the transient groundwater flow equation into the eikonal equation using an asymptotic approach (Virieux et al., 1994). The eikonal equation can be solved with ray tracing

techniques, which allow the calculation of pressure propagation along trajectories (e.g. Vasco et al. 1999; 2000; Vasco and Datta-Gupta, 1999; Vasco and Karasaki, 2006; Kulkarni et al., 2001; Datta Gupta et al., 2001; Brauchler et al., 2003, 2007; 2010; He et al., 2006). Ray tracing techniques are computationally very efficient and allow the inversion of hundreds of travel times derived from hydraulic cross-well short term tests using a common PC within a few seconds. However, this method estimates only the diffusivity, neglecting the separation of diffusivity into its component hydraulic conductivity and specific storage. In order to overcome this problem Brauchler et al. (2011) performed another inversion, which is based on the relationship between attenuation of a hydraulic signal traveling between source and receiver, and the specific storage of the investigated media. Since the attenuation is determined solely by the specific storage, this new inversion can help evaluate the specific storage independently as a complementary approach to the travel time based inversion.

1.3 Outline

For a highly efficient and highly spatially resolved aquifer characterization, three inversion approaches are coupled in this study. The goal is to reconstruct the spatial distributions of hydraulic diffusivity (D), hydraulic conductivity (K), and specific storage (S_s) separately and complementarily in two and three dimensions. Since the computationally efficient steady shape inversion proposed by Bohling et al. (2002, 2007) is only sensitive for K values but not for S_s values, it is an attractive complementary method to the abovementioned hydraulic travel time and attenuation inversions proposed by Brauchler et al. (2003 and 2011). Hydraulic travel times are governed by D, the ratio of K to S_s, whereas the steady shape drawdown configuration and hydraulic attenuation are determined solely by K and S_s, respectively. Thus, combining travel time and steady shape inversions will allow the direct identification of D and K, from which the estimate of S_s can be consequentially derived. Similar to this coupled inversion scheme, combining travel time and attenuation inversions can allow the direct identification of D and S_s, which leads to the estimate of their product: the K value. Hence, with the D values serving as an interconnection, there are two methods to reconstruct both the K and S_s distributions. The three most important hydraulic subsurface parameters can thus be determined independently from each other and proven by each other.

7

In Chapter 2, the relevant inversion methodology is briefly introduced.

In Chapter 3, a numerical study is introduced for the hydraulic tomographic approach, coupling hydraulic travel time and steady shape inversions. Thereby, this coupled inversion scheme is developed and tested using two- and three-dimensional synthetic data sets derived from an aquifer analogue outcrop study performed by Bayer, 1999. Based on this analogue study, the developed methods can be evaluated as a case where the true result is already known. First, the hydraulic diffusivity tomography approach of Brauchler et al., 2003 is utilized to construct zones of constant diffusivity. In a second step, hydraulic conductivity estimates are determined for each zone by means of steady shape analysis of tomographic measurements. In a third step, the specific storage of each zone is calculated from the hydraulic conductivity and diffusivity estimates.

In Chapter 4, the hydraulic tomographic approach, coupling hydraulic travel time, attenuation, and steady shape inversions is assessed in the field at the test site "Stegemühle" in the Leine River valley in Göttingen, Germany. The database for the hydraulic inversion consists of a series of 60 short-term pumping tests performed with a tomographic configuration. That is, during these series of tests, the positions of the sources (pumping interval) and the receivers (observation ports), isolated with double packer systems and multi chambers, are varied. Based on the three inversions, the K, S_s and D values can be independently estimated. In order to validate the inversion results, a large amount of results from traditional aquifer characterization methods such as grain size analyses, pumping tests, slug tests and tracer tests performed in this test site are introduced and compared with the inversion results. In addition, the inversion results are compared with the three-dimensional inversion results based on cross-well slug tests from Brauchler et al. (2011), in order to prove the potential of the hydraulic tomography in the aquifer reconstruction.

2   METHODOLOGY OF INVERSION

2.1   Hydraulic travel time inversion

Hydraulic travel time inversion is based upon the transformation of the transient groundwater flow equation into the eikonal equation (e.g. Vasco et al., 2000; Kulkarni et al., 2001) using an asymptotic approach developed by Virieux et al. (1994). A relationship between the diffusivity value and the hydraulic travel time was found to describe the similarity between groundwater flow and seismic wave propagation phenomena. With this approach, the pressure propagation along trajectories can be calculated between the source and the receiver. Thus the two- or three-dimensional problem of calculating pressure is reduced to a sequence of one-dimensional problems. Hence, the travel time inversion is computationally efficient and robust. Besides that, the hydraulic travel time is only determined by the diffusivity of the material between the source and receiver and is not influenced by variations of material properties in the vicinity of the wells (Vasco et al., 2000).

The main methodology for travel time inversion in this work, as well as the further modification of this travel time inversion is based on the findings by Vasco et al. (2000) and Brauchler et al. (2003). For detailed information and further discussions, the interested readers are referred to the above-mentioned studies for extended reading. For this application and for some further developments to the inversion approach made in this work, the main theory of travel time inversion, briefly summarized, is presented in the following sections.

2.1.1   Governing equations

The developed approach is to transform the groundwater flow equation first into the frequency domain by means of Fourier transformation. Based upon an asymptotic solution for the flow in the frequency domain, the flow equation can thus be transformed into the eikonal equation. Through inverse Fourier transformation, the flow equation will be transformed back into the time domain and will be combined with the solution of the eikonal equation. Through these derivations a relationship between the diffusivity and the travel time of a hydraulic signal can then be established with the following line integral (Vasco et al., 2000; Kulkarni et al., 2001):

$$\sqrt{t_{peak}(x_2)} = \frac{1}{\sqrt{6}} \int_{x_1}^{x_2} \frac{ds}{\sqrt{D(s)}} \; ,$$

Eq. 2.1

where t_{peak} is the travel time of the peak of a Dirac signal from the point x_1 (source) to the observation point x_2 (receiver) and D is the diffusivity. Based on this line integral, the travel time of a hydraulic signal is directly related to the reciprocal value of diffusivity. In the following a brief introduction of the derivation of the proposed procedures from Vasco et al. (2000) and Kulkarni et al. (2001) is given.

In a heterogeneous medium, the time (t) and space (x) dependent head $h(x,t)$ is described by Bear (1972) and de Marsily (1986) with the following equation:

$$K(x)\nabla^2 h(x,t) + \nabla K(x)\nabla h(x,t) = S(x)\frac{\partial h(x,t)}{\partial t} \; ,$$

Eq. 2.2

where $K(x)$ denotes the hydraulic conductivity and $S(x)$ denotes the storage coefficient. This equation can be transformed into the frequency domain by means of the Fourier transformation

$$H(x,\omega) = \frac{1}{2\pi} \int_{-\infty}^{\infty} h(x,t)e^{i\omega t} dt \; .$$

Eq. 2.3

In the frequency domain,

$$\frac{1}{2\pi} \int_{-\infty}^{\infty} S(x)\frac{\partial h(x,t)}{\partial t} dt = i\omega S(x)H(x,\omega) \; .$$

Eq. 2.4

Thus the diffusion equation in a heterogenous medium in the frequency domain, which describes the evolution of head H with dependence on frequency ω and space x is

$$K(x)\nabla^2 H(x,\omega) + \nabla K(x)\nabla H(x,\omega) = i\omega S(x)H(x,\omega) \; .$$

Eq. 2.5

The equation 2.5 can be written as

$$\nabla^2 H(x,\omega) + \Lambda(x)\nabla H(x,\omega) - i\omega\Delta(x)H(x,\omega) = 0 \; ,$$

Eq. 2.6

by defining

$$\Lambda(x) = \frac{\nabla K(x)}{K(x)}$$

<div align="right">**Eq. 2.7**</div>

$$\Delta(x) = \frac{S(x)}{K(x)} = \frac{1}{D(x)}$$

<div align="right">**Eq. 2.8**</div>

where $\Delta(x)$ is the inverse of the diffusivity.

An asymptotic solution of Equation 2.6 is given by Virieux et al. (1994) and Fatemi et al. (1995), by which the medium is assumed to have a smooth variation in conductivity $k(x)$:

$$H(x,\omega) = e^{\left[-\sqrt{-i\omega}\tau(x)\right]} \sum_{n=0}^{\infty} \frac{A_n(x)}{\left(\sqrt{-i\omega}\right)^n} .$$

<div align="right">**Eq. 2.9**</div>

This kind of asymptotic expansion is the one that has been used in the ray theory except that the $i\omega$ term for wave propagation has been replaced by $-\sqrt{-i\omega}$ for diffusive transport. This replacement can later help simplify equation 2.6 into the eikonal equation. In this expansion $\tau(x)$ represents the phase of a propagating wave. It corresponds to the geometry of a propagating front and has a dimension of square root of time. ω is the frequency of the wave and $A_n(x)$ are real functions that relate to the amplitude of the wave.

Asymptotic expansions have been widely used in the electromagnetic and wave propagation. The expansion with inverse power of ω has the initial terms of the series which represent rapidly varying (large ω, high frequency) components of the solution and the successive terms are associated with lower frequency behaviour (Vasco and Datta-Gupta, 1999). Although this expansion has a sum of an infinite number of functions $A_n(x)$, the propagation of a sharp front is described only by the initial terms of the sum, which can be related to important physical quantities.

In order to obtain expressions for these quantities the sum (Equation 2.9) is substituted into Equation 2.6. This substitution leads to an expression with an infinite number of terms and each term contains $\sqrt{-i\omega}$ to some order. The equations with terms of $\sqrt{-i\omega}$ and $\left(\sqrt{-i\omega}\right)^2$ retain one's attention because solving them will give the propagating phase $\tau(x)$ and the amplitude $A_0(x)$ used for the zero-order term of the solution. These are identical to both the eikonal and the transport equations used for

<div align="center">11</div>

ray tracing of seismic waves and permit us to compute $\tau(x)$ and $A_0(x)$ with any standard ray-tracing program (Virieux et al., 1994; Lambare, 1992). In the case of this study the terms of order $\left(\sqrt{-i\omega}\right)^2$ are considered, leading to the following equation

$$i\omega\nabla\tau(x)\nabla\tau(x)A_0(x) - i\omega\Delta(x)A_0(x) = 0.$$

Eq. 2.10

Assuming that $A_0(x)$ and ω are unequal to zero, Equation 2.10 can be expressed as follows

$$\nabla\tau(x)\nabla\tau(x) - \Delta(x) = 0.$$

Eq. 2.11

Equation 2.11 is known as the eikonal equation, which describes many types of propagation processes e.g. wave propagation. In this case it relates the function $\tau(x)$ to the flow properties as contained in $\Delta(x)$. A physical interpretation of $\tau(x)$ is obtained if the zeroth-order term in expansion of Equation 2.9 is considered

$$H(x,\omega) = A_0(x)\, e^{\left[-\sqrt{-i\omega}\,\tau(x)\right]}.$$

Eq. 2.12

Taking the inverse Fourier transformation with respect to ω, Virieux et al. (1994) transformed Equation 2.12 back to the time domain under the assumption of a Dirac source at the origin

$$h(x,t) = A_0(x)\frac{\tau(x)}{2\sqrt{\pi t^3}}\, e^{\left[-\tau^2(x)/4t\right]}.$$

Eq. 2.13

The first derivative of Equation 2.13 at a fixed position x

$$\frac{\partial h(x,t)}{\partial t} = e^{\left[-\tau^2(x)/4t\right]}\left[-3/2\sqrt{t^5} + \tau^2(x)/4\sqrt{t^7}\right]\cdot A_0(x)\frac{\tau(x)}{2\sqrt{\pi}}$$

Eq. 2.14

vanishes at the maximum (peak) drawdown, when $t = \tau^2(x)/6$. Hence, the travel time of the peak arrival of a Dirac impulse is $\tau^2(x)/6$. Equation 2.11 shows that the travel time is a function of $\Delta(x)$, the inverse of the diffusivity of the medium. The spatially varying quantity $A_0(x)$ will generally ensure that the amplitude of the peak drawdown observed at various positions will differ.

Now, it is possible to derive a line integral by defining a trajectory $s(t)$ between a source (x$_1$) starting at *t* = 0 and a receiver (x$_2$) using a curvilinear coordinate system. In these coordinates $\tau(x)$ only varies with *(s)* and $\nabla \tau$ is tangent to the *s* coordinate curve. Thus from Equation 2.11, it is possible to define the following

$$\nabla \tau = \frac{d\tau}{ds} = \sqrt{\Delta(s)}.$$

Eq. 2.15

By substituting $\tau(x)$ with $\sqrt{t} = \dfrac{\tau}{\sqrt{6}}$ one gets

$$\sqrt{t_{peak}(x_2)} = \frac{1}{\sqrt{6}} \int_{x_1}^{x_2} \sqrt{\Delta(s)}\,ds = \frac{1}{\sqrt{6}} \int_{x_1}^{x_2} \frac{ds}{\sqrt{D(s)}}\,,$$

Eq. 2.16

where t_{peak} is the travel time of the pressure from the source to the receiver and D is the diffusivity. Note that this equation is a result of a high frequency assumption. Since a smooth continuous medium is necessary for the asymptotic approach of Virieux et al. (1994), it is assumed that the permeability and porosity vary smoothly with respect to the spatial wavelength of the propagation (Vireux et al., 1994; Vasco et al., 2000). The resulting limits of this inversion technique based on the asymptotic approach are also discussed in Chapters 3.2 and 4.4.

2.1.2 Travel time inversion with transformation factor for a Dirac source

The travel time integral (Equation 2.1) is only valid for an impulse source (Dirac pulse). However, Vasco et al. (2000) have shown that the pressure response of a Heaviside source can be transformed into a pressure response of an impulsive source (Dirac source) by differentiation of the transient head data. This allows us to apply the inversion scheme to the pressure responses of constant rate pumping tests. For illustration, Figure 2.1(a) shows a drawdown curve from a simulated pumping test; Figure 2.1(b) depicts the slope of this drawdown (m/s), derived by differentiating the head data.
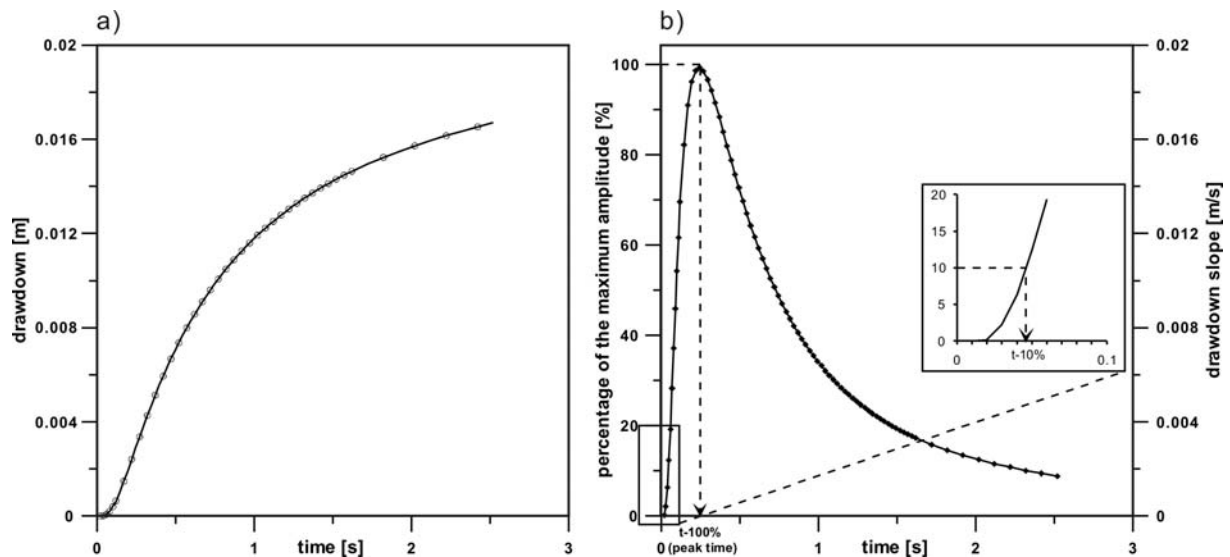
Figure 2.1: a) Drawdown curve from a simulated pumping test; b) slope of this draw-down (m/s) and percentage (%) of maximum amplitude at peak time.

The travel time inversion yields a reconstructed diffusivity distribution (in the following termed tomograms) for the area between pumping and observation wells. Brauchler et al. (2007) and Cheng et al. (2009) found that the tomograms based on the inversion of early travel time (in the following called travel time diagnostics, e.g. t-10% in Figure 2.1(b)) show more details about subsurface heterogeneity than the ones based on later travel time diagnostics (e.g. t-100% or t-peak). A travel time diagnostic is defined as the time of occurrence of a certain feature of the transient pressure pulse. For example, the t-10% diagnostic is the time at which the pressure pulse rises to 10% of its ultimate peak value (Figure 2.1(b)). In this sense, the peak value is defined as the t-100% diagnostic. As described by Fermat's principle, the hydraulic signal follows the fastest way between source and receiver. Thus early travel times are more characteristic for the preferential flow paths. In contrast, later travel times, which characterize the final part of the signal, reflect the integral behaviour throughout the whole area of investigation.

Hence, in this work the travel time inversion approach is focused on the inversion of early travel time diagnostics besides the peak time. Equation 2.1 or 2.16, respectively, relate only the travel time t_{peak} of the pressure signal to the diffusivity. For the inversion of additional travel time diagnostics besides the peak time a transformation factor was introduced by Brauchler et al. (2003):

$$\sqrt{t_{\alpha,d}} = \frac{1}{\sqrt{6 f_{\alpha,d}}} \int\limits_{x_1}^{x_2} \frac{ds}{\sqrt{D(s)}} \quad ,$$

<div align="right">**Eq. 2.17**</div>

where $t_{\alpha,d}$ is the respective travel time diagnostic and $f_{\alpha,d} = t_{peak}/t_{\alpha,d}$ is the related transformation factor. The subscript *d* denotes a Dirac source. The transformation factor is defined as follows:

$$f_{\alpha,d} = -W\left(-\frac{\alpha_d^{2/3}}{e} \right) \, .$$

<div align="right">**Eq. 2.18**</div>

W denotes Lambert's *W function*, which is a set of functions, namely the branches of the inverse relation of the function $f(w) = we^w$, where e^w is the exponential function and *w* is any complex number. The head ratio α_d enables the comparison of the peak time with the respective travel time diagnostic: $h_d(r,t) = \alpha_d h_d(r, t_{peak})$, where $h_d(r,t)$ is the hydraulic head depending on space and time.

Equation 2.17 demonstrates that it is possible to relate any recorded travel time $t_{\alpha,d}$ with the diffusivity by using the corresponding transformation factor $f_{\alpha,d}$. The choice of the travel time diagnostic is in dependence on different factors, such as the test setup, pressure measurement technique and the material characteristic of the aquifer. Hence, different early time diagnostics should be chosen for different situations. In this work, for the numerical study based on the aquifer analogue, the hydraulic travel time inversion is mainly based on the t-10% diagnostic. Whereas for the achievement of a better data quality during the field application, other early travel time diagnostics such as t-50% can be used, if pressure data at t-10% is not available due to early time data noise.

2.1.3 Travel time inversion based on specific data subsets

Another important point for the quality of subsurface transport predictions is the continuity and interconnectivity of the hydraulically significant subsurface features. To address this, I introduced the travel time inversion based on specific data subsets in addition to the inversion of a whole data set.

Similar to cross-hole radar tomography, if the angular aperture is limited, the vertical resolution will be greater than the horizontal resolution (Menke, 1984). Usually, the upper and lower part of the investigated area is less covered with travel time in-

formation as is the central part. Based on different inversion parameters (e.g. initial velocity and constraints), a certain amount of mathematically equivalent solutions exist, which cause the result of cross-hole tomography to be non-unique (Vasco et al., 1996). In common cross-hole radar tomography, a homogeneous starting model is employed and the whole travel time data set is used for the inversion. If one follows this conventional approach, anomalies may be insufficiently resolved and the images may be contaminated with artifacts (Becht et al., 2004).

To reduce the problems of the conventional approach and the ambiguity in the inversion results, constraints based on information of geological structure are implemented in the inversion. Instead of inverting the whole travel time data set, I introduce the travel time inversion based on specific data subsets. This specific data subset refers to selected travel time series from the whole data set, which has a constraint on the angle between the horizontal and a straight line connecting the source and receiver |α|.
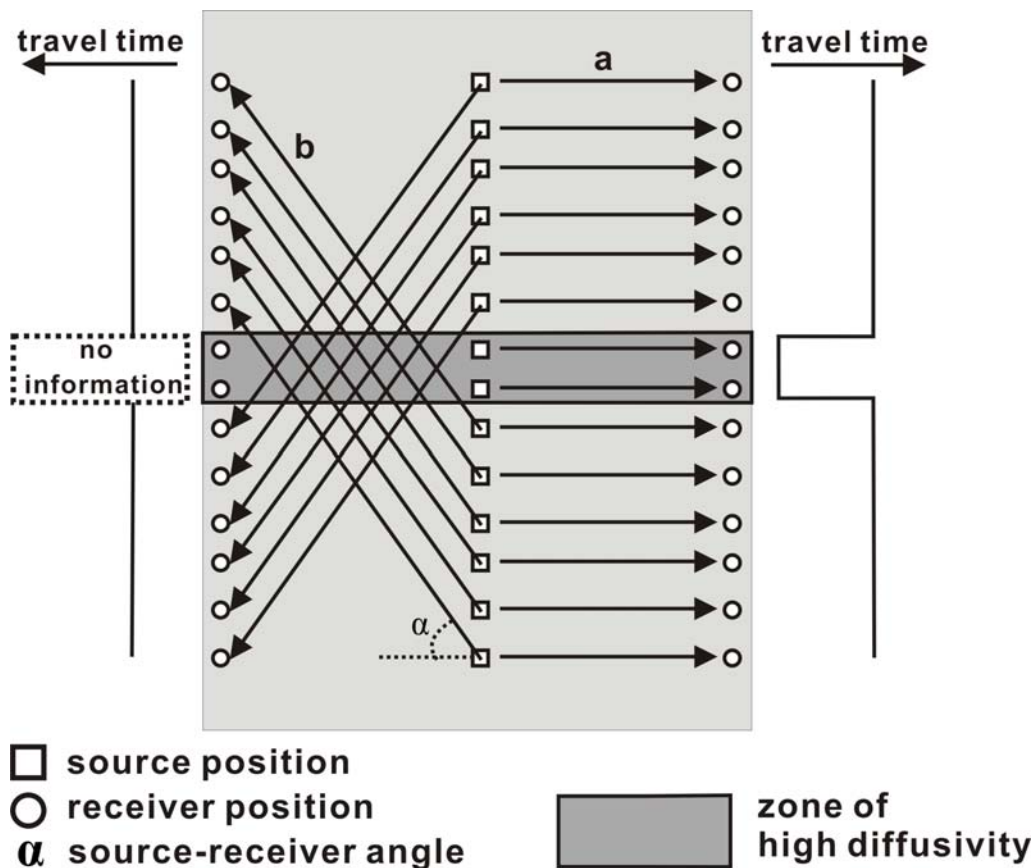
Figure 2.2: Illustration of travel times based on data subsets with different source-receiver angles (Hu et al, 2010).

As shown in Figure 2.2, trajectories with small source-receiver angles, e.g. trajectory "a" with α=0°, contain mainly information about vertical variations of the average

velocity (top and bottom boundary of a horizontal layer). Travel times of trajectories with larger source-receiver angles (e.g. trajectory "b") indicate horizontal velocity changes (e.g. pinching out of a horizontal layer) and do not contribute much to the vertical resolution of the layered zones. Under perfect conditions, the latter will improve the inversion. In practice, however, due to sparse data, and spatially varying trajectory density and data inaccuracy, a potentially ill-posed inverse problem has to be solved (Tarantola, 2005). Under such conditions there is a risk that the gain from travel times with small information content is masked by the non-uniqueness of the inversion solution. This can lead to smearing effects, ambiguity and undesirable artefacts (Becht et al. 2004; Brauchler et al., 2007).

Both the aquifer analogue and the aquifer of the test field in this study, which both are geomorphologically from a fluvial unconsolidated sedimentary outcrop, are dominated by horizontal features. Hence I decide to compare different subsets of smaller source-receiver angles.

2.2 Hydraulic attenuation inversion

Hydraulic travel times are determined by the hydraulic diffusivity, a combination of hydraulic conductivity and specific storage, whereas the hydraulic attenuation is determined solely by specific storage. Therefore the hydraulic attenuation inversion is naturally complementary to the hydraulic travel time inversion. The detailed information about this inversion approach is described in Brauchler et al. (2011). For detailed information and discussions, interested readers are directed to their work. In the following, the theory and the derivation procedures of hydraulic attenuation inversion are briefly introduced.

After Häfner et al., (1992), the solution of the diffusion equation (in radial coordinates) in an infinite domain for a Dirac source is

$$h_d(r,t) = \frac{\pi r_c^2 H_0}{\sqrt{(4\pi kt)^3 / S_s}} e^{\left(-\frac{S_s r^2}{4kt}\right)},$$

Eq. 2.19

where r_c is the casing radius and H_0 the initial displacement and $h_d(r,t)$ is the hydraulic head depending on space and time. The subscript d stands for a Dirac source. The peak time of a pressure pulse can be determined by means of the first derivative of Equation 2.19

$$\frac{\partial h_d}{\partial t} = \left[-1.5 \frac{\pi r_c^2 H_0}{\sqrt{(4\pi k)^3 t^5 / S_s}} + \frac{\pi r_c^2 H_0}{\sqrt{(4\pi k t)^3 / S_s}} \frac{S_s r^2}{4kt^2} \right] \cdot e^{\left(-\frac{S_s r^2}{4kt} \right)} .$$

Eq. 2.20

The first derivative becomes zero when

$$t = t_{peak} = \frac{S_s r^2}{6k} .$$

Eq. 2.21

Consequently, the peak time t_{peak} can be expressed in dependence of the hydraulic properties S_s and K and the distance r. The amplitude of the signal can be determined by inserting t_{peak} into Equation 2.19

$$h_{peak} = h_d(r, t_{peak}) = \frac{\pi r_c^2 H_0}{\sqrt{\left(\frac{2\pi}{3}\right)^3 S_s r^3}} e^{\left(-\frac{3}{2} \right)} .$$

Eq. 2.22

Equation 2.22 states that the decay of the amplitude (total attenuation) of an impulse source is only a function of the flow property specific storage S_s and the distance r apart from test specific parameters. The test specific parameter can be summarized introducing the parameter B:

$$B = \frac{\pi r_c^2}{\sqrt{\left(\frac{2\pi}{3}\right)^3}} e^{-\frac{3}{2}} .$$

Eq. 2.23

Inserting equation 2.23 into equation 2.22 the following relationship is received:

$$\left(\frac{h(r, t_{peak})}{H_0} \frac{1}{B} \right)^{-\frac{1}{3}} = \left(\frac{1}{S_s} \right)^{-\frac{1}{3}} r ,$$

Eq. 2.24

where $h(r, t_{peak})$ is the peak response at position r.

Based on equation 2.24 a trajectory describing the attenuation of a hydraulic pressure pulse in a medium with a heterogeneous distribution of the parameter specific storage can be defined.

$$\left(\frac{h(x_2)}{H_0} \right)^{-\frac{1}{3}} = B^{-\frac{1}{3}} \int_{x_1}^{x_2} \left(\frac{1}{S_s(s)} \right)^{-\frac{1}{3}} ds$$

Eq. 2.25

Equation 2.25 relates the attenuation of a pressure signal to a Dirac source signal at the origin to changes in specific storage S_s integrated along the trajectory defined by start and end points x_1 and x_2. Note, the proposed integrals (Equations 2.1, 2.17 and 2.25) are a result of a high frequency assumption, i.e. that the hydraulic parameters vary smoothly with respect to the spatial wavelength of the propagation and attenuation of the pressure pulse (Vasco et al., 2000).

2.3 Steady shape inversion

The key point of this study is to combine hydraulic travel time inversion and the steady shape analysis to separate the diffusivity value into its components K and S_s. Under steady shape conditions, drawdown varies with time but the hydraulic gradient does not. Jacob (1963) and Krusemann and de Ridder (1990) describe the steady shape flow regime as steady-radial flow and transient steady-state flow regimes, respectively.
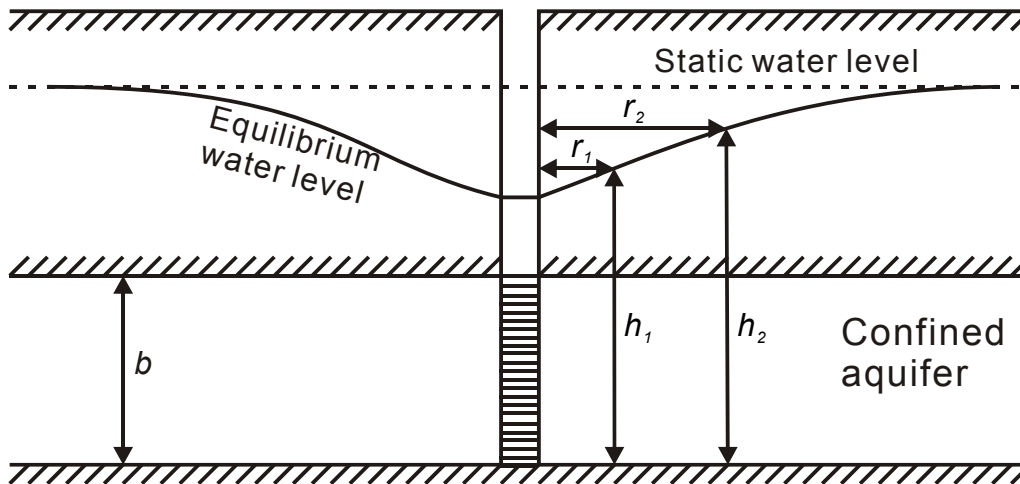
Figure 2.3: Equilibrium drawdown in a confined aquifer (after Fetter, 1994).

Figure 2.3 shows a well penetrating a confined aquifer. Under steady state conditions the rate that water is pumped from the well is equal to the rate that the aquifer transmits water to the well. This problem was first solved by Thiem (1906). From Darcy's law:

$$Q = (2\pi r b)K\left(\frac{dh}{dr}\right) = 2\pi T\left(\frac{dh}{dr}\right)$$

Eq. 2.26

Where:

Q is the pumping rate

r is the radial distance from the circular section to the well

b is the aquifer thickness

K is the hydraulic conductivity

dh/dr is the hydraulic gradient

T is the transmissivity,

Equation 2.26 can be rearranged as:

$$dh = \frac{Q}{2\pi T} \frac{dr}{r}$$

Eq. 2.27

If there are two observation wells the head is h_1 at a distance r_1 from the pumping well and h_2 at a distance r_2. One can integrate both sides of Equation 2.27 with these boundary conditions:

$$\int_{h_1}^{h_2} dh = \frac{Q}{2\pi T} \int_{r_1}^{r_2} \frac{dr}{r}$$

Eq. 2.28

$$h_2 - h_1 = \frac{Q}{2\pi T} \ln\left(\frac{r_2}{r_1}\right)$$

Eq. 2.29

$$K = \frac{Q}{2\pi b (h_2 - h_1)} \ln\left(\frac{r_2}{r_1}\right)$$

Eq. 2.30
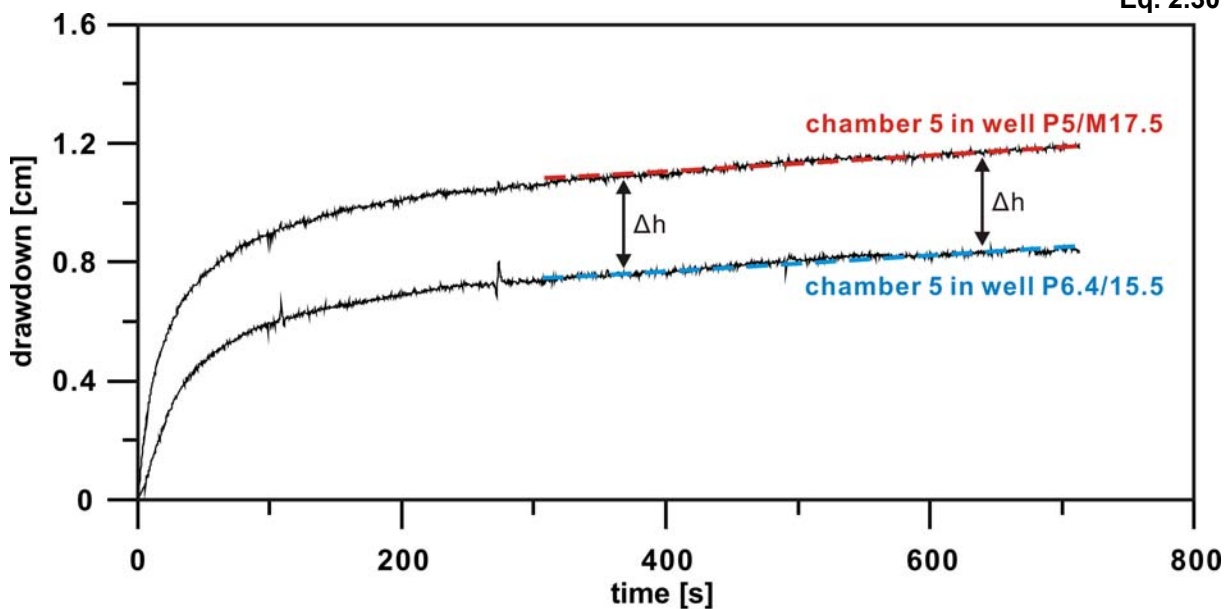
Figure 2.4: **Drawdown versus time plot for a multilevel pumping test (drawdown measured in chamber 5 of multilevel sampling wells P5/M17.5 and P6.4/M15.5, which are positioned on a straight line at distances of 9 m and 11.5 m, respectively, from the pumping well P0/M25).**

Equation 2.30 is known as the Thiem equation. Figure 2.4 displays a field example of the steady shape conditions observed during a short time pumping test in the field at the test site Stegemühle (Figure 4.3). As shown in this figure, although the flow system has not yet attained a steady state condition, steady shape condition is already established. This means the head difference between two observation points does not vary and is characteristic for the K value prior to the time when boundary conditions exert significant influence on the head response. Butler (1988) discussed how steady shape conditions can be exploited to use the Thiem equation to analyze transient drawdown data and proved that the hydraulic gradients under steady shape conditions are the same as those that will exist under true steady state conditions, if those conditions are ever achieved. The equivalence of hydraulic gradients at steady state and steady shape conditions serves as the theoretical basis of the steady shape inversion developed by Bohling et al. (2002) in detail.

Thus, I decide to use a steady state model to analyze the transient data of a series of short term pumping tests to increase the computational efficiency. Thereby, the hydraulic travel time inversion is utilized to construct zones of constant diffusivity. Subsequently hydraulic conductivity estimates can be determined for each zone by means of steady shape analysis of tomographic measurements. With this steady state model, the calculated steady shape head differences between two observation points are recorded and compared with the observed head differences. Note that according to the Thiem equation head differences rather than absolute head values are used in the approach of this study. Using the automatic parameter estimator PEST (Doherty, 2003), the hydraulic conductivity field is found that minimizes the error between all calculated and observed head differences. Since the specific storage does not have any influence on the head difference in this model and K is the only parameter to be determined, non-uniqueness that typifies such parameter estimation problems can be strongly reduced while the calculation efficiency of the steady shape approach is improved.

2.4 Inversion technique

2.4.1 Hydraulic travel time and attenuation inversion

The travel times for the diffusivity reconstructions are inverted using the software GeoTom3D, which is based on the Bureau of Mines tomography program 3DTOM (Jackson and Tweeton, 1996). The program was originally developed for seismic ray tomography and is based on the SIRT (Simultaneous Iterative Reconstruction Technique) algorithm. This algorithm allows the calculation of curved ray paths through the target area and is therefore well suited for applications in seismic tomography (Gilbert, 1972). The determination of the seismic velocities by integration of travel times is described as follows:

$$t = \int_{x_1}^{x_2} \frac{ds}{v(s)}$$

Eq. 2.31

Since the derivation of the hydraulic travel time integral is based on the transformation of the transient groundwater flow equation into the eikonal equation (Virieux et al., 1994), the eikonal equation can thus be solved with ray tracing techniques, which allow the calculation of pressure propagation along trajectories. Hence the similarity between the seismic and hydraulic travel time inversions (Equation 2.1 and 2.31) allows us to use the same application software GeoTom3D to solve hydraulic tomographic problems. With this software the ray tracing methods are applied in order to determine the trajectory paths. Similar to the rays in seismic tomography, a trajectory is determined if the source point, observation point (receiver) and the incident angle are fixed. Fermat's principle governs the geometry of the trajectory paths. This principle states that a trajectory travels not through the shortest way between two points, but through the way which takes the least time. Normally the curved-ray/trajectory calculations are slower than the straight-ray/trajectory calculations, but are more accurate for strong contrasts. The diffusivity values of the investigated geological media may vary over several orders of magnitude. This leads to a large variation of the travel times of a hydraulic signal. For this reason, it is assumed that the trajectories are curved and the travel time based inversions throughout this study are conducted with curved trajectory tracing.

Generally for the seismic travel time inversion, a model of GeoTom3D will be created with a homogeneous starting value for the velocity field, which is derived from

the mean values of the measured source-receiver-combinations. With the SIRT and ray tracing algorithm this initial model can be modified by repeated cycles of three steps: forward computation of model travel times, calculation of residuals, and application of velocity corrections. The cycle repeats through a specified number of iterations to choose a velocity distribution which minimizes the functional J:

$$J = \sum_{i=1}^{n} (\sqrt{t_i^m} - \sqrt{t_i^e})^2$$

Eq. 2.32

where t_i^e and t_i^m are the estimated and measured travel times for the i'th measurement and n is the number of measurements.

For the hydraulic travel inversion with the manipulation and modification introduced in this work, in order to achieve optimized diffusivity distribution, GeoTom repeats the cycle to minimize the overall residual $S^{0.5}$:

$$S^{0.5} = \sqrt{\sum_{i}^{n} (\sqrt{t_i^m \, 6 f_\alpha} - \sqrt{t_i^e \, 6 f_\alpha})^2} = \sqrt{6 f_\alpha J} \,,$$

Eq. 2.33

where the f_α stands for the transformation factor.

The detailed introduction of the curved ray/trajectory tracing technique, as well as the detailed derivation of the SIRT algorithm with regard to the inversion of transient pressure responses would go beyond the scope of this thesis and interested readers are referred to the studies by Brauchler et al. (2007).

For the hydraulic attenuation inversion, the analogy between Equation 2.1 and 2.25 allows calculating the specific storage distribution with the same trajectory tracing technique as for the hydraulic travel time inversion, after the amplitude data have undergone proper data processing.

2.4.2 The application of staggered grids

Different hydraulic travel times and attenuations reflect the spatial parameter distribution. Furthermore, the results of travel time based inversions depend also on the arrangement of the grids, i.e. the model cells. Since the geological and hydraulic properties are averaged over one cell, one anomaly of important properties might distribute at the border between cells and is thus separated into two or more cells. This can lead to an apparent dilution of the anomaly. In order to avoid such dilution effects

by an unlucky choice of the grid position the method of staggered grids proposed by Vesnaver and Böhm (2000) for seismic tomography is applied.
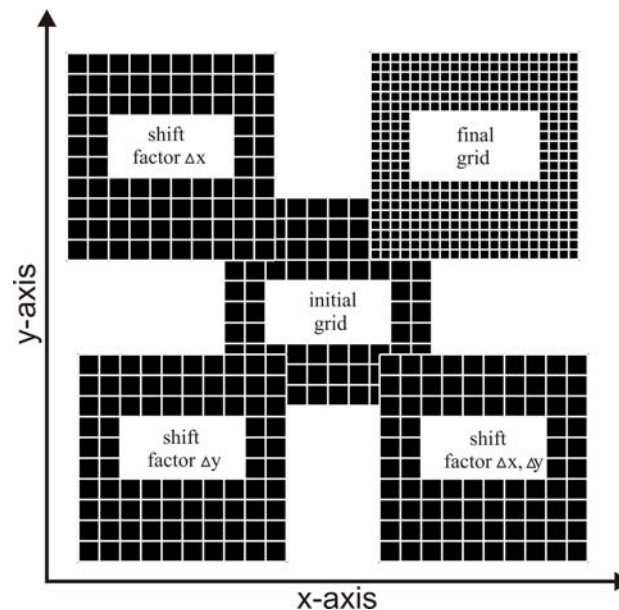
Figure 2.5: **Two-dimensional of the displacement of the initial grid. The shift factors Δx and Δy are half of the voxel lengths in the x and y directions, respectively (Brauchler et al, 2003).**

As shown in Figure 2.5 and assessed by Brauchler et al. (2003), this method is based on different viewpoints accomplished by shifting the grid. A displacement of the initial grid three times in two directions is performed. The displacements Δx and Δy are half of the cell length in x- and y-directions, respectively. For each grid a slightly different image of the parameter distribution is received because inside each voxel a different averaged value is determined. The data set is inverted four times and afterwards the arithmetic average of all grids is determined by staggering them.

As a result, the final grid can be composed of four times the cell amount, which will largely increase the resolution of the reconstruction and decrease the possibility of dilution effects through the inversion.

2.4.3 Steady shape inversion

The steady shape inversion is carried out by means of parameter estimation with the automatic parameter estimator PEST (Doherty, 2003). For parameter estimation, PEST employs the Levenberg-Marquardt algorithm (Marquardt, 1963) to optimize the parameter set, based on which the sum of squared deviations between observed and calculated values reaches the minimum (Doherty 2003). In the case of this study, this is described with the following objective function:

$$ J = \sum_{i=1}^{n} (d_{ob(j)} - d_{cal(j)})^2 \ , $$

<div align="right">**Eq. 2.34**</div>

where J is the sum of square weighted residuals, $d_{ob(j)}$ is the weighted head difference of the j'th observation pair and $d_{cal(j)}$ is the calculated weighted head difference for the j'th observation pair of the steady state model. The smaller the object function is, the better will be the parameter estimation.

For the evaluation of the model calibration, the root mean squared error (RMSE) is used as a standard error measurement. However, the value of the RMSE is case-specific, which makes it is difficult to evaluate the estimation using just the value of RMSE, if comparison with other estimations is needed. Hence, the correlation coefficient as another general measure of goodness of fit is introduced, which is provided by the correlation coefficient as defined in Cooley and Naff (1990). "Unlike the objective function, the correlation coefficient is independent of the number of observations involved in the estimation process and of the absolute level of uncertainty associate with these observations" (Doherty 2003). Hence use of the measure of goodness of fit allows the results of different parameter estimation procedures to be directly compared.

The correlation coefficient R is calculated as

$$ R = \frac{\sum (w_i d_i - m)(w_i d_{oi} - m_o)}{\left[\sum (w_i d_i - m)(w_i d_i - m) \sum (w_i d_{oi} - m_o)(w_i d_{oi} - m_o)\right]^{\frac{1}{2}}} \ , $$

<div align="right">**Eq. 2.35**</div>

where

d_i is the i'th observation value,

d_{oi} is the model-generated counterpart to the i'th observation value,

m is the mean value of weighted observations,

m_o is the mean value of weighted model-generated counterparts to observation values, and

w_i is the weight associated with the i'th observation value. (Doherty 2003)

3   NUMERICAL STUDY BASED ON SYNTHETIC DATA

3.1   Work steps

The coupled approach of hydraulic travel time with steady shape inversion is tested by a transient groundwater model using MODFLOW-96 (Harbaugh and McDonald, 1996). Based on two- and three-dimensional numerical data sets derived from an aquifer analogue outcrop study performed in a braided river environment-derived hydrogeology, the ground water model is set up to simulate short term pumping tests arranged in a tomographic array between five wells, in which the positions of the pumping intervals (sources) and the observation intervals (receivers) are varied between the tests. Based on the hydraulic travel times between different sources and receivers, the hydraulic diffusivity tomography approach is utilized to construct zones of constant diffusivity. Consequently, through a steady state model with the same zonation of diffusivity, the hydraulic conductivity estimates are determined for each zone by means of steady shape analysis of tomographic measurements. In the last step, the specific storage of each zone is calculated from the hydraulic conductivity and diffusivity estimates.

3.1.1   Aquifer analogue outcrop study

Theoretical numerical studies are often a cost effective way to develop and evaluate new investigation techniques. However, there is still a question remaining: Are the results from the studies representative for a real aquifer? Transferability into practice can only be answered by testing in the field. Even then, the quality of measured data interpretation can hardly be assessed exactly as the true field conditions are not fully known. In order to maximize the expressiveness of numerical studies, they therefore should resemble field conditions as realistically as possible.

An attractive approach is to make use of aquifer analogues. Such analogues are often derived from mapping outcrops and have mainly been used in the petroleum industry for reservoir characterization (Flint and Bryant, 1993). In particular structural and textural features can be deduced that represent the characteristics of the hardly accessible reservoir rocks. In hydrogeology, emphasis is set on outcrop analogues of complex sedimentary formations, which are of special interest due to their relevance as hosts of highly productive aquifers. Using such analogues, detailed inspection of

natural heterogeneity of hydraulic properties is possible (Teutsch et al., 1998; Hug-genberger and Aigner, 1999).

The database of the numerical investigations, presented in the following study, is from the aquifer analogue outcrop study close by the village Herten in SW Germany performed by Bayer (1999). Six parallel profiles of an unconsolidated sedimentary body with a size of 16 m × 10 m × 7 m are provided. During a period of six months, the gravel quarry was excavated in a stepwise fashion as the quarry face was moved back 10 m in total. Every two meters, high resolution photographs were taken of each exposed face, yielding six parallel images (e.g. Figure 3.1(a)). The outcrop photographs were then interpreted to yield facies maps of lithology, using observed texture, sediment grain size, and GPR (Ground Penetrating Radar) surveys. From a hydrogeological perspective, focus is set on hydrofacies, i.e. zones of similar hydraulic conductivity and porosity. Hence, for each lithological unit, laboratory measurements for hydrofacies classification were performed (e.g. Figure 3.1(b)-(c)). Maji and Sudicky (2008) present a geostatistical analysis of the generated hydrofacies mosaics. Based on transition probability Markov chain geostatistics, they interpolated between the six profiles and translated the gathered information into a three-dimensional (3-D) hydraulic parameter distribution. The 3-D characterization of the aquifer analogue makes the highly resolved parameter distribution unique with a resolution of 5 cm × 5 cm × 5 cm (Figure 3.1(d)).
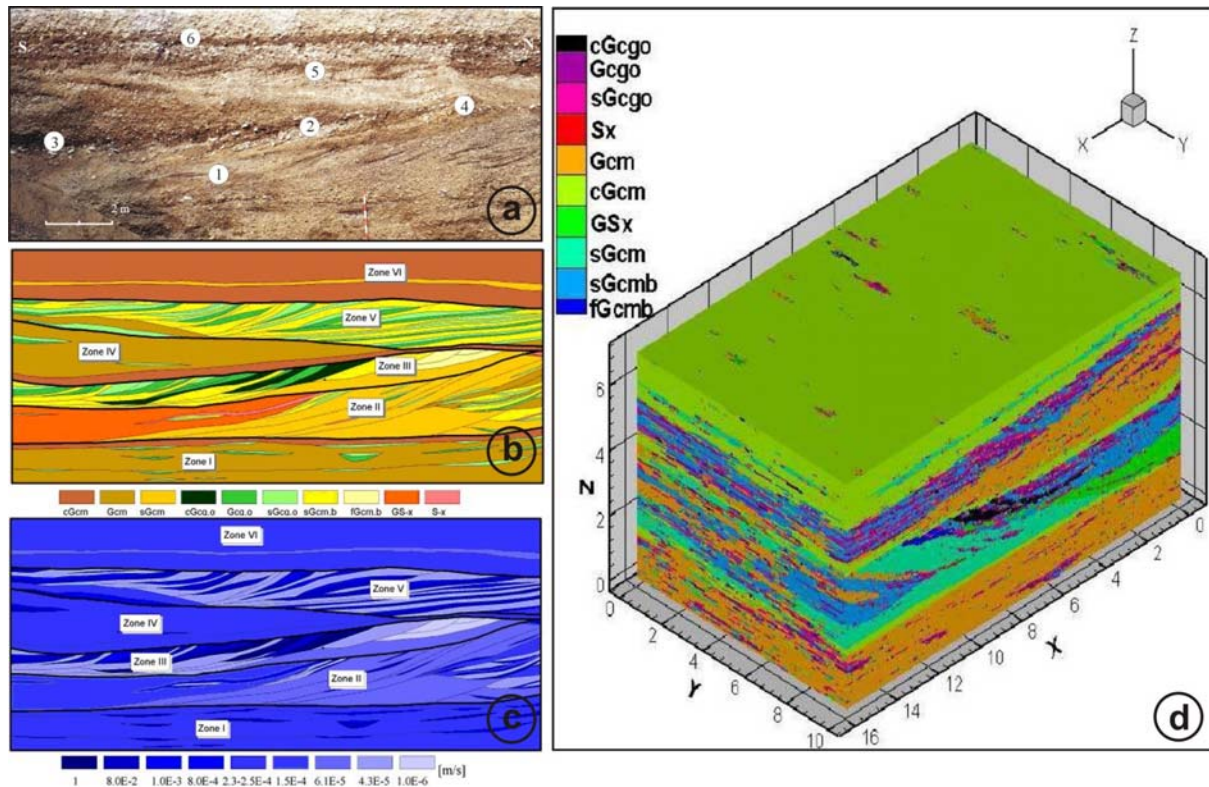
Figure 3.1: Aquifer analogue outcrop study: (a) photograph of an outcrop, (b)-(c) derived hydrofacies and permeability distribution (Bayer, 1999); (d) 3-D interpolation of hydraulic parameter distribution (Maji and Sudicky, 2008).

The Herten analogue serves as a basis for the numerical groundwater model, which is utilized in the present study to simulate short term pumping tests arranged in a tomographic array. The hydrofacies-specific hydraulic conductivity values are taken from Bayer (1999). The specific storage values are oriented to representative data reported in the literature (Domenico and Mifflin, 1965). For this, four main hydrofacies groups are distinguished, each with one characteristic specific storage value (Table 3.1).

Table 3.1: Lithofacies, hydrofacies, and their corresponding values for hydraulic conductivities (m/s) and specific storages (m^{-1}).

Lithofacies code	Characterization	Hydrofacies code	Characterization	Hydraulic Conductivity [m/s]	Specific Storage [m^{-1}]
Gcg, a	Gravel Matrix free Well rounded	Gcgo	Gravel, open framework	8.0×10^{-2}	3.62×10^{-5}
		cGcgo	Stone-rich gravel	1	
		sGcgo	Stone-rich gravel (coarse)	1.0×10^{-3}	
Gcm	Gravel Well- to rounded Moderate to poor sorting	cGcm	Stone-rich gravel	2.3×10^{-4}	4.90×10^{-5}
		Gcm	Sand-rich gravel	2.5×10^{-4}	
GSx	Gravel/sand mixtures Well sorted and rounded	fGcmb	Bimodal silt-gravel mixture	6.0×10^{-7}	1.02×10^{-4}
		sGcmb	Bimodal sand-gravel mixture	4.3×10^{-5}	
		sGcm	Sand-rich gravel	6.1×10^{-5}	
		GSx	Sand/silt-gravel mixture	1.5×10^{-4}	
S-x	Sand	S-x	Pure sand accumulation	8.0×10^{-4}	2.00×10^{-4}

For computational reasons, the original analogue data set is scaled up to 10 cm × 10 cm × 10 cm. Since the porosity was found to be normally distributed over the entire aquifer analogue dataset, the upscaling is performed using the arithmetic mean of the surrounding porosity values, and the geometric mean for the hydraulic conductivity (Renard and de Marsily, 1997) as shown in Figure 3.2.
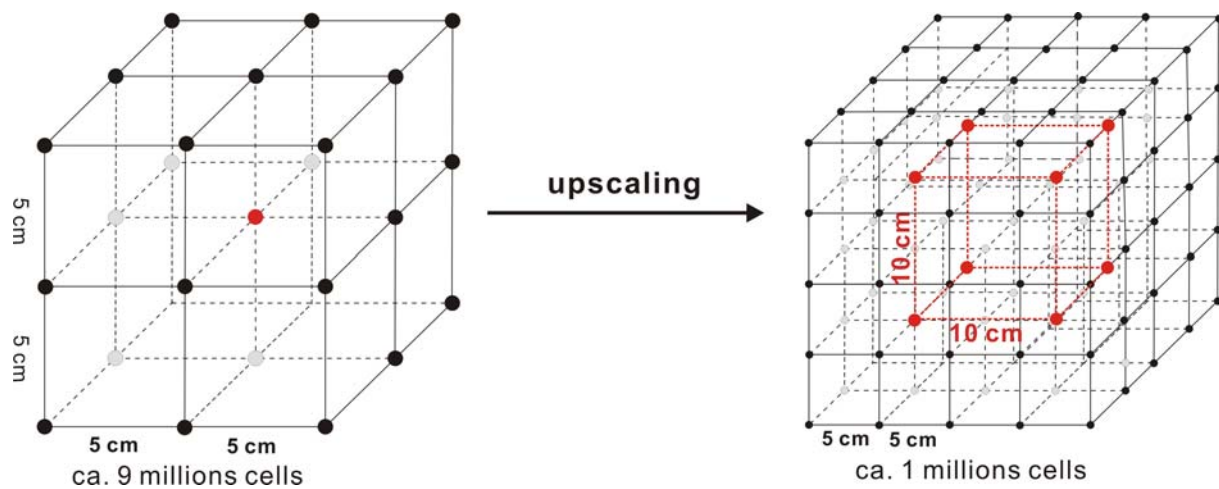
Figure 3.2: The upscaling of the original analogue data set.

This upscaling results in a reduction of the total number of cells from approx. 9 Mio. to approx. 1 Mio. Figure 3.3 shows a 3-D image of the hydraulic conductivity and specific storage distribution. Although the resolution reduction and the rigorous definition of specific storage are a compromise between data quality and practicability, the images illustrated in Figure 3.3 still maintain highly resolved sedimentary structures such as small scale layering and cross-beddings, which are reflected by the corresponding hydrofacies distribution.
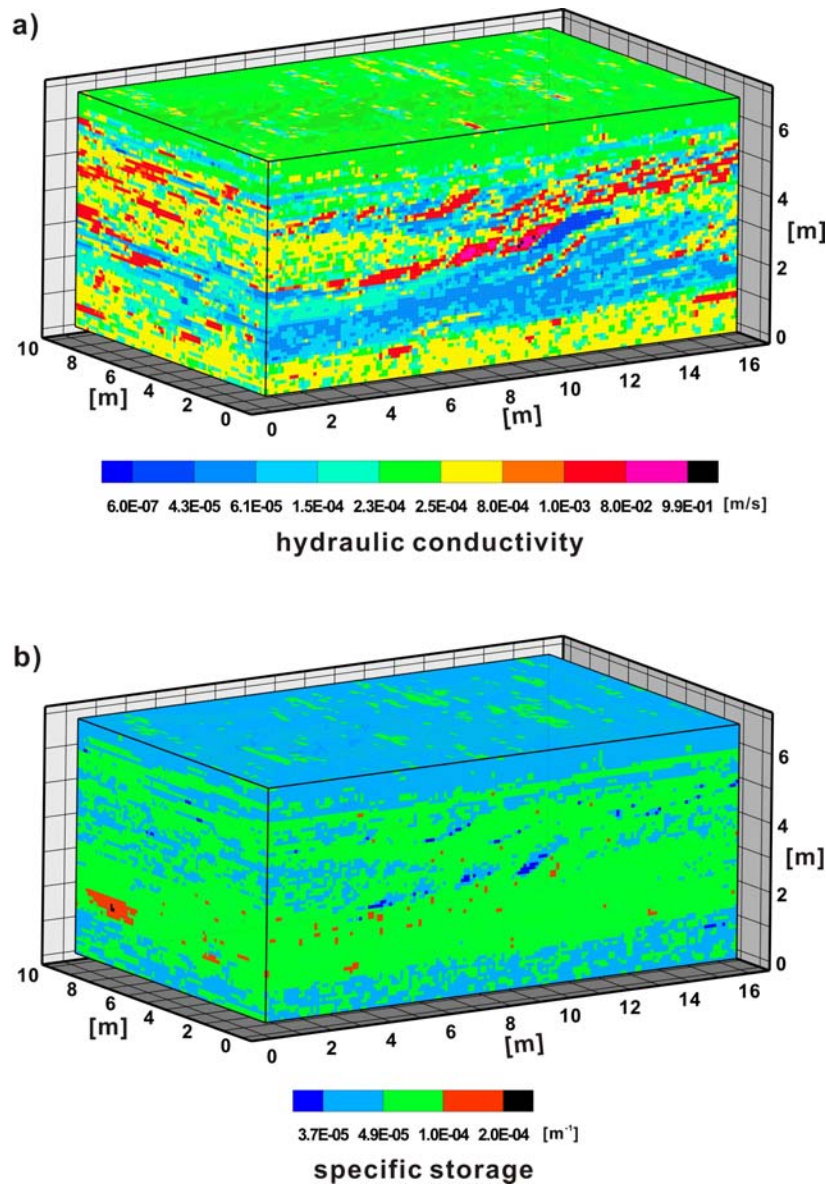
Figure 3.3: Three-dimensional (3-D) images of the upscaled distribution of (a) hydraulic conductivity and (b) specific storage for the Herten aquifer analogue.

3.1.2 Numerical simulation of short term pumping tests

Model domain

A groundwater model using MODFLOW-96 (Harbaugh and McDonald, 1996) is set up to simulate short term pumping tests arranged in a tomographic array. The aquifer analogue data set with a volume of 16 m × 10 m × 7 m is embedded in the center of the model domain on a uniform 10 cm grid. Outside of this area the mesh is telescopically coarsened and increasing cell sizes are employed, ranging from 10 cm at the central domain of interest to 100 m at the model boundaries. The distance from the center to the constant head boundary is about 600 m (Figure 3.4). The hydraulic parameters for the cells of the extended area are the mean values taken from the

aquifer analogue data set (hydraulic conductivity: 2.1×10^{-3} m/s; specific storage: 6.6×10^{-5} m^{-1}).
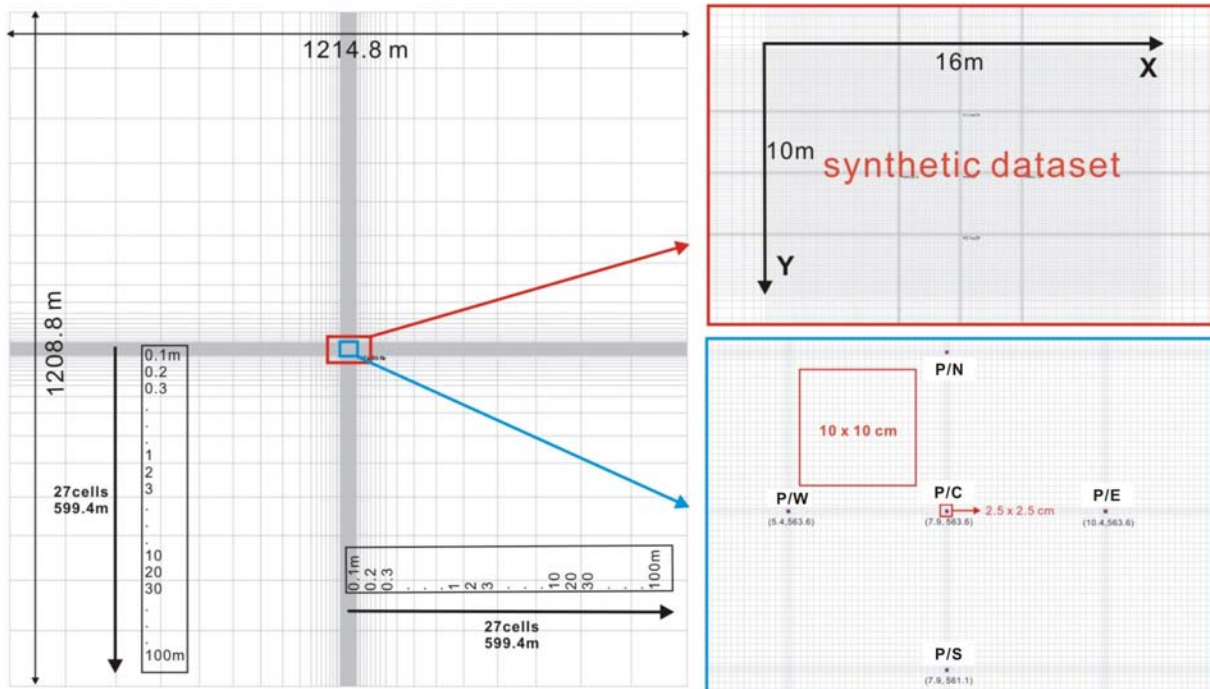
Figure 3.4: Model domain (top view) used for the forward model based on the synthetic dataset with a zoomed-in section of the central well positions.

Five wells with a diameter of 0.05 m are positioned in the center of the model domain. The wells are arranged in a five point star configuration, with the four outer wells located at a distance of 2.5 m from the center well (Figure 3.4 - zoomed-in section and Figure 3.5 – (a) and (b)). The initial head and the constant head at the boundaries are set 0.2 m above the aquifer top, and confined conditions are confirmed during the simulation of pumping tests. For each pumping test, the simulation length is 300 seconds and six stress periods with 100 increasing time steps in total are applied to simulate the drawdown phase.

Simulated tests

For the hydraulic tomography a large number of short term pumping tests in a tomographical array are simulated. During each test, extraction from a defined vertical well screen section (the source) stimulates transient pressure changes in the surrounding observation wells. These are simultaneously recorded at different depths (the receivers).

For each short term pumping test, the pumping well is screened every 0.5 m. In successive tests, the position of the well screen is moved to the adjacent vertical position, so that 14 tests with one pumping well are performed in total. The same verti-

cal resolution is assigned to the observation wells, and accordingly hydraulic heads are recorded at 14 different depths (Figure 3.5(c)). Each pair of pumping-observation wells delivers 14×14 recorded transient pressure responses, which together forms a cross-well vertical profile between the two wells.
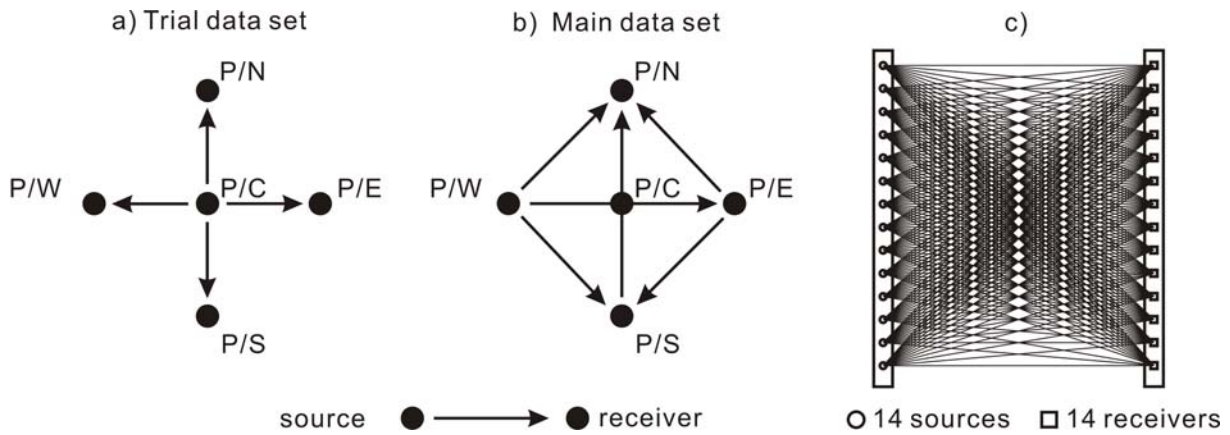
Figure 3.5: Spatial position of pumping and observation wells of (a) trial data set for preliminary testing and (b) main data set. (c) Vertical position of the pumping and observation intervals of a recorded tomographic profile.

For this work, a trial data set is first generated for fast preliminary testing. The trial data set includes four profiles, where the center well of the five point star configuration serves as the source and the four surrounding wells are the observation wells (Figure 3.5(a)). Using the trial data set and two-dimensional (2-D) travel time inversions, a strategy based on (i) the inversion of data subsets and (ii) the inversion of early travel times is developed.

In the subsequent main simulation campaign, additional cross-well configurations are used to generate a complete 3-D main data set. This contains six profiles recorded between each two of the four outer wells (Figure 3.5(b)). Different from the first trial data set, this main data set is a complete data set, which covers not only the profiles of the North-South (N-S) and West-East (W-E) directions, but also the four sides of the five-well area. From the recorded pressure responses, the derived travel times will be inverted through a 3-D inversion applying the developed inversion strategy.

Model verification

In order to verify the validity and plausibility of the numerical model, a pumping test with full penetration is first simulated. The test is analyzed with the analytical solution developed by Theis (1935). The pumping well is the well P/C in the middle and

the other four wells are the observation wells. The mean values of the evaluated K and S_s can be compared with the mean values of the aquifer analogue data set.

Subsequently, the head data of 28 simulated pumping tests with partial penetration from the data set described in Figure 3.5(b) is extracted. They can be evaluated with analytical solutions developed by Theis (1935) and the steady shape forward calculation based on the Thiem equation (1906) (Equation 2.30).

During the first series of 14 tests for the direction South-North the water was pumped out of every 50 cm interval for over 7 meters of the well P/S and the hydraulic heads generated by each test in the well P/C and P/N in the same depth as the pumping interval are recorded. During the second series of 14 tests for the direction West-East, the same set-up is used between the pumping well P/W and the observation wells P/C and P/E.

Using the analytical solution developed by Theis (1935) and taking partial penetration effects into account, the 28 drawdown curves recorded in the well P/N and P/E at 14 different depths can be analyzed. Besides that, through each pumping test, the head difference between the two observation wells (P/C-P/N, P/C-P/E) at the same depth is also recorded. With the Thiem equation (Eq. 2.30), the hydraulic conductivity values for the 14 depths in the directions South-North and West-East can be calculated. The calculated and evaluated K values with respect to the vertical variation can be compared with the "true" values from the aquifer analogue data.

3.1.3 Inversion

The proposed inversion scheme based on synthetic data couples two different techniques: travel time and steady shape inversions. The goal is to reconstruct the spatial distribution of the parameters hydraulic conductivity and specific storage with high accuracy in two and three dimensions. Hydraulic travel times are governed by the hydraulic diffusivity, the ratio of hydraulic conductivity to specific storage, whereas the steady shape drawdown configuration is determined solely by hydraulic conductivity. Thus, combining these two approaches will allow the identification of the three parameters hydraulic conductivity, diffusivity and specific storage. The entire inversion procedure is shown in the following flowchart (Figure 3.6).
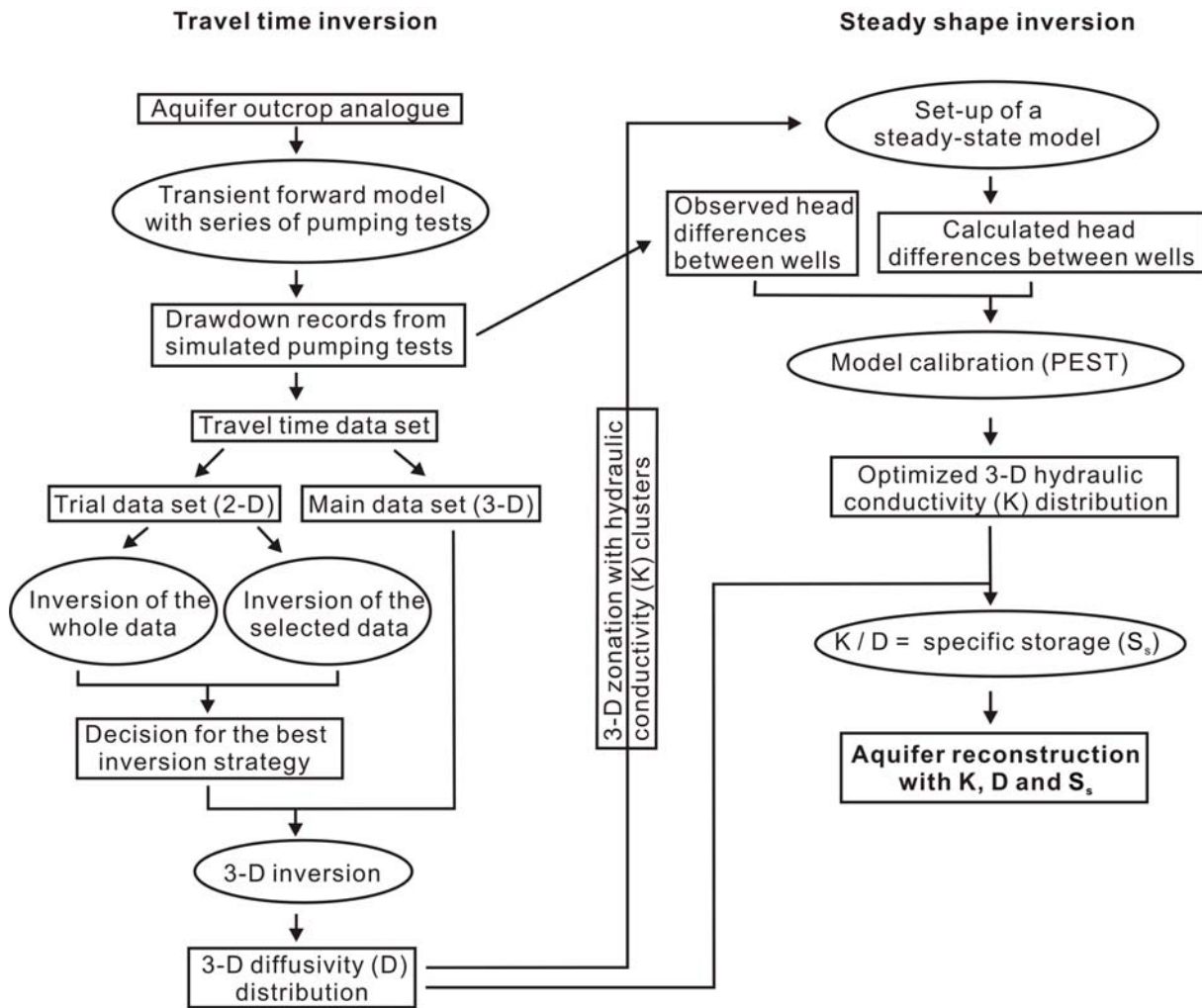
Figure 3.6: Flowchart of the entire inversion procedure used throughout the numerical study.

The 2-D trial data set will be utilized for fast preliminary testing, in order to optimize the travel time inversion strategy for the 3-D main data set. From the full 3-D travel time inversion, a spatial diffusivity pattern and the zonation of hydraulic conductivity are derived. This zonation is implemented in a steady-state model for the next step, the steady shape inversion. This new flow model simulates the same configuration of pumping tests as examined with virtual reality, i.e. the original transient forward model. The model is then calibrated by adjusting the zoned hydraulic conductivities. This is done by minimization of head differences between zoned and original models. Based on the optimized hydraulic conductivity distribution from the steady shape inversion and the diffusivity distribution from the hydraulic travel time inversion, the specific storage values can be calculated for the corresponding zonation and the aquifer can be fully reconstructed with these three parameters.

Travel time inversion

In this work the travel time inversion approach is focused on the inversion of additional travel times (in the following, called travel time diagnostics) besides the peak time. A travel time diagnostic is defined as the time of occurrence of a certain feature of the transient pressure pulse. For example, the t-10% diagnostic is the time at which the pressure pulse rises to 10% of its ultimate peak value (Figure 2.1(b)). In this sense, the peak value is defined as the t-100% diagnostic.

In order to test different inversion strategies, 2-D inversions based on the trial data set and the travel time diagnostic t-10% are carried out first. The inversion yields a reconstructed diffusivity distribution (in the following, termed tomogram) for each profile between pumping and observation wells. The decision to use the travel time diagnostic t-10% is based on the findings by Brauchler et al. (2007) and Cheng et al. (2009) that the tomograms based on the inversion of early travel time diagnostics show more details about subsurface heterogeneity. As described by Fermat's principle, the hydraulic signal prefers to follow the fastest way between source and receiver. Thus early travel times are more characteristic for the preferential flow paths. In contrast, later travel times, which characterize the final part of the signal, reflect the integral behavior throughout the whole area of investigation.

Steady shape inversion

The key point of this study is to combine hydraulic travel time inversion with the steady shape analysis to separate the diffusivity value into its components K and S_s. Under steady shape conditions, drawdown varies with time but the hydraulic gradient does not. This means the head difference between two observation points does not vary and is characteristic for the K value, prior to the time when boundary conditions exert significant influence on the head response. Thus, a steady state model is used to analyze the transient data to increase the computational efficiency. Since the specific storage does not have any influence on the head difference in this model and K is the only parameter to be determined, non-uniqueness that typifies such parameter estimation problems can be strongly reduced while the calculation efficiency of the steady shape approach is improved.

The steady shape inversion is performed with the new steady state flow model from MODFLOW-96 (Harbaugh and McDonald, 1996). This model has the zonation of hydraulic conductivity derived from travel time inversion (Figure 3.6). The steady shape model domain can be separated into two parts. The center part, reflecting the

five point star configuration with a diagonal length of 5 m and an aquifer height of 7 m, is discretized by voxels with an edge length of 0.44 m × 0.44 m × 0.44 m. Thereby, the cell length of the steady shape model was adapted to the voxel length of the three-dimensional diffusivity reconstruction. Outside this area, the model is extended about 600 m in order to avoid any boundary effects. The model edges are represented by constant head boundaries (Figure 3.7).
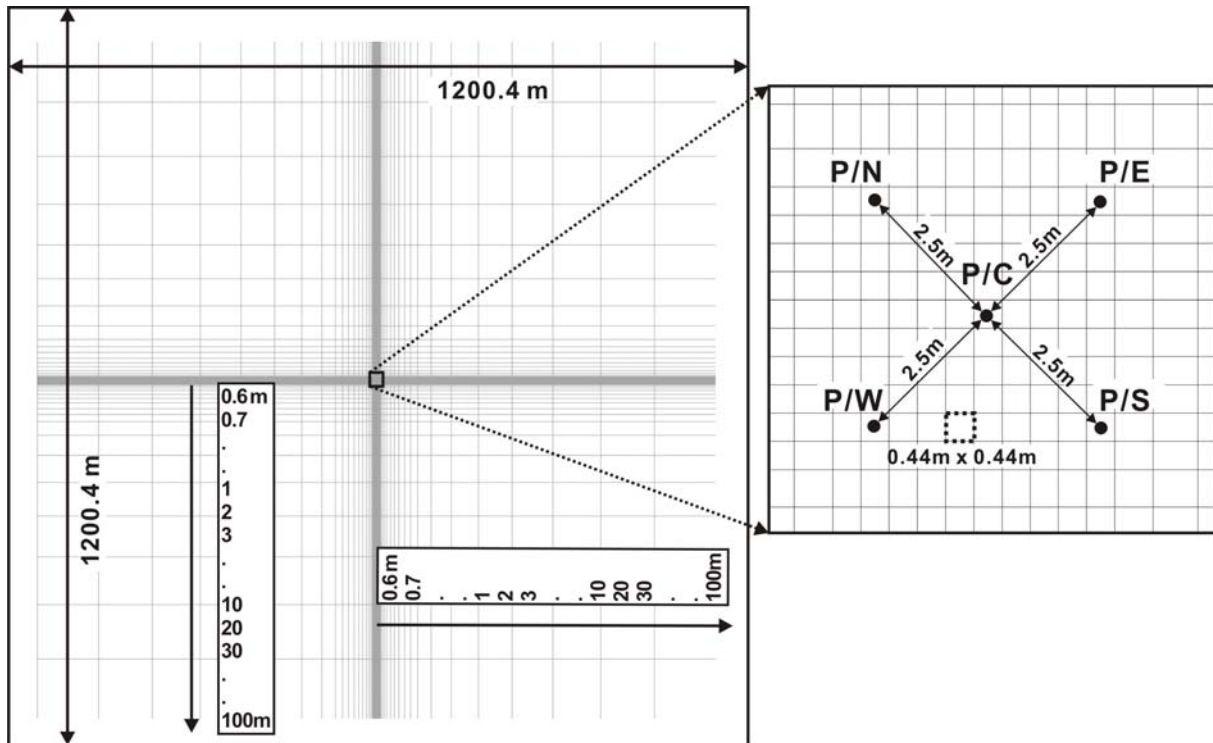
Figure 3.7: Model domain used for the steady shape inversion with a zoomed-in section of the central well positions.

Using this model, pumping tests with the same configurations as in the full model based on analogue data are simulated. The calculated steady shape head differences between two observation points are recorded and compared with those "observed" with the "true" analogue data model. Using the automatic parameter estimator PEST (Doherty, 2003), the hydraulic conductivity field is found that minimizes the error between all calculated and observed head differences. As standard error measurement, the root mean squared error (RMSE) is used. Since the value of the RMSE is case-specific and in particular dependent on the number of observations to be calibrated, the correlation coefficient as another general measure of goodness of fit is introduced.

37

For the parameter estimation 392 (14×14+14×14) recorded head differences from a series of 28 short term pumping tests are used. The recorded head differences can be divided into two directions (Figure 3.8). Direction South-North is based on 14 pumping tests with the pumping well P/S. Consistent with the tomograms of the full data set, the pumping well is screened every 0.5 m during each pumping test. The head differences generated by each pumping test are recorded at 14 different depths between the center well P/C and well P/N. Direction West-East is recorded using the same set-up between the pumping well P/W and the observation wells P/E and P/C.
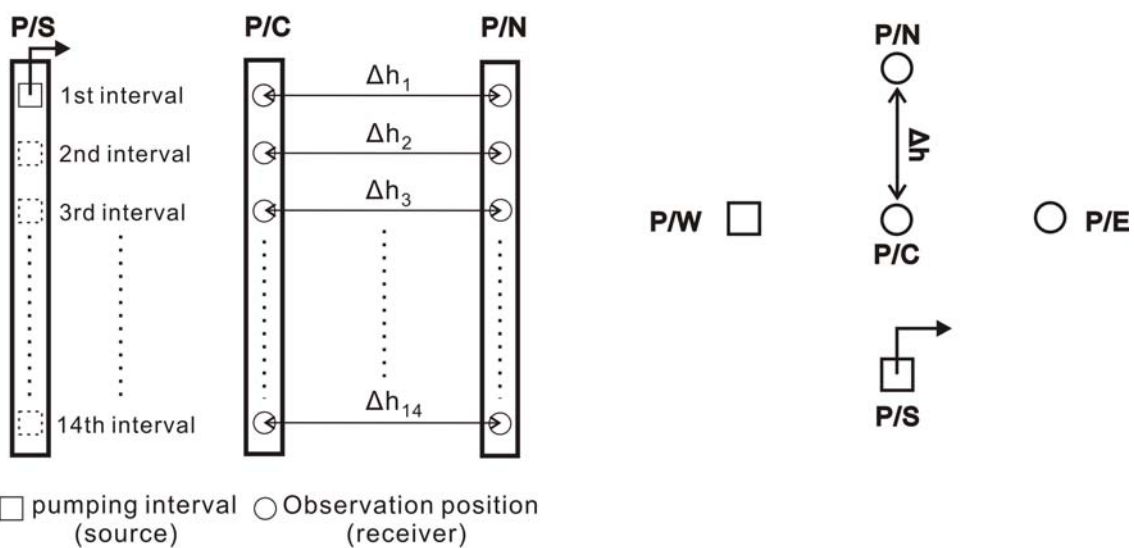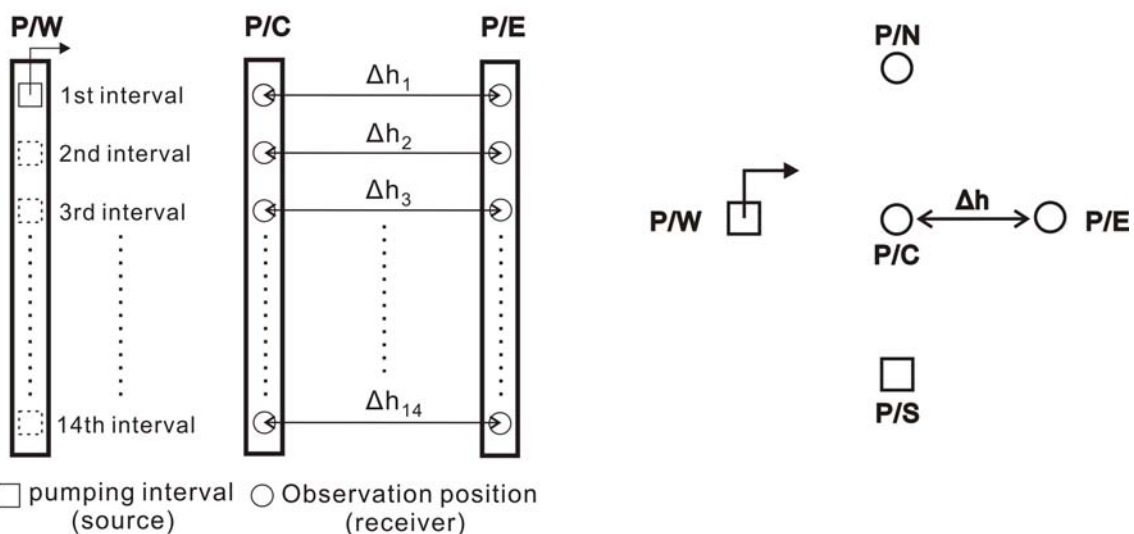
Figure 3.8: Head differences recorded in two directions for the steady shape inversion: (a) South-North direction with pumping well P/S; (b) West-East direction with pumping well P/W.

38

3.2 Results

3.2.1 Model verification

The first result of model verification based on a pumping test with full penetration is shown in the Table 3.2. The hydraulic parameters match the corresponding mean values of the analogue data set, which indicates success with respect to the fact that the groundwater model is able to successfully run based on the analogue data set.

Table 3.2: Evaluated hydraulic conductivity and specific storage values in comparison with the "true" values of the aquifer analogue.

hydraulic conductivity [m/s]		specific storage [m^{-1}]	
true	evaluated	true	evaluated
2.11×10^{-3}	2.05×10^{-3}	6.60×10^{-5}	1.1×10^{-5}

Based on the pumping tests with partial penetration, the model is verified in two directions. The vertical variation of evaluated hydraulic conductivity values from analytical solutions and steady shape forward calculations are displayed in Figure 3.9. Note that the 14 "true" K values in this figure are the calculated arithmetic mean values from the analogue data set of every 50 cm over the total depth of 7 meters within the corresponding well area.
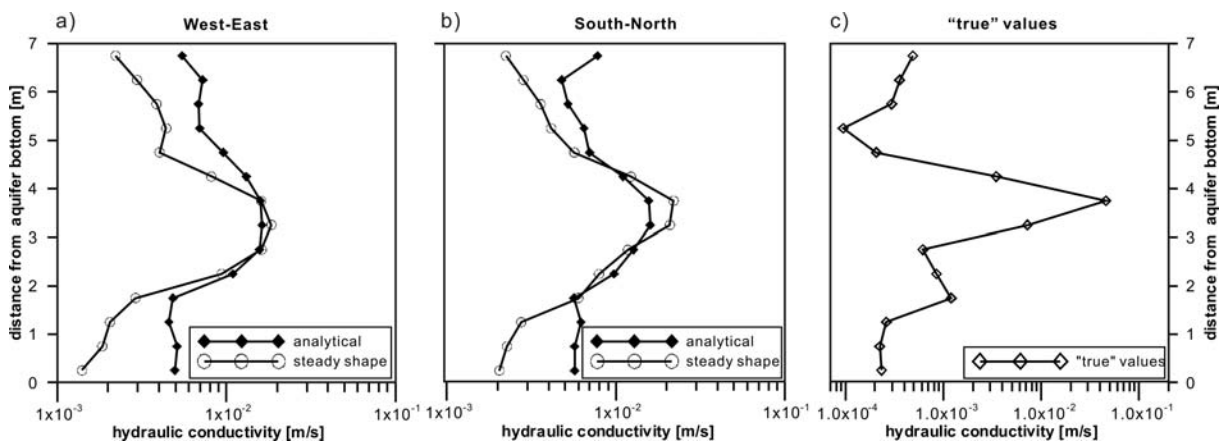
Figure 3.9: The evaluated hydraulic conductivity values with analytical and steady shape solutions in the (a) West-East (W-E) direction and the (b) South-North (S-N) direction. (c) The "true" K values of the analogue dataset.

Different from the "true" K values, which vary from approx. 1×10^{-4} to 4.6×10^{-2} m/s, the evaluated K values vary in a smaller range of approx. $1.4 \times 10^{-3} \sim 2.2 \times 10^{-2}$ m/s with less variation in the vertical direction. Based on the integral information over the

area of investigation, the multilevel pumping tests have their limitation with resolving the vertical variance of the horizontal hydraulic conductivity. The results represent the bulk average in a fairly limited region around the pumping intervals and in the immediate vicinity of the observation wells.

Nevertheless, the distribution of the high-*K* and low-*K* zones of the aquifer from both analytical and steady shape methods are clearly recognizable. These results reflect the hydraulic properties of the different layers of the aquifer very well and strongly support the validity and plausibility of the numerical model.

3.2.2 Hydraulic travel time inversion

The trial data set includes four profiles that form a cross with the central well P/C serving as pumping well. Travel time based inversion is applied to arrive at four independently inverted profiles. In West-East (W-E) and South-North (S-N) direction, the two adjacent profiles each are combined and two composite tomograms are derived. Tomogram W-E represents the reconstructed aquifer between the wells P/C – P/W and P/C – P/E. Profile S-N is perpendicularly oriented and based on the profiles between the wells P/C – P/S and P/C – P/N (Figure 3.5(a)).

The hydraulic travel time based inversion is fulfilled through GeoTom3D. It performs inversions with the simultaneous iterative reconstruction technique, or SIRT (Gilbert, 1972). SIRT calculations modify an initial velocity model by repeated cycles of three steps: forward computation of model travel times, calculation of residuals, and application of diffusivity corrections. The cycle repeats through a number of iterations, which is specified before the inversion. For this specification, the peak times (t-100%) of the whole travel time data set from profile W-E are inverted with different number of curved-ray iterations and the results are shown in the Figure 3.10.
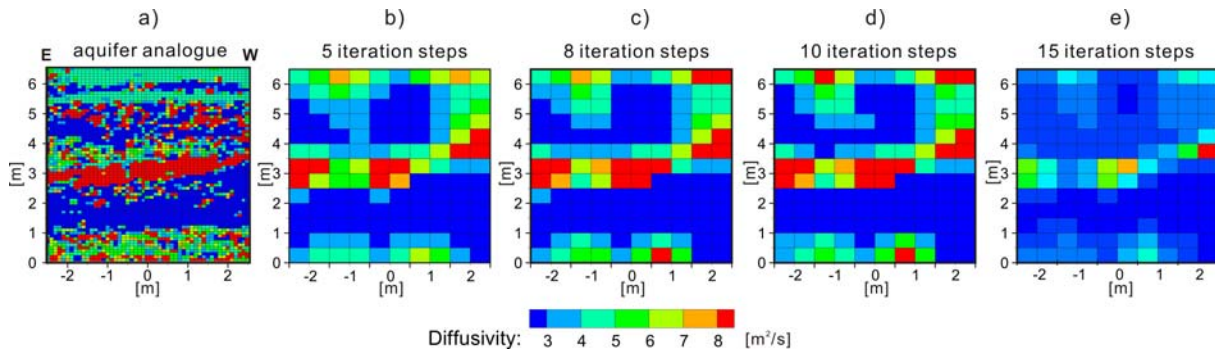
Figure 3.10: Diffusivity tomograms of profile W-E based on the inversion of peak time with different numbers of iterations. (a) The "true" profile from the aquifer analogue. (b)-(e) Inversion results of 5, 8, 10, and 15 iterations, respectively.

With respect to the reconstruction of the high-D zone in the middle of the aquifer and the low-D zone under it, the inversions of 8 and 10 iterations have the best results. In Figure 3.11, the overall residual $S^{0.5}$ (Equation 2.33) for 15 iteration steps of this 2D inversion in shown. The $S^{0.5}$ decreases in a quasi-exponential manner and fluctuates after 8 steps. Based on this fact, the following 2-D inversions are preferred to be conducted with 8 iteration steps and each inversion takes around 10 seconds on a 3.2 GHz Pentium CPU.
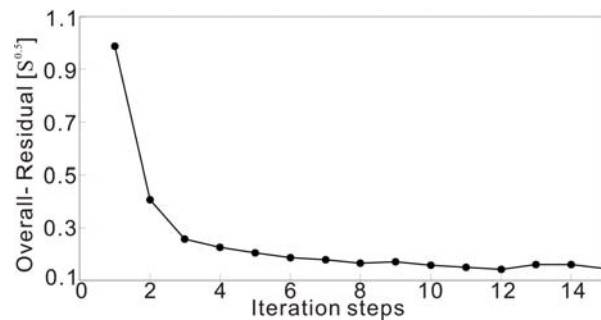
Figure 3.11: Overall residual for 15 iteration steps of a 2-D inversion of profile W-E.

Due to Fermat's principle, the hydraulic signal follows the fastest way between source and receiver. Thus, early travel times are more characteristic for the preferential flow paths. This results in a difference between tomograms based on inversions of different travel time diagnostics, with respect to the reconstruction of the high-D zone of the aquifer. In order to test this characteristic, the whole data set of profile W-E is used again to compare inversion results of different early travel time diagnostics.
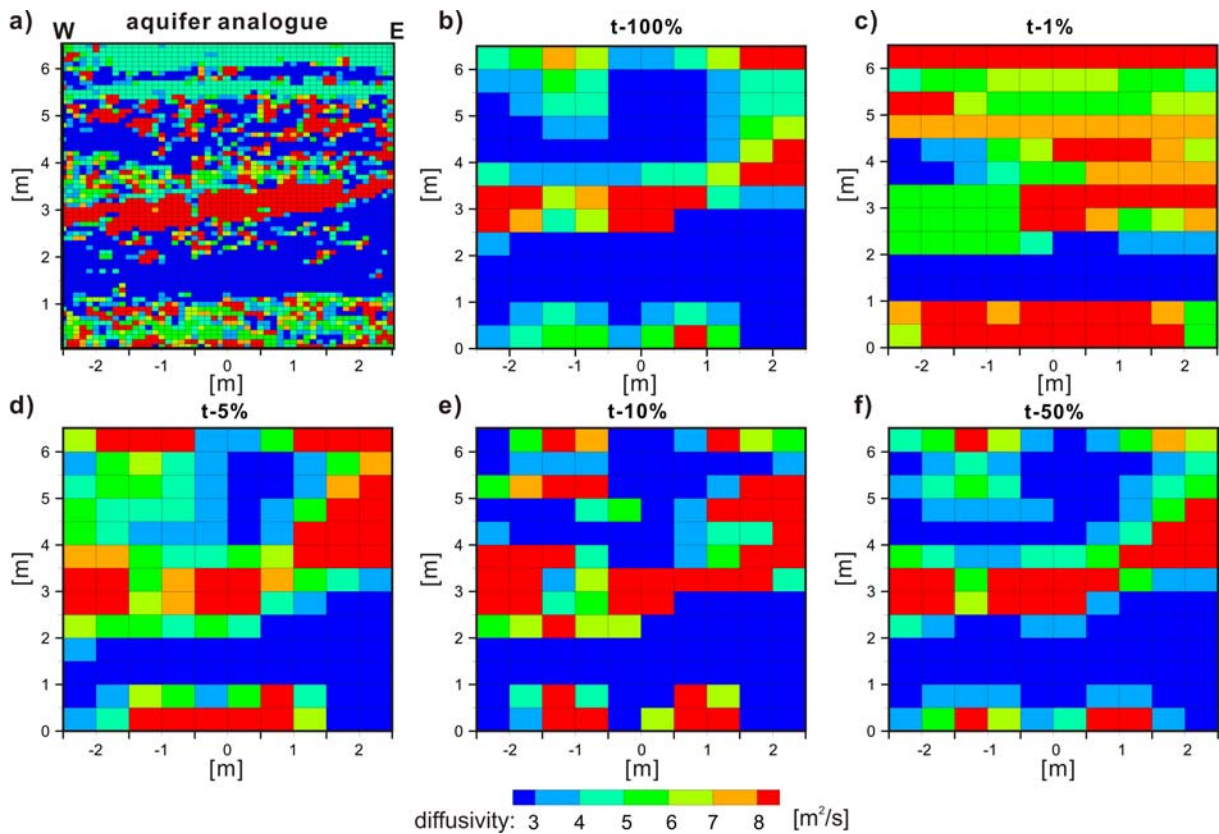
Figure 3.12: Comparison of inversions for the profile W-E with different early travel time diagnostics: (a) the "true" profile W-E of the aquifer analogue; (b)-(f) the inversions of t-peak (t-100%), t-1%, t-5%, t-10%, and t-50%, respectively.

As displayed in Figure 3.12, the inversion result of t-100% (t-peak) evaluates the aquifer as being more homogeneous. Due to the limitation of modelled time steps, insufficient travel time data was gained at the very early phase of pumping test (within 0.04 seconds after pumping). Hence, compared with the results of travel time diagnostic t-10% and t-50%, the results of travel time diagnostic t-1% and t-5% cannot reflect the "true" data of the aquifer analogue very well. The main structure of the aquifer analogue data, as well as the heterogeneity of the mixing layers of high- and low-diffusivities is reflected the best by the t-10% result. Hence, the travel time diagnostic t-10% is used to fulfill all inversions with different strategies.
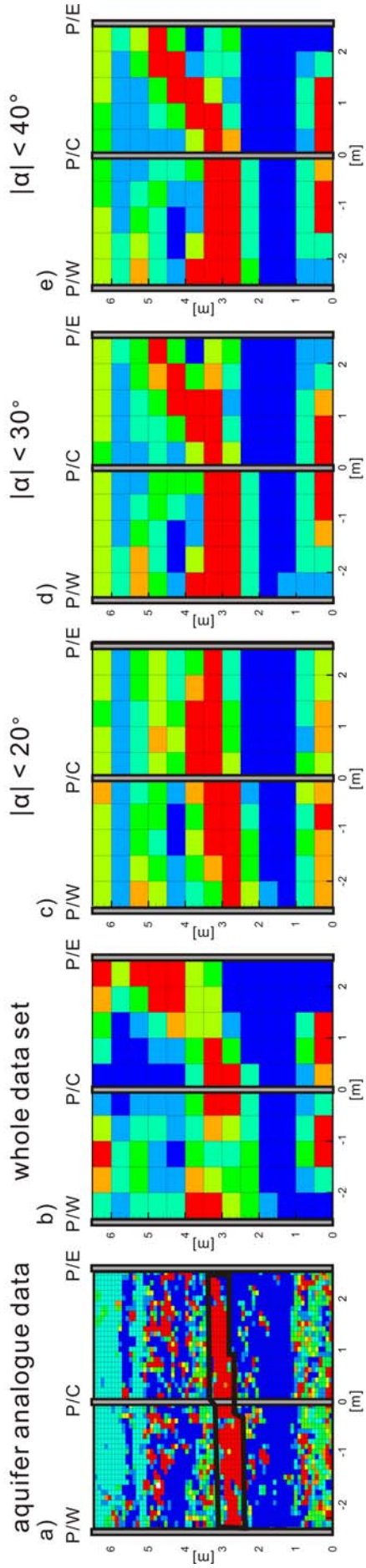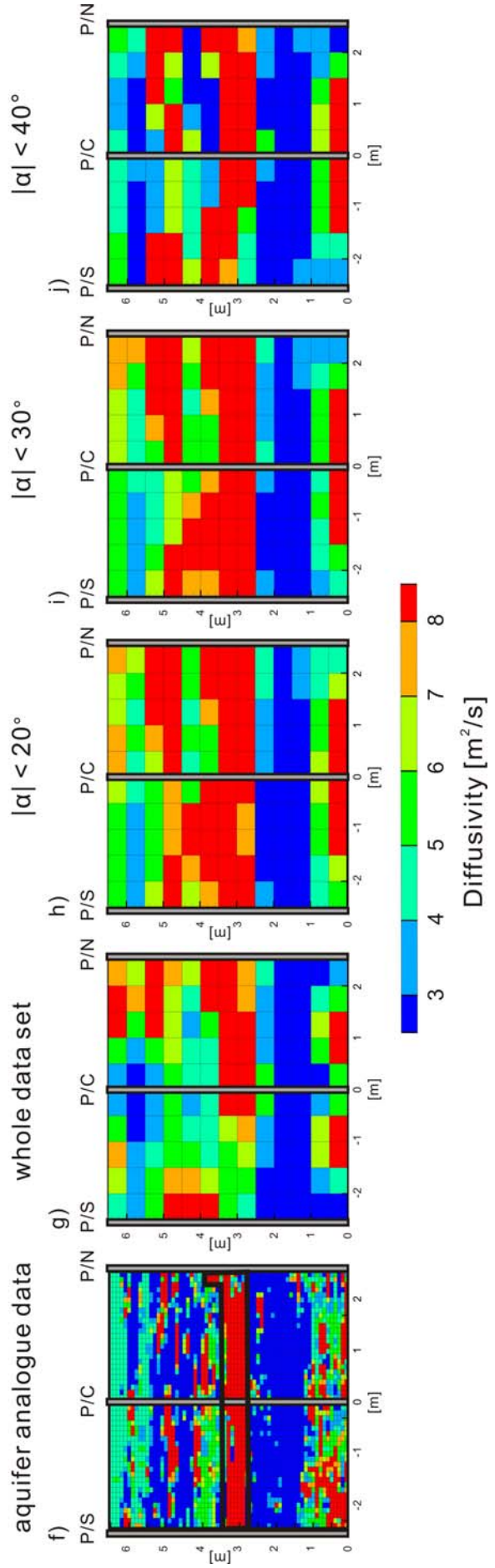
Figure 3.13: Comparison of the aquifer analogue data with the reconstructed diffusivity values: (a)-(e) profiles in West-East direction and (f)-(j) profiles in South-North direction.

43

Figures 3.13(b) and 3.13(g) display the obtained composite diffusivity tomograms, using the whole data set of travel times. Comparison with the "true" high resolution aquifer analogue data (Figure 3.13(a) and 3.13(f)) reveals that significant hydraulic features of the aquifer could be reconstructed. This means the comparatively coarse resolution of the tomograms can only reproduce a distorted image of those zones with small scale variability of the hydraulic parameters. However, they capture in particular the extensive and continuous portions such as the horizontal low-diffusivity zone in the lower half of the analogue. Even the high diffusivity zone in the center of both analogue sections (bold black lines in Figures 3.13(a) and 3.13(f)) is detected, especially in the S-N-tomogram. However the reconstruction of the laterally continuous high diffusivity zones in the middle of the aquifer, as well as of the low-diffusivitity zone close to the aquifer top, is still not satisfactory.

In order to improve the interpretation, travel time inversion based on specific data subsets in addition to the whole trial data set is suggested. As shown in Figure 3.13, the inversion results based on the trajectories with $|\alpha| < 20°$, $|\alpha| < 30°$ and $|\alpha| < 40°$ also reflect the main hydraulic significant features. Additionally, all these reconstructions indicate that the high permeability zone in the center of the S-N as well as of the W-E section is continuous. These results are in agreement with the findings of Brauchler et al. (2007), which demonstrated for a synthetic case that the resolution of horizontally arranged layers can strongly be improved using data subsets with small source-receiver angles. However, in the case of this study there is a risk that better characterization of horizontal features would occur at the expense of reconstructing vertical or inclined structures, since at some depths the aquifer analogue is also highly heterogeneous in the horizontal direction. As a compromise, the constraint on the source–receiver angle should not be too strict, and $|\alpha| < 40°$ is chosen for the subsequent full 3D inversion of the main data set.
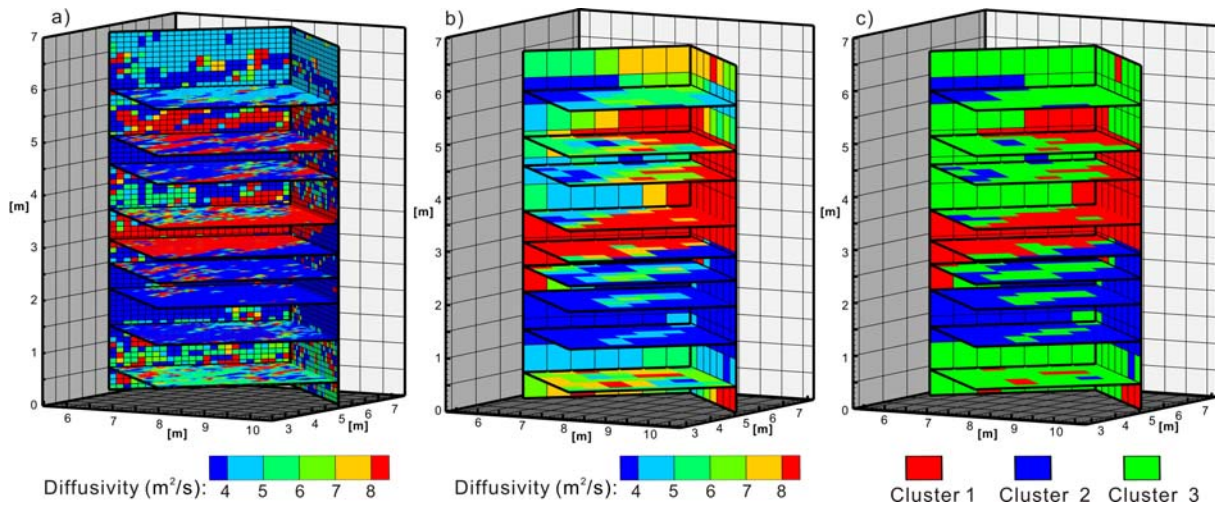
Figure 3.14: (a)-(b) Comparison of the aquifer analogue data with the three-dimensional diffusivity reconstruction. (c) Hydraulic zonation based on the result of the three dimensional hydraulic travel time inversion.

The 3-D inversion with the data subset of $|\alpha| < 40°$ yields tomograms of a resolution of 8 × 8 × 14 voxels. For this application, the procedure takes 10 seconds on a 3.3 GHz Pentium CPU. Comparison of the reconstructed diffusivity field (Figure 3.14(b)) with the "true" field (Figure 3.14(a)) shows that, at this resolution, significant hydraulic features can be reconstructed with adequate precision. The 3-D reconstruction appears to be of higher quality than the 2-D results illustrated in Figure 3.13. An apparent reason for these differences is that the simulated pressure pulses in fact propagate in three dimensions. The 2-D inversion of the pressure responses can hardly reflect 3-D processes and thus it is more approximate and can lead to ambiguous results.

3.2.3 Steady shape inversion

For the flow model of the following steady shape inversion, the zonation of equal hydraulic conductivity (Figure 3.14(c)) is defined based on the results of the 3-D hydraulic travel time inversion (Figure 3.14(b)). A principal advantage of the introduced zonation is its ability to overcome the shortcoming of the travel time based inversion approach to reconstruct discrete changes in hydraulic properties. The aquifer analogue data set, for example, exhibits that open framework gravel layers with a K value of approx. 10^{-2} m/s (some even of 1 m/s) are deposited next to sand-gravel mixtures with a K value of 5×10^{-5} m/s. Figure 3.14 (mainly at depth of 3~4 m) shows that travel time based inversion fails to reconstruct such discrete changes but reconstructs smoothed interfaces with continuously changing parameter distributions.

Three clusters of constant diffusivity values are distinguished. Note that in this study the clusters denote diffusivity classes (i.e. "facies"), whereas zones represent volume elements of the same diffusivity class. Due to the small number of clusters the derived model in Figure 3.14(c) consists of three zones, which are fewer than those of the high-resolution original. Though they are non-uniform, of different size and thus replicate the complex composition of the investigated medium, sediments with identical hydraulic properties (i.e. of the same hydrofacies) are deposited at different positions of the aquifer and are separated from each other.

The small number of clusters is chosen in accordance with the achievable resolution by the diffusivity tomogram, and it facilitates computationally efficient steady shape inversion. In further applications the distinction of clusters could be supported by geophysical measurements, borehole cores or logs. The clusters here are characterized as follows:

Cluster 1 represents the highest permeable zones in the center of the diffusivity tomogram, located between 3 m to 3.5 m and 4.5 to 5 m above aquifer analogue bottom. This domain is characterized mainly by matrix free gravel, which is indicated by diffusivity values larger than 8 m^2/s.

Cluster 2 covers the lowest permeable area located between 1 m to 3 m above the bottom directly below the high permeability zone represented by Cluster 1. A smaller section is located close to the top of the aquifer between 5.5 m to 6 m above bottom. Gravel sand mixtures dominate this cluster, leading to diffusivity values less than 4 m^2/s.

The domain close to the top and bottom of the aquifer analogue is represented by *Cluster 3*, which denotes intermediate diffusivity values. In the aquifer analogue, this area is mainly characterized as sand-rich / stone rich gravel, which is reflected by diffusivity values between 4 m^2/s and 8 m^2/s.

Outside of the center part of the model a constant K value of 2×10^{-3} m/s for the surrounding aquifer is assigned. Table 3.3 summarizes the starting values and the upper and lower bounds used for the steady shape inversion. The parameter estimation procedure required 127 model runs on a PC with a 3.33 GHz CPU, and each run of the steady shape model took about 25 seconds. The minimized root mean squared error (RMSE) from the calculated and observed head difference is 0.4 mm and the mean value of the 392 residuals between calculated and observed head differences is 4 mm.

46

Table 3.3: Initial parameters and value bounds used for the steady shape inversion.

Cluster No.	Diffusivity [m^2/s]	Hydraulic conductivity [m/s]		
		starting value	lower bound	upper bound
1	>8	1.0×10^{-4}	1.0×10^{-7}	1
2	<4	1.0×10^{-4}	1.0×10^{-7}	1
3	4~8	1.0×10^{-4}	1.0×10^{-7}	1

The correlation coefficient R for the calculated and measured head differences from the calibrated model is 0.8, which is considered acceptable keeping in mind the coarse resolution considered for the tomograms. Table 3.4 lists the estimated K values as well as the respective specific storage values for the three clusters. The specific storage values are calculated as the quotient of hydraulic conductivity over diffusivity. Additionally the arithmetic and harmonic means for the zones of the aquifer analogue are given. These means represent the upper and lower bound of the equivalent conductivity of an upscaled heterogeneous block, respectively (see e.g., Cardwell and Parsons 1945).

Table 3.4: Arithmetic means (arithm.) and harmonic means (harm.) as "true" values of hydraulic conductivity, specific storage, and diffusivity for the three clusters and the corresponding estimated (est.) values.

Cluster No.	Hydraulic conductivity [m/s]			Diffusivity [m^2/s]			Specific storage [m^{-1}]		
	arithm.	harm.	est.	arithm.	harm.	est.	arithm.	harm.	est.
1	3.0×10^{-2}	1.5×10^{-5}	1.7×10^{-2}	773	0.2	20	7.7×10^{-5}	9.2×10^{-5}	8.5×10^{-4}
2	1.3×10^{-4}	8.9×10^{-5}	1.6×10^{-4}	1.6	1.0	2.1	9.4×10^{-5}	9.0×10^{-5}	7.6×10^{-5}
3	3.4×10^{-4}	2.7×10^{-4}	4.0×10^{-4}	6.6	5.0	5.8	5.4×10^{-5}	5.3×10^{-5}	6.9×10^{-5}

The comparison between the K values derived from the steady shape inversion with the mean true value ranges show a good agreement for all of the three clusters. The estimated vales tend to be closer to the arithmetic mean. This reflects the mostly horizontal orientation of the sedimentary structures, in small angle with the direction of the inspected trajectories. The diffusivity and derived specific storage values also lie in or close to the expected value ranges except for *Cluster 1*, which represents the high-D zone. Apparently, the travel time inversion approach is not able to reconstruct the full range of diffusivity within *Cluster 1*. Figure 3.15 shows a histogram of the diffusivity distribution of this cluster. The diffusivity values range from 10^{-1} to 3×10^4 m^2/s with an arithmetic mean of 773 m^2/s, whereby the reconstructed diffusivity values

range from 8 to 200 m^2/s with an arithmetic mean of 20 m^2/s. The reason for these differences is the strong heterogeneous composition of the outcrop analogue data. The stone rich gravel (matrix free hydrofacies cGcg,o in Table 3.1) characterized by diffusivity values between 2×10^4 and 3×10^4 m^2/s is not arranged in a horizontal layer but is distributed in small clusters.
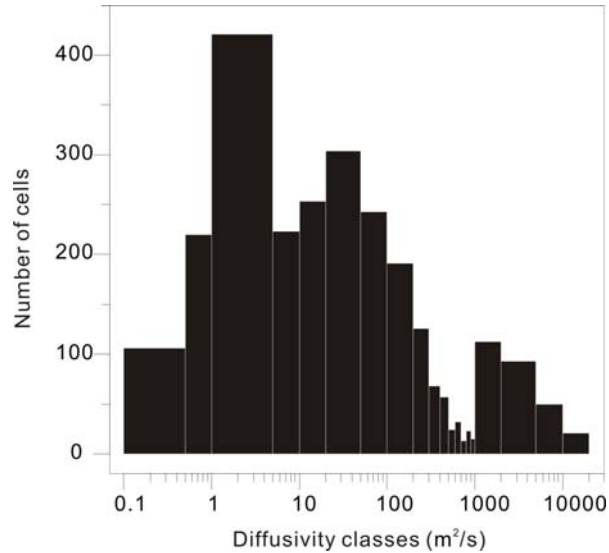
Figure 3.15: Histogram of the diffusivity distribution of Cluster 1, representing the high-diffusivity zone in the center of the aquifer analogue data set.

Numerical and experimental studies performed by Vasco et al. (2000) and Brauchler et al. (2007) have shown that parameter variations of several orders of magnitude can be reconstructed. However, for the transformation of the diffusivity equation into the eikonal equation a hydraulic parameter distribution is assumed, which varies smoothly with respect to the spatial wavelength of the propagation of the pressure pulse. Therefore, the small clusters of stone rich gravel characterized by extremely high diffusivity values cannot be reconstructed. Nevertheless, the good agreement between the reconstructed and true hydraulic conductivity values, representing the most significant hydraulic properties, shows the potential of the coupled inversion approach to characterize hydraulic properties of the subsurface with high resolution.

3.3 Potential development

The resolution and accuracy of the travel time-based inversion strongly depends on the number of the travel times that can be inverted, i.e. the number of source-receiver combinations. In order to test the potential of this travel time based inversion

technique, pumping tests with large numbers of observation points are also simulated. Taking the profile W-E again as an example, a series of 14 pumping tests are simulated, with the well P/C as the pumping well. During each test, the water is pumped out of a 50 cm interval from the well P/C, which is the same as for the pumping tests for the trial data set for the inversion in Chapter 3.1.3. At this time in the observation wells P/W and P/E, the pressure changes are recorded for each 10 centimeters over a depth of 7 meters, which forms a dense net of 1960 source-receiver combinations.
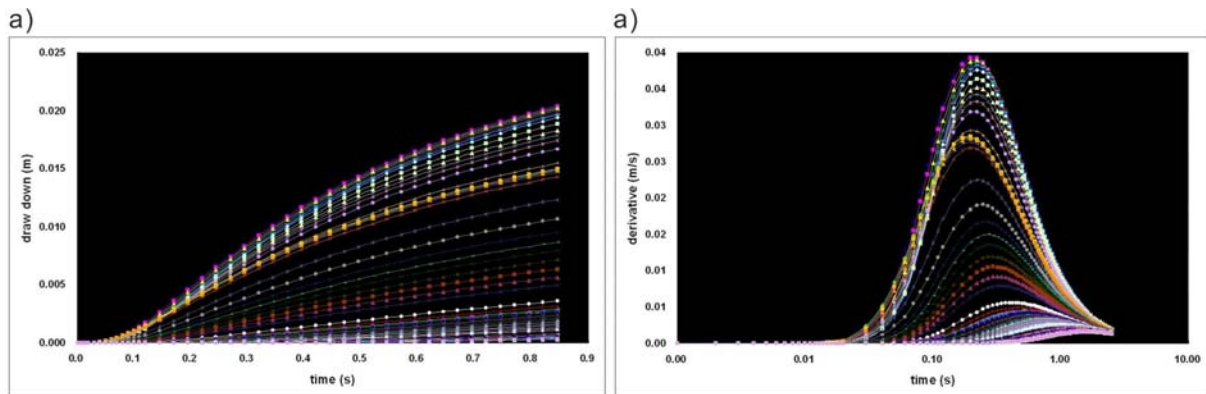
Figure 3.16: (a) Drawdown curves recorded in the observation well P/W (pumping interval: P/C, 1.0-1.5m under aquifer top). (b) Corresponding first derivatives of drawdown curves in (a).

As an example, Figure 3.16(a) shows the drawdown curves recorded in the observation well P/W from receivers located in different depths during one of the pumping tests (pumping interval: 1.0-1.5 m under aquifer top from the well P/C). The first derivation of the drawdown curves with a logarithmic time scale clearly show the curves with different peak times, representing each corresponding receivers in different depths (Figure 3.16(b)). Each minor difference between the travel times is recognizable and characteristic for the heterogeneity of the aquifer. Hence, this large amount of different travel times can significantly enhance the uniqueness of the inversion.

With the same strategy, which derives from the inversion results based on the trial data set in Chapter 3.2.2, i.e. the inversion using an early travel time diagnostic of t-10% and the selected data subset, a new diffusivity tomogram is reconstructed and shown in the Figure 3.17(b).

Same as for the 2-D inversion, for the 3-D travel time inversion one can also achieve a higher resolution result, benefiting from the larger amount of source-receiver combinations (also 70 observation points in every observation well over the 7 meter depth). A 3-D interpolation of the diffusivity reconstruction with *D* value iso-

surfaces is demonstrated in Figure 3.17(d). With this interpolation of high resolution, even the small embedded element, e.g. the low-D area at approx. 5.5 m from the aquifer bottom, can be detected.

diffusivity: 3 4 5 6 7 8 9 10 [m²/s]
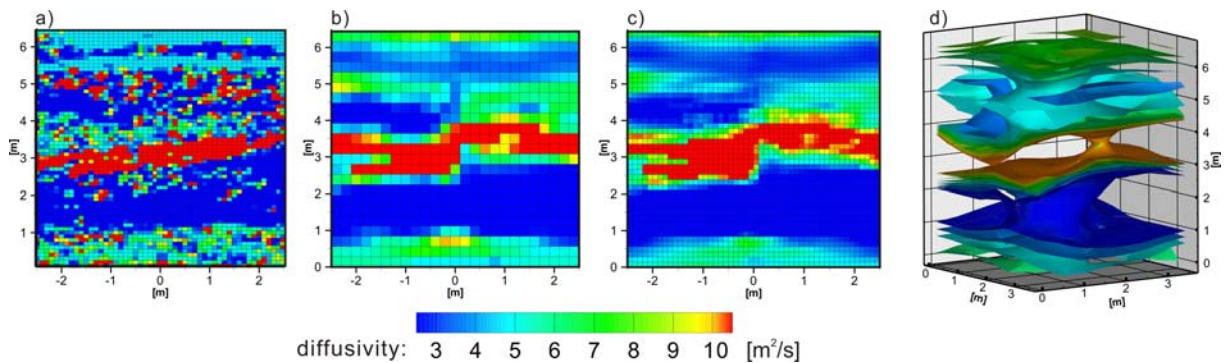
Figure 3.17: (a) The "true" profile W-E of the aquifer analogue. (b) Inversion result with 140 (70×2) receivers. (c) Further development of the inversion with the staggered grids technique.

With the application of the staggered grid approach introduced in Chapter 2.4.2, the reconstruction result is shown in Figure 3.17(c). As a result, the final grid is composed of 2500 cells, 50 in the horizontal direction and 50 in the vertical direction in comparison to the original grid, which consisted of 625 cells (25 in horizontal direction and 25 in vertical direction). Comparison between the tomograms shows that the method of staggered grids leads to an increase in the nominal resolution. In particular, the dilution effects at the boundary between the low permeability zone and the homogeneous background could be strongly reduced.

With the application of the staggered grid approach, the resolution of this diffusivity reconstruction is successfully enhanced to 10 cm × 14 cm. With this resolution, even the distribution of high-diffusivity elements inside the zone of lower diffusivity is reconstructed. Thousands of travel times gained from the synthetic data do not cause any calculation problems and the inversion needs only a few seconds on the computer.

However, without question, in the field application it is really time-consuming to get such a great amount of travel time information. Nevertheless, for certain engineering purposes the potential of travel time based inversion offers us the possibility, to reconstruct the subsurface with high resolution and accuracy, which is significant for environmental engineering purposes, e.g. to develop transport models for groundwater remediation with the increased concern regarding groundwater contamination.

4   FIELD ASSESSMENT

The potential of the introduced approach coupling hydraulic travel time and steady shape inversion, which has been numerically developed, was then applied to hydraulic tomographic field measurements performed at the experimental test site "Stegemühle," which consists of a network of 26 wells comprising 1", 2" and 6" as well as multi-chamber wells. In addition to the method of S_s estimates obtained with the coupled inversion approach (based on the relationship $S_s = K / D$) introduced in Chapter 3 for the numerical study based on an aquifer analogue, the S_s estimates in the field were also verified with the direct results of hydraulic attenuation inversion. The final parameter (K, D and S_s) estimates were compared to those obtained over similar vertical intervals using a variety of other approaches and the results from a great deal of previous work, such as geophysical measurements, grain size analysis, slug tests, pumping tests, and tracer tests.

4.1   The test site

The test site is located in the Leine River valley in the south of Göttingen, Germany (Figure 4.1). This test site is part of the water protection area of Stegemühle waterworks which is organized by Stadtwerke Göttingen AG, the local Göttingen water supplier. The test site terrain (approx. 110 m x 95 m) is bounded to the west by the River Leine and to the east by the Channel Mühlengraben. There is a barrage at the southern tip of the test site where the Channel Mühlengraben separates from the River Leine, with approx. 2~3 m difference in water level. Due to this head difference, the ground water of this test area is assumed to have a general flow direction from Southeast (the channel) to Northwest (the river) (Figure 4.3).
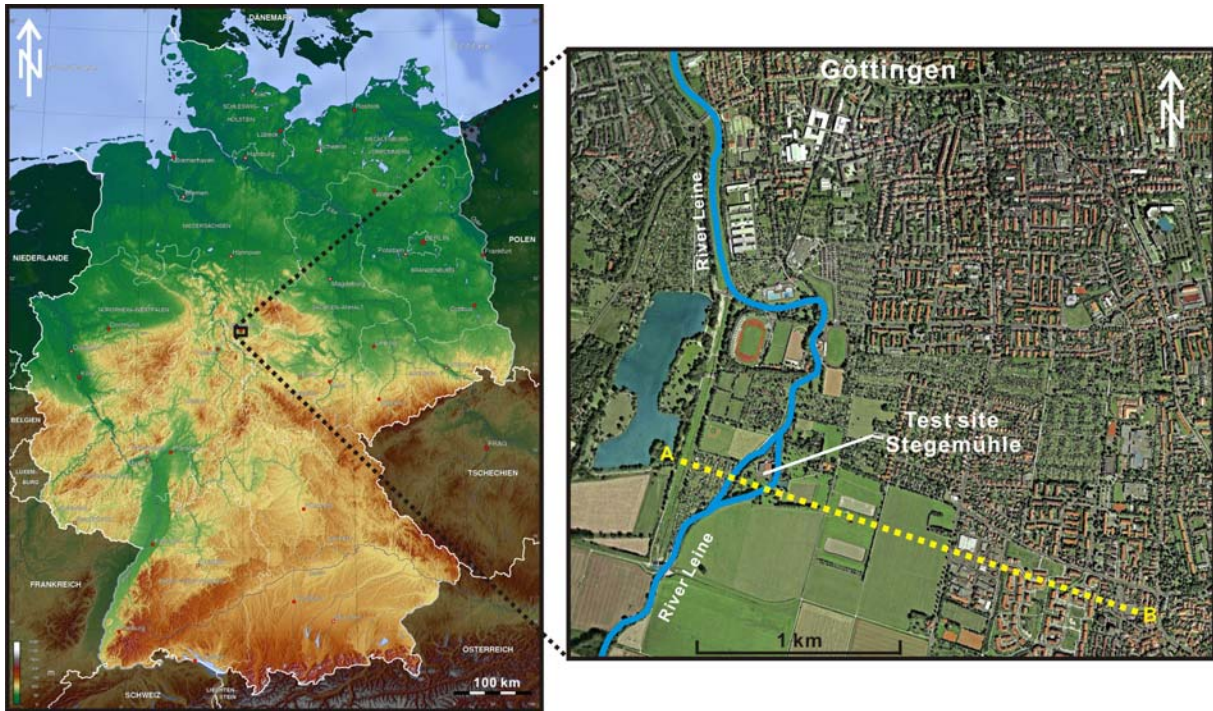
Figure 4.1: The location map of the test site Stegemühle. Source of topographic map: http://de.wikipedia.org (2006). Source of satellite image: Google Earth (2011).

Preliminary studies (e.g. Schlie, 1989) on the hydrogeology of Stegemühle have shown that the pore water from the River Leine's Pleistocene gravels is delivered through this waterworks but these studies were not focused on the exact test site area (Figure 4.2). Thus, only rough information about the hydrogeological situation inside the test site area was known.
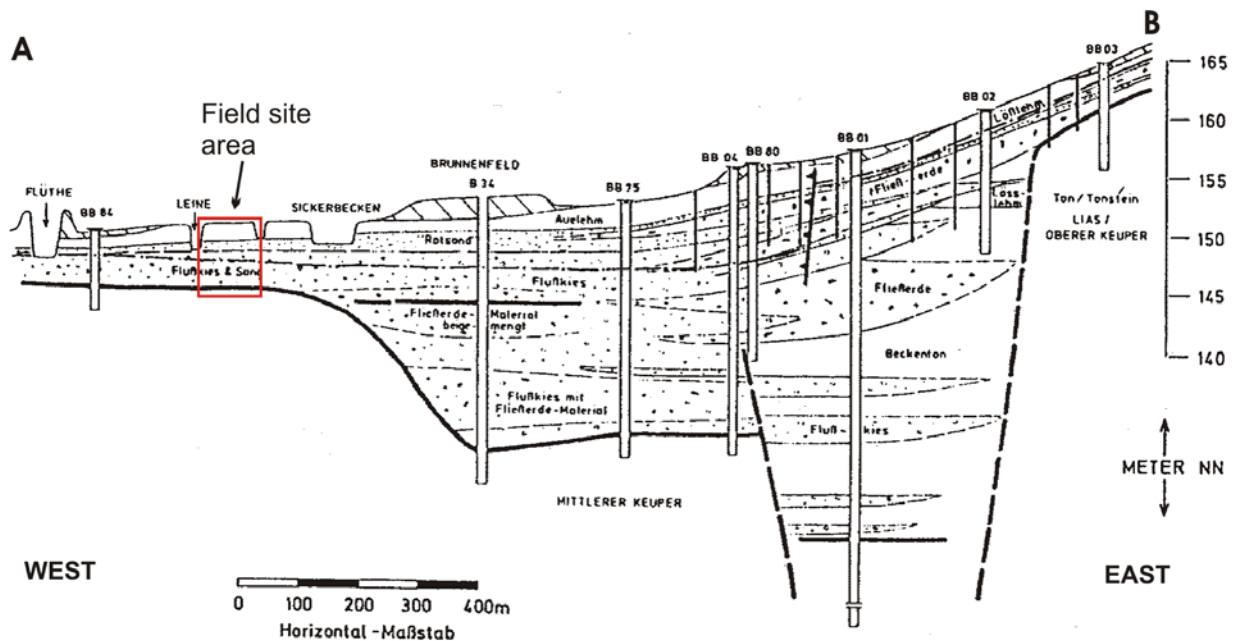
Figure 4.2: W-E cross-section of the Leine River Vally in the South of Göttingen. The position of the cross section A-B is shown in Figure 4.1 (Schlie, 1989).

For the intended further hydrogeological research work, the test site Stegemühle was first constructed in 2007 (Hu, 2007 and Vogt, 2007). Five 1", eleven 2", and three 6" observation wells were constructed in order to facilitate hydrogeological field investigations under controlled natural conditions. In 2009, seven new wells were constructed at this test site. Two of them are 2" wells and five of them are multi-chamber wells, installed with the intention that they may provide a better monitoring network for field work, involving advanced characterization techniques such as tracer tests and hydraulic tomography. All twenty-three 1", 2", and multi-chamber wells were installed using direct-push technology (e.g. Dietrich and Leven, 2006). For each of these wells, a 3.25" probe rod was driven through the alluvial clay and the Leine gravels into the Keuper silt and clay stones by the DP Geoprobe® machine. Afterwards, the pipes were put into the rods. At the lower end of these rods an expendable drive point had been positioned, which remained in the Keuper stones after the rods were pulled out of the ground. The pipes of the 1" and 2" wells consist of HDPE and the screen pipes are laterally slotted (0.3 mm slot width). By retracting the drive rods, the formation was allowed to collapse back against the HDPE pipes. All well screens are completely in the saturated zone. The three 6" wells were installed by means of dynamic pipe ramming. For the well construction, the bore hole was expanded with a 325 mm auger. Subsequently the HDPE tubes were installed with an outer diameter of 180 mm. The screen pipes are vertically slotted (0.3 mm slot width) and fully penetrate the aquifer. As for the 1" and 2" wells, the remaining space between well pipe and borehole was filled up with filter gravel pack (2.0 mm ~ 3.15 mm particle size) and clay pellets. Different from the filter medium of the 1" and 2" wells, Geotextile clay seal rings (OD 280 mm x ID 180 mm) were placed additionally within the filter gravels for the 6" wells. The clay seal rings have a vertical distance of approx. 50 cm and can reduce vertical flow in the filter gravel during hydraulic aquifer tests (e.g. flowmeter-test) or multilevel-sampling (Ptak and Teutsch, 1994).
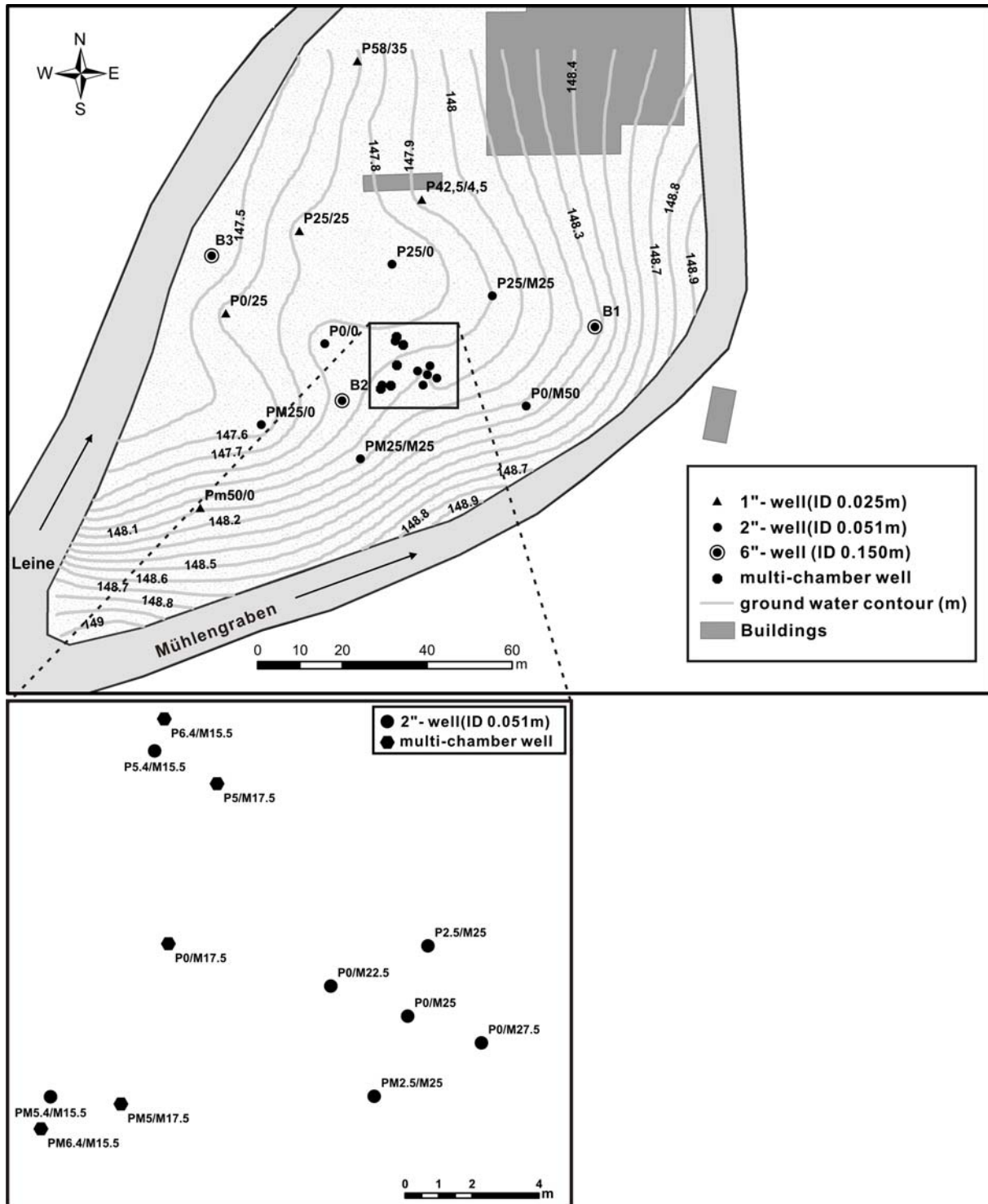
Figure 4.3: Map of the installed well network at the test site Stegemühle with enlarged investigation area of this study and related studies.

The subsurface of the unconsolidated river sediments (approx. 7 meters thick) was characterized with a variety of different approaches, such as soil core samplings, grain size analysis, direct-push electrical conductivity logging, and borehole Gamma-ray logging. Note the direct-push electrical conductivity logging, termed in the following DP-EC logging (e.g. Christy et al., 1994; Schulmeister et al., 2003) is performed

54

prior to well installation, which allows the determination of the aquifer bottom by penetrating the first few centimeters of the bedrock. Borehole Gamma-ray logging is performed inside each well and cannot be used to gain information on the aquifer bottom material. In the following, current characterization results based on these methods, as well as the preliminary work from Hu (2007) and Vogt (2007) are summarized.

For the geological characterization, soil cores of the subsurface were taken during the drilling process and grain size analyses were performed (see Chapter 4.2.2) on the soil cores. The soil cores and the grain size analyses show that the aquifer has a thickness of 1.0~3.3 meters and consists of a sequence of the River Leine's Weichselian Age gravels. The aquifer has an average saturated thickness of approximately 2.0 m, overlain by 1.9~4.5 m of silty to fine sandy alluvial clay and underlain by a hydraulically tight silt and mudstone formation of Triassic bedrock (Middle Keuper Age). The aquifer material is classified as sandy to pure gravel with very low silt and clay content. According to the geological interpretation based on the soil cores and the grain size analyses, the sedimentation regime is defined as a braided river system. Therefore, a vertical stratigraphical differentiation of the gravels is considered to be unlikely (Vogt, 2007).

With the geophysical investigation methods such as DP-EC logging and borehole gamma-ray logging, reliable information about the subsurface composition can also be provided. Hence, they are additionally performed to characterize the shallow subsurface, especially for the determination of aquifer top and bottom. The DP EC logging produces sharp, continuous profiles and allows a vertical differentiation of the alluvial clay. In contrast to the EC logs, the Gamma-ray logs show lithological boundaries more gradually, but also reflect the general subsurface composition. The patterns of the two logs are correlated with the geological profiles and are considered as important complementary information about the subsurface. For example, at some lithological boundaries, some of the soil cores were compacted during ramming (e.g. well P0/M17.5 Figure 4.4). The elevation of those boundaries can be provided through EC or Gamma-ray logs. Note that the gravel-bedrock boundary indicated by the logs is generally several cm lower than the boundary determined through soil cores. All recorded logs and groundwater level measurements show similar subsurface structure with variable thicknesses of the confining unit (silt and clay layers) and

the aquifer material (sand and gravel). Within the aquifer, no correlations between local heterogeneities are obvious (Hu, 2007; Vogt, 2007).

Groundwater level measurements indicate that due to differences in water table (approx. 2~3 m with seasonal fluctuation) between the River Leine and Channel Mühlengraben, a complex groundwater flow system is produced. The receiving streams from the channel cause a decreasing groundwater level from the channel to the river. The gradient (5~7%) in close proximity to the channel is much larger than the gradient (0.3~0.7 %) in close proximity to the river (see groundwater contours in Figure 4.3).

Based upon the investigations described above, further aquifer characterization based on numerous traditional hydraulic tests as well as hydraulic tomographical research work were carried at this test site (e.g. Hu, 2007; Vogt, 2007; Brauchler et al., 2007; Möck, 2009; Brauchler et al., 2010; Brauchler et al., 2011). All investigations indicate that, on average, the aquifer is approximately 2 m thick, highly conductible (with averaged hydraulic conductivity of 5.0×10^{-4} m/s from pumping tests), and behaves as a confined system (see also Figure 4.4).

4.2 Traditional aquifer characterization

In this study, different hydraulic tests such as pumping tests, slug tests, and tracer tests are performed to characterize the aquifer. These tests are evaluated with analytical solutions and compared with respect to spatial resolution of the hydraulic parameters. The results of these traditional methods, combined with the information gained from grain size analysis, DP-EC, and Gamma-Ray logging, serve as prior information for the aquifer reconstruction based on the hydraulic tomographical approach. In the following, these traditional methods with their relevant results and interpretations are introduced.

4.2.1 The structure of the subsurface

For the aquifer characterization, the determination of the structural geometry of the subsurface, in particular the definition of the aquifer top and bottom is the most important prior information to the hydraulic tests.

The geological information gained from the relevant soil samples (Figure 4.4), combined with DP-EC logs and Gamma-Ray logs, shows the interpreted subsurface profile between Well P0/25 and P0/M50. As displayed in Figure 4.4, the subsurface

consists of a silt and clay layer (approx. 3.5 m thick) overlying the aquifer layer of sand and gravel (2~3 m thick). Under the aquifer is the bedrock, which consists of Triassic (Middle Keuper) silt and clay stones.
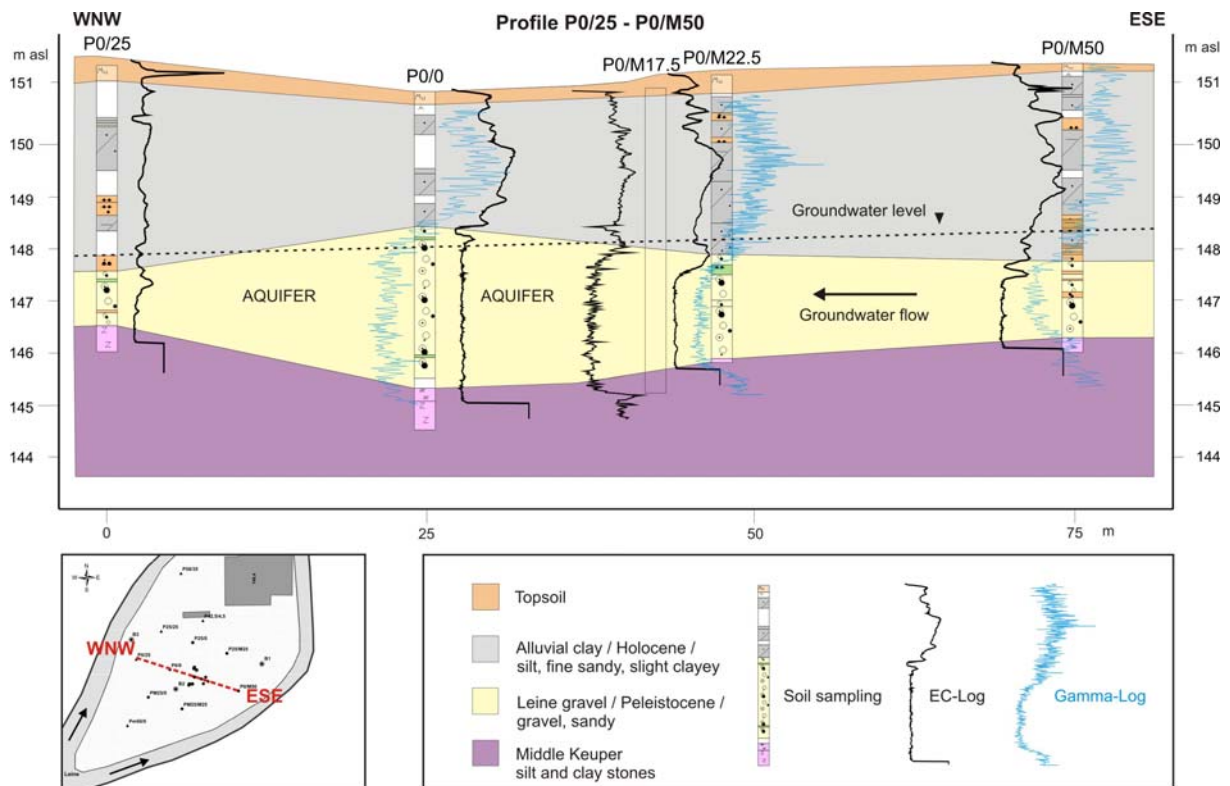
Figure 4.4: Subsurface profile between well P0/25 and P0/M50 with geological and geophysical information. Note the DP-EC logs are recorded at a distance of one meter from the wells, while the borehole Gamma-ray loggings are performed inside each well.

Based on the detailed information gained, the main investigation area for hydraulic tests (zoomed area in Figure 4.3) is chosen to be centered around well P0/M25 with four wells each located at a distance of 2.5 m to it (in the following termed five-point star area) and four multi-chamber wells at a distance of 9~11.5 m to it. In this area, aquifer thickness is sufficiently even at approx. 2 m and average hydraulic conductivity is 5.0×10^{-4} m/s (Hu, 2007). In the five-point star area, multi-level single-well and cross-well slug tests as well as pumping tests (fully penetrating) were carried out. For the investigation area outside the five-point star area, pumping tests with tomographical configuration were performed. In this case, P0/M25 was the pumping well and wells PM6.4/M15.5, P6.4/M15.5, PM5/M17.5 and P5/M17.5 were the observation wells. As an example, the subsurface profile between well P0/M25 and PM6.4/M15.5 is shown in Figure 4.7.

Recorded gamma ray and DP-EC logging data on the subsurface was further interpolated for the high resolution structural characterization and horizontal changes in lithology were able to be visualised as is illustrated in Figure 4.5.
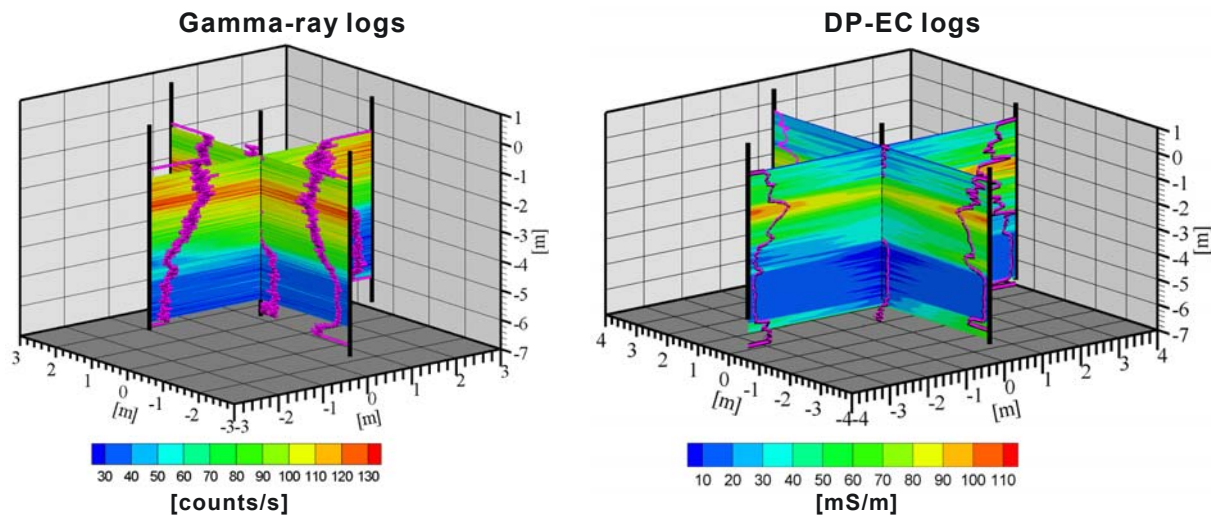
Figure 4.5: Interpolated images of the gamma ray and direct-push electrical conductivity logs. Note the distance between the DP-EC logs is 3.5 m in comparison to the 2.5 m of the gamma ray logs (Brauchler et al, 2010).

The five DP-EC and Gamma-ray logs have the same pattern as the logs recorded for the well P0/M22.5 illustrated in Figure 4.4, meaning that the high values of the logs in the upper 3.5 m of the subsurface represent the confining layer of silt and clay and the lower values of 3.5~6 m indicate the spatial position of the confined aquifer layer of sand and gravel. The interpolation between the logs demonstrates that the horizontal changes of the aquifer top and bottom do not exceed 0.5 meters (Brauchler et al., 2010). Note the DP-EC logs are recorded at a distance of one meter from the wells.

4.2.2 Grain size analysis

The samples for the grain size analysis are only taken from the aquifer material and are obtained by continuous dynamic penetration coring. All core samples (38 mm Ø) are portioned into 11 grain size fractions with dry sieving. The sieving is performed with a vibration-sieving machine (Company Retsch), a wire texture sieve set (Company Retsch, DIN ISO 3310-1, mesh sizes of 0.063, 0.125, 0.25, 0.5, 1, 2 mm) and a quadrate-hole sieve set (Company Geotechnik Hannover, DIN-ISO 3310-2, mesh sizes of 4, 8, 16, 31.5 and 63 mm).

In order to get a complete grain size distribution of the aquifer material, the dried and homogenized fine fractions of grains (<0.063 mm) are analyzed by a Laser Diffraction Particle Size Analyzer (Company Beckmann Coulter, type LS13320). This laser diffraction method is able to analyze a size range from 0.4 μm to 2000 μm.

Consequently, the statistical distribution of the grain size fractions can be illustrated through a grading curve, from which the non-uniform degree U of the soil can be obtained:

$$U = \frac{d_{60}}{d_{10}}$$

<div align="right">**Eq. 4.1**</div>

With the cumulative grading curve, the undirected hydraulic conductivity (K) of each sample can be determined by the empirical relationship after Hazen (1893). According to Hazen (1893) the hydraulic conductivity of sandy soils is determined in m/s as follows:

$$K = 0.0116 \times (d_{10}[mm])^2 \;, \quad for \quad U \leq 5 \,.$$

<div align="right">**Eq. 4.2**</div>

The value d_{10} is termed "effective grain size" because the finest 10% of the complete material is the main factor for the hydraulic conductivity of unconsolidated sediments.

In the Figure 4.6, the K values at the wells within the five-point star area and the well PM5.4/M15.5 are plotted against the depth.
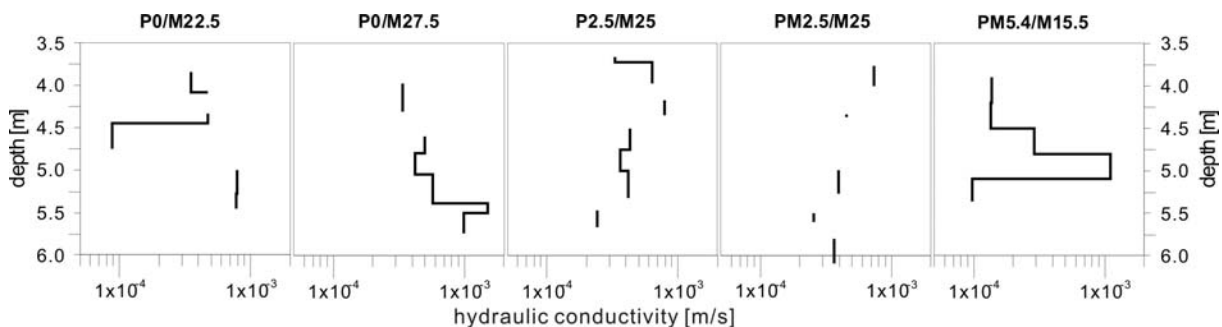
Figure 4.6: *K* values estimated by grain size analysis in the five-point star area and well PM5.4/M15.5.

With respect to aquifer characterization, this method has the disadvantage that the results from different analyses are only meaningful for different small volumes of the aquifer. Hence, an interpretation of the results based on the statistic data of the K values estimated through the grain size analysis is shown in the following table.

Table 4.1: Statistical data of the *K* values (m/s) from grain size analyses within the five-point star area and at the well PM5.4/M 15.5 after Hazen (1893).

Sampling well	Number of samples	Minimum	Maximum	Mean	Variance [(m/s)^2]
P0/M22.5	6	8.79×10^{-05}	7.84×10^{-04}	4.94×10^{-04}	8.79×10^{-08}
P0/M27.5	7	3.39×10^{-04}	1.51×10^{-03}	7.23×10^{-04}	2.00×10^{-07}
P2.5/M25	8	2.43×10^{-04}	7.92×10^{-04}	4.58×10^{-04}	3.66×10^{-08}
PM2.5/M25	5	2.57×10^{-04}	7.40×10^{-04}	4.43×10^{-04}	3.28×10^{-08}
PM5.4M/15.5	10	9.70×10^{-05}	1.11×10^{-03}	3.53×10^{-04}	1.47×10^{-07}
Sum/Mean	36	2.05×10^{-04}	9.87×10^{-04}	4.94×10^{-04}	1.01×10^{-07}

For the information provided through the grain size analyses in the other parts of the test site area, I also represent the statistic data of 67 grain size analysis from Hu (2007), in order to show the general view about the *K* values of this area.

Table 4.2: Statistical data of the *K* values (m/s) of 67 samples from the whole test site (Hu 2007).

Sampling well	Number of samples	Minimum	Maximum	Mean	Variance [(m/s)^2]
P0/0	10	6.77×10^{-05}	8.82×10^{-04}	3.62×10^{-04}	6.97×10^{-08}
P0/M50	9	1.62×10^{-04}	8.46×10^{-04}	5.51×10^{-04}	5.37×10^{-08}
P25/25	3	1.92×10^{-04}	4.96×10^{-04}	3.44×10^{-04}	4.62×10^{-08}
P25/M25	9	1.57×10^{-04}	1.00×10^{-03}	5.28×10^{-04}	9.45×10^{-08}
P42.5/4.5	9	2.76×10^{-04}	1.03×10^{-03}	5.80×10^{-04}	4.81×10^{-08}
PM25/0	10	4.88×10^{-05}	1.15×10^{-03}	5.23×10^{-04}	1.45×10^{-07}
PM25/M25	8	1.12×10^{-04}	3.56×10^{-04}	2.05×10^{-04}	1.05×10^{-08}
PM50/0	1	3.39×10^{-04}	3.39×10^{-05}	3.39×10^{-06}	-
P58/35	5	4.60×10^{-05}	8.85×10^{-04}	5.30×10^{-04}	1.21×10^{-07}
B1	1	2.80×10^{-04}	2.80×10^{-04}	2.80×10^{-04}	-
B2	1	4.15×10^{-04}	4.15×10^{-04}	4.15×10^{-04}	-
B3	1	1.27×10^{-03}	1.27×10^{-03}	1.27×10^{-03}	-
Sum/Mean	67	2.75×10^{-04}	7.83×10^{-04}	5.08×10^{-04}	7.36×10^{-08}

Table 4.1 and 4.2 show that the aquifer has an averaged hydraulic conductivity of approximately 5.04×10^{-4} m/s. This indicates a highly conductive aquifer derived from a braided-river system. Sandy gravel dominates the aquifer whereas the silt and clay content is very low.

Although the grain size analyses show a variation of hydraulic conductivity from 4.6×10^{-5} to 1.5×10^{-3} m/s, the aquifer cannot be simply divided into different continuous hydraulic horizons. This is because every K estimate is only representative of the points where the respective samples are taken from. Samples from varying depths in a single borehole show K value variations in the vertical direction, which indicate the presence of small sandy or gravel zones. These zones are not necessarily related with similar zones at other boreholes. Therefore, the results from grain size analyses only serve as complementary information for the aquifer characterization. In Chapter 4.2.6, the K values determined by the grain size analyses are compared with other results from hydraulic test such as slug tests and pumping tests.

4.2.3 Pumping tests

For more than a century, pumping tests have successfully been relied upon for diagnosing aquifer characteristics based on the evaluation of aquifer response data. These tests are commonly performed by pumping water out of a well while measuring the changes in water level (drawdown) in this well or, if present, in nearby observation wells (Butler, 1998). The drawdown can be analyzed using various models to obtain estimates of the aquifer parameters, which characterize the transmissive and storage characteristics of the aquifer (Butler, 2008) and the flow system boundaries. Note that in this work, all of the pumping tests performed at the test site are constant-rate pumping tests.

Conventional pumping tests

In this work, conventional pumping tests with fully penetrating wells were performed at first, irrespective of vertical variation of hydraulic parameters. Hydraulic parameters were determined by matching the measured time-drawdown curves with known type curves of appropriate models or solutions to the groundwater flow equation. The solutions for the type curves require several assumptions e.g. unsteady flow, which is horizontal when the pumping well is fully penetrating and the aquifer is homogenous and isotropic with uniform thickness and infinite areal extent. The water is assumed to be released instantaneously from storage with decline of hydraulic head. Heterogeneous natural conditions in this aquifer do exist and therefore the assumptions which are being made are being implemented with the awareness that simplifications are the result. Groundwater penetrates through fully screened wells and the system is stressed over the entire depth of the aquifer, resulting in depth-averaged

drawdown measurements. K and S_s are therefore average values for the saturated aquifer thickness over the sphere of influence of the pumping well. The aquifer parameters are representative of a much larger volume than the small-scale methods such as grain size analysis and slug tests described above (Ptak et al., 1996).

Conventional pumping tests are classified as a direct field method for local to regional three-dimensional determination of hydraulic conductivity (Hofmann et al., 1991). When treated as the first step in aquifer investigation, the conventional pumping test can provide information of great practical value about the average hydraulic parameters over the whole investigation area and the boundaries of the flow system, which is essential for design of other more advanced hydraulic tests.

As the first hydraulic tests, two short pumping tests were performed, conforming to DVGW worksheet W 111. Pumping Test (1): In the five-point star area, the 2" well P0/M25 served as the pumping well, which is surrounded by the adjacent four observation wells. Pumping Test (2): The 6" well B2 was the pumping well and P0/M22.5, which is 18.7 meters away from B2, serves as the observation well. For both pumping tests, the pumping period was 60 minutes with a minimum recovery of half the pumping period. Groundwater removal was performed with a Grundfos® underwater pump MP1 (max. discharge flow of 2.5 m³/h, 230V, inner well diameter min. 5 cm), whose pumping rate was determined with a Woltmann meter (WP H 4000, DN 80, measurement range 0.3-200 m³/h). During both tests, the pumping rates in the wells P0/M25 and B2 were constant and adjusted to 0.175 and 0.59 l/s, respectively, in order to keep the aquifer under confined condition throughout the tests. The extracted water was drained off over PVC-fabric-hoses (Ø 20 mm) directly into the receiving stream. The relative drawdown and recovery in the pumping and observation wells were recorded with a small diameter pressure transducer (PDCR 35/D-8070) connected to a data logger (Campbell Scientific® CR 1000). The head data during the tests were monitored simultaneously and saved on a field laptop.

All data series (each with drawdown and recovery times for every pumping and observation well) were analyzed with the software Aqtesolv. All solutions used in this work, if not mentioned, are described in detail by Kruseman and De Ridder (1994). The initial saturated aquifer thickness was taken from the observation well to avoid problems with solutions offered by Aqtesolv.

After Cooper-Jabob (1946) and Theis (1935) both drawdown and recovery phases of each tests were analyzed, respectively. The following table shows the

evaluated hydraulic conductivity values within the five-point star area. Note that the values for each well are averaged with the values analyzed from drawdown and re-covery curves.

Table 4.3: The K and S_s values obtained from pumping tests within the five-point star area.

	P0/M25	P0/M22.5	P0/M27.5	P2.5/M25	PM2.5/M25	Mean
K [m/s]	1.4×10^{-03}	1.8×10^{-03}	2.1×10^{-03}	1.9×10^{-03}	1.5×10^{-03}	1.8×10^{-03}
S_s [m^{-1}]	-	8.4×10^{-08}	3.3×10^{-7}	3.0×10^{-6}	8.5×10^{-7}	1.1×10^{-7}

In the pumping test with pumping well B2, head changes were recorded both in B2 and in P0/M22.5. After Theis (1935) and Barker (1988) the evaluated hydraulic conductivity based on the head change in B2 is 5×10^{-4} m/s (Table 4.4).

Table 4.4: The K and S_s values obtained from the pumping test between B2 and P0/M22.5.

	B2	P0/M22.5
K from whole curve (Theis 1935 and Barker 1988) [m/s]	5.0×10^{-04}	-
K from drawdown (Cooper-Jacob 1946) [m/s]	6.6×10^{-04}	3.0×10^{-03}
K from recovery (Theis 1935) [m/s]	-	1.5×10^{-03}
S_s from drawdown (Cooper-Jacob 1946) [m^{-1}]	-	5.0×10^{-05}

For the analysis of the head data recorded in well P0/M22.5, the same analytical solutions for the wells in the five-point star area were used. The evaluated hydraulic conductivity varies from 1.5×10^{-3} to 3.0×10^{-3} m/s. Note that during this test, the pump-ing rate had to be set very low (0.175 l/s) to prevent a dry up of the pumping well. Therefore, the drawdown in the observation well was very low, which introduced an insufficient signal-noise ratio, especially for the data at later time. Hence, the obser-vation well data is difficult to analyze and the results should be carefully interpreted.

The evaluated S_s values within the five-point star area at Well P0/M25 are small values with a strong variation from 8.4×10^{-8} to 3.0×10^{-6} m^{-1} (Table 4.3), while the re-sult of the test with B2 as pumping well shows an S_s value of 5.0×10^{-5} m^{-1}, evaluated at the observation well P0/M22.5 (Table 4.4).

Pumping tests are normally performed to obtain estimates of large volumetric av-erages of K (or T) and S_s. The S_s estimates are very often problematic, since the variation in S_s is produced by many factors, especially by the large impact of spatial

variations in K of the aquifer material between the pumping well and the observation well (e.g., Butler, 1988; Butler, 1990; Butler, 1998; Schad and Teutsch, 1994; Sánchez-Vila et al., 1999). This problem occurs because the hydraulic diffusivity D (K/S_s) and K from drawdown are only directly estimated in the absence of boundary effects. Those parameters represent conditions in different portions of the aquifer (Butler, 2008). The diffusivity estimate is primarily a function of aquifer material between the pumping and observation wells, whereas the K estimate represents an average over a much larger area (e.g., Butler, 1990; Butler, 1998; Schad and Teutsch, 1994). Through the S_s estimate, the large volumetric average of K is used to represent the local aquifer material between the pumping and observation wells and then that K value is substituted into the diffusivity relationship. Thus, spatial variations in K can introduce error into the S_s estimate. Results from numerous multi-well pumping tests have also shown that it is common to obtain a near-constant K but large variations in S_s from analyses of drawdown at different observation wells (e.g., Schad and Teutsch, 1994; Butler, 1998). Therefore, one should expect more representative S_s estimates as the distance between the pumping and observation wells increases.

The pumping tests introduced above are focused mainly on the five-point star area. For the general information about the whole test site Stegemühle, the statistic data of pumping tests from Hu (2007) and Vogt (2007) are shown in the following table as complementary information for the aquifer characterization in this work.

Table 4.5: Statistical data of K values obtained from other pumping tests within the whole test site.

	Minimum	Maximum	Mean	Variance
K [m/s]	1.84×10^{-05}	2.59×10^{-03}	1.04×10^{-03}	3.93×10^{-07}

These pumping tests were carried out from different wells within the whole test site and the statistic data is based on the evaluations of 31 response curves. The similarity of the mean and low variance of K from this method, like the results from the grain size analysis, show that the aquifer at the test site Stegemühle is highly conductive.

Cross-well multi-level short term pumping tests

The conventional pumping tests were performed with fully penetrating wells. Unlike the sieve analysis and the slug tests, the hydraulic conductivity cannot be differentiated into vertical profiles. The parameters determined by a pumping test are

not an arithmetic mean, but a spatially integrated physical average that is caused through the radial flow process (Ptak et al., 1996).

In order to estimate the vertical changes of hydraulic parameters, I performed cross-well multi-level pumping tests, implementing a tomographic array along a straight line between a pumping well and two observation wells. The distance between the pumping well (P0/M25) and the first observation well (PM5/M17.5) is 9 m (Figure 4.7) and the distance between the two observation wells (PM5/M17.5 and PM6.4/M15.5) is 2.5 m.
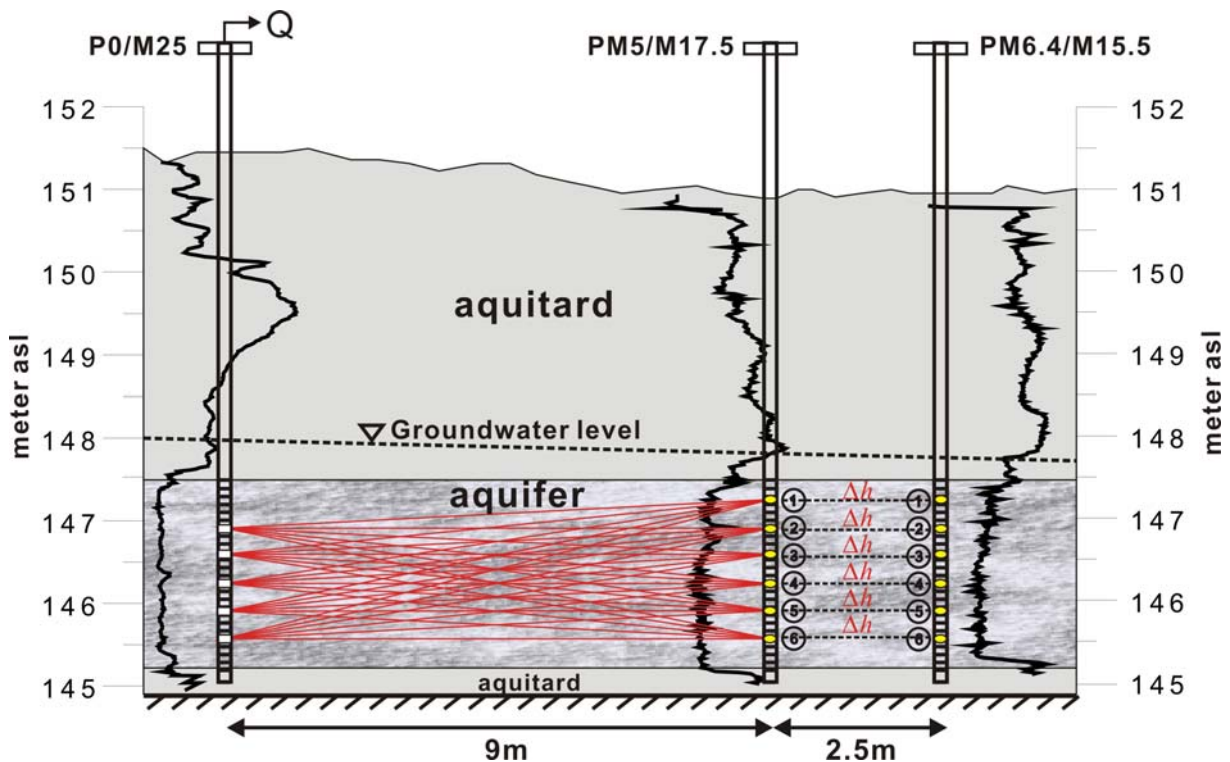
Figure 4.7: Schematic of the multi-level pumping test design with the DP-EC log near the wells. Note that the red trajectories do not represent the real flow paths, but only the connections between the middle point of pumping intervals (white box) and the observation points at multi-chambers (yellow circles). The numbers 1~6 represent the chambers of the multi-chamber wells.

During the pumping test, the water was partially pumped out of the pumping well P0/M25 (Figure 4.7) with an internal tube diameter (ID) of 0.031 m by employing double packer systems with a screened interval of 0.25 m. The observation wells PM6.4/M15.5 and PM5/M17.5 (Figure 4.7) are multi-chamber wells based on the Continuous Multi-channel Tubing (CMT) System (Einarson and Cherry, 2002). This system is originally developed for the multi-level sampling and consists of a pipe with seven continuous separate channels or chambers (ID = 0.014 m), which are ar-

ranged in a honeycomb shape (Figure 4.8). Prior to the well installation, individual chambers, leading to different depths, with 0.08 m long openings, which are covered with sand filters, were installed into the tube. This design allows the measurement of water level changes at different depths of the aquifer.
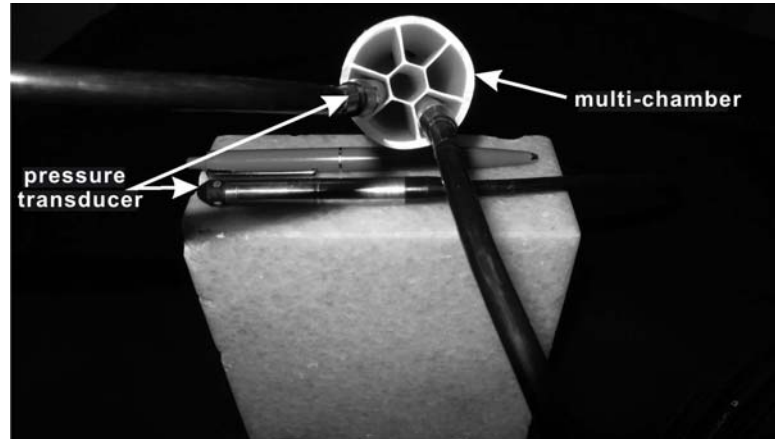
Figure 4.8: Photograph of the pressure transducer (PDCR 35/D-8070) and the multi-chamber tube installed using the Continuous Multi-channel Tubing (CMT) system.

For one profile between the pumping well and one of the observation wells, five short-term pumping tests were carried out. For every short-term pumping test and every pumping interval, the pressure changes in the six different depths of the multi-chamber wells were recorded at a frequency of 50 Hz with the pressure transducer (PDCR 35/D-8070) connected to a data logger (Campbell Scientific® CR 3000). By varying the pumping interval, a total number of 30 (5 × 6) drawdown curves for one profile were recorded. Note that in the central chamber of the multi-chamber wells (Figure 4.8) no pressure change was recorded because this chamber has only a limited hydraulic connection to the aquifer.

The performance of the respective pumping tests in series produced a pattern of crossing trajectories between the test well and observation wells, similar to the paths of a radar or seismic experiment. The travel times between well P0/M25 and the two observation wells can be inverted to obtain a reconstruction of the diffusivity distribution. The head differences between the two observation wells during the pumping tests can be used as observed data for the *K* estimation based on a steady shape inversion. The inversion approach and results are introduced in Chapter 4.3. Here, only an introduction to the evaluation of some selected tests based on the analytical solutions is presented.

For the analytical evaluation of short term pumping tests, the straight line method from Cooper-Jacob (1946) was used. This solution can be used for the evaluation of

pumping tests in a confined homogeneous and isotropic aquifer. The solution is based on the assumption that the wells are screened over the whole thickness of the aquifer. The solution can also be applied for a partially penetrating well, if the observation well has a distance of at least $1.5b\sqrt{K_h/K_v}$ from the pumping well (Hantush, 1964). The parameter b describes the thickness of the aquifer and K_h and K_v stand for the horizontal and vertical hydraulic conductivity, respectively. Based on hydraulic tomographical inversions of the data derived from cross-well slug tests, the aquifer characterization results from Brauchler et al. (2010) show that close to well P0/M25, the horizontal hydraulic conductivity is larger than the vertical hydraulic conductivity by a factor of 5~8. With an average aquifer thickness of 2 m and an assumed anisotropy of the hydraulic conductivity of 8, the distance between pumping and observation wells after Hantush (1964) should not be less than 8.48 m. Given all these local information, all required conditions are met to evaluate the short-term pumping tests with the straight line method developed by Cooper and Jacob (1946).

Figure 4.9 (c)-(f) shows five drawdown curves and their corresponding curve fitting regressions. These drawdown curves are derived from five pumping tests, where the middle points of pumping and the observation intervals are at the same depth. They are recorded at five different depths of the aquifer in observation well PM5/M17.5. The straight line method is only applied to fit the respective values at the right side of each dashed line in order to meet the minimum-time criterion (Cooper & Jacob, 1946). This minimum-time criterion is determined by the relationship $t = r^2 S / 0.04T$, where r represents the distance between pumping and monitoring intervals, S is the storage, and T is the transmissivity. The r in this case is 9 m, which exceeds the calculated minimum distance of 0.5 m by Hantush (1964). The depths in Figure 4.9 refer to the depths of the middle points of the pumping and observation intervals. The evaluated hydraulic conductivity and specific storage values are displayed in Figure 4.9(a) as a function of depth. The values show only small variation from 1.6×10^{-3} m/s to 2.2×10^{-3} m/s for hydraulic conductivity and from 1.2×10^{-4} m^{-1} to 2.0×10^{-4} m^{-1} for the specific storage.

The drawdown curves recorded at the observation well PM6.4/M15.5 are evaluated by the same means of analytical method and the results are shown in Figure 4.9(b). The hydraulic parameters at well PM6.4/M15.5 are consistent with the results shown in Figure 4.9(a) and display the same small variation.
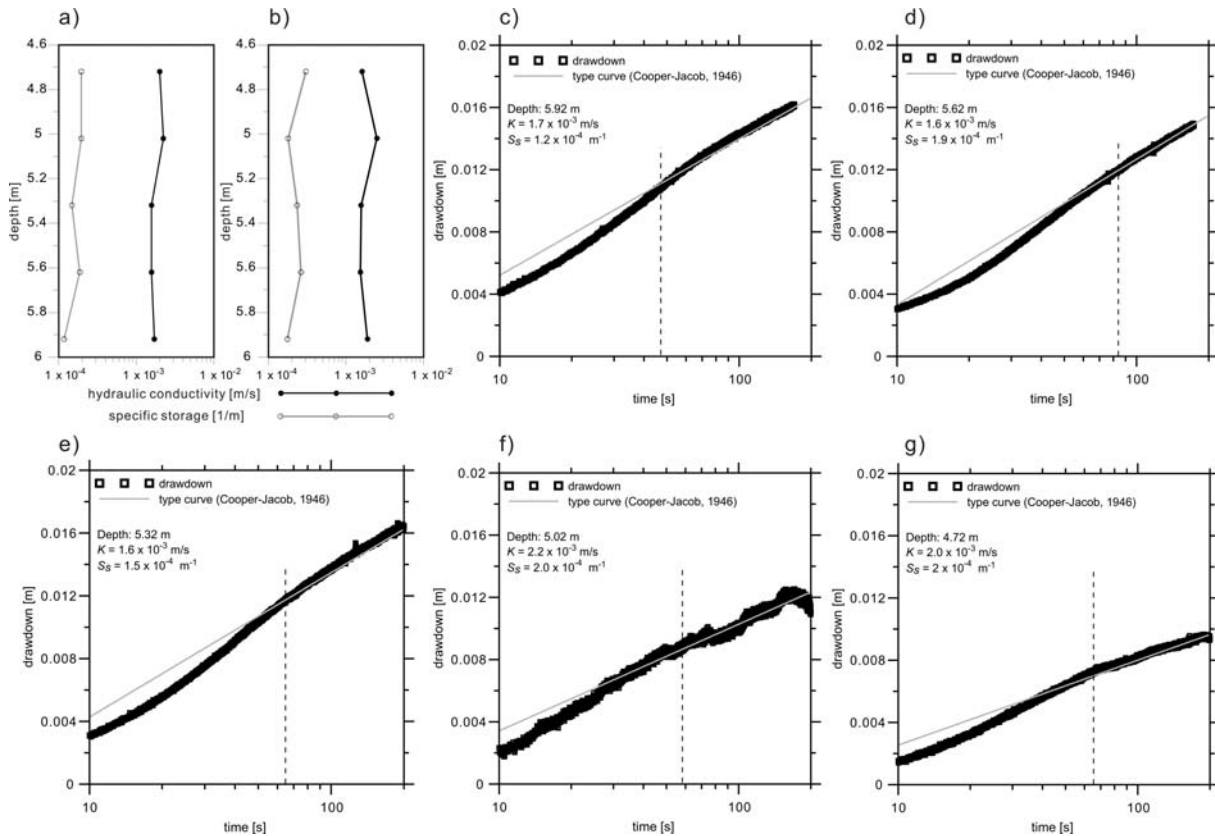
Figure 4.9: (a) Results of the short-term pumping tests between the 2"well P0/M25 and the multi-chamber well PM5/M17.5 conducted at five different depths. (b) Results of the short-term pumping tests between the 2" well P0/M25 and the multi-chamber well PM6.4/M15.5 conducted at five different depths. (c)-(f) The individual drawdown curves, plotted logarithmically as a function of time for the five short-term pumping tests shown in (a).

Compared to the results of the grain size analysis, the analytically evaluated K and S_s values through multi-level short-term pumping tests show no vertical and lateral changes in the hydraulic properties of the aquifer. For purposes such as contaminant movement predictions and remediation system designs, the large volumetric average of hydraulic parameters without spatial variation is not sufficient due to the strong effects local heterogeneities may have on contaminant movement (e.g. Zheng and Gorelick, 2003; Liu et al., 2004; Butler, 1998). Thus, through conventional pumping tests, only little information can be gained about the variations in important hydraulic parameters e.g. hydraulic conductivity on the scale of interest for solute-transport investigations.

4.2.4 Slug tests

Slug tests have conventionally been utilized as a means to determine the hydraulic conductivity of an aquifer at a relatively smaller scale, compared with pumping tests. The slug test approach consists of measuring the recovery of head in a well after a near-instantaneous change in head at that well. Head data are analyzed, using various models of the well-formation configuration (Butler, 1998). Varying K values obtained from slug tests are attributed to the properties of the aquifer material in the immediate vicinity of the screened interval (Beckie and Harvey, 2002). Therefore, at a site with an extensive network of wells, slug testing is a valuable tool for aquifer characterization (Yeh et al., 1995). When performed in a cross-well mode, a slug test can provide considerable information for describing spatial variations in hydraulic properties.

The slug test has been frequently used due to its unique advantages over the other hydraulic approaches (e.g. pumping tests and tracer tests). The most significant advantages are the low costs involved, the relative simplicity of the method, the short duration (at least in high permeability media), and the consideration that no water needs to be handled, which is very beneficial at sites of suspected groundwater contamination (Butler, 1998).

Slug tests can be implemented through a variety of different techniques. In this study, the slug tests were implemented by the pneumatic approach (Figure 4.10) in order to avoid significant fluctuation in initial readings of the response signal (Butler, 1998). This pneumatic approach involves pressurizing the air column in a sealed well by the injection of compressed air. Increased pressure in the air column of the sealed part of the well results in a depression of the water level in the well as water is driven out of the well screen. The change in water level and the change in pressure of the air column is recorded with small diameter pressure transducers (PDCR 35/D-8070) connected to a data logger (Campbell Scientific® CR 1000 or CR3000). The head data during a test can be monitored simultaneously and saved on a field laptop. The pressure transducer in the water column is placed close to the static water table to avoid the problem that transducer readings tend to vary with installation depth and thus may not accurately measure the water-level position if placed at inconsistent locations (Butler et al., 2003).

In this study the relevant multi-level single-well slug tests and cross-well interference tests within the investigation area as shown in the enlarged plan-view section of Figure 4.3 are introduced.

Multi-level single-well slug tests

Multi-level single-well slug tests were first performed in each well within the five-point star area to determine the vertical changes of hydraulic conductivity within the aquifer. Figure 4.10 displays the hypothetical cross section of a single-well slug test.
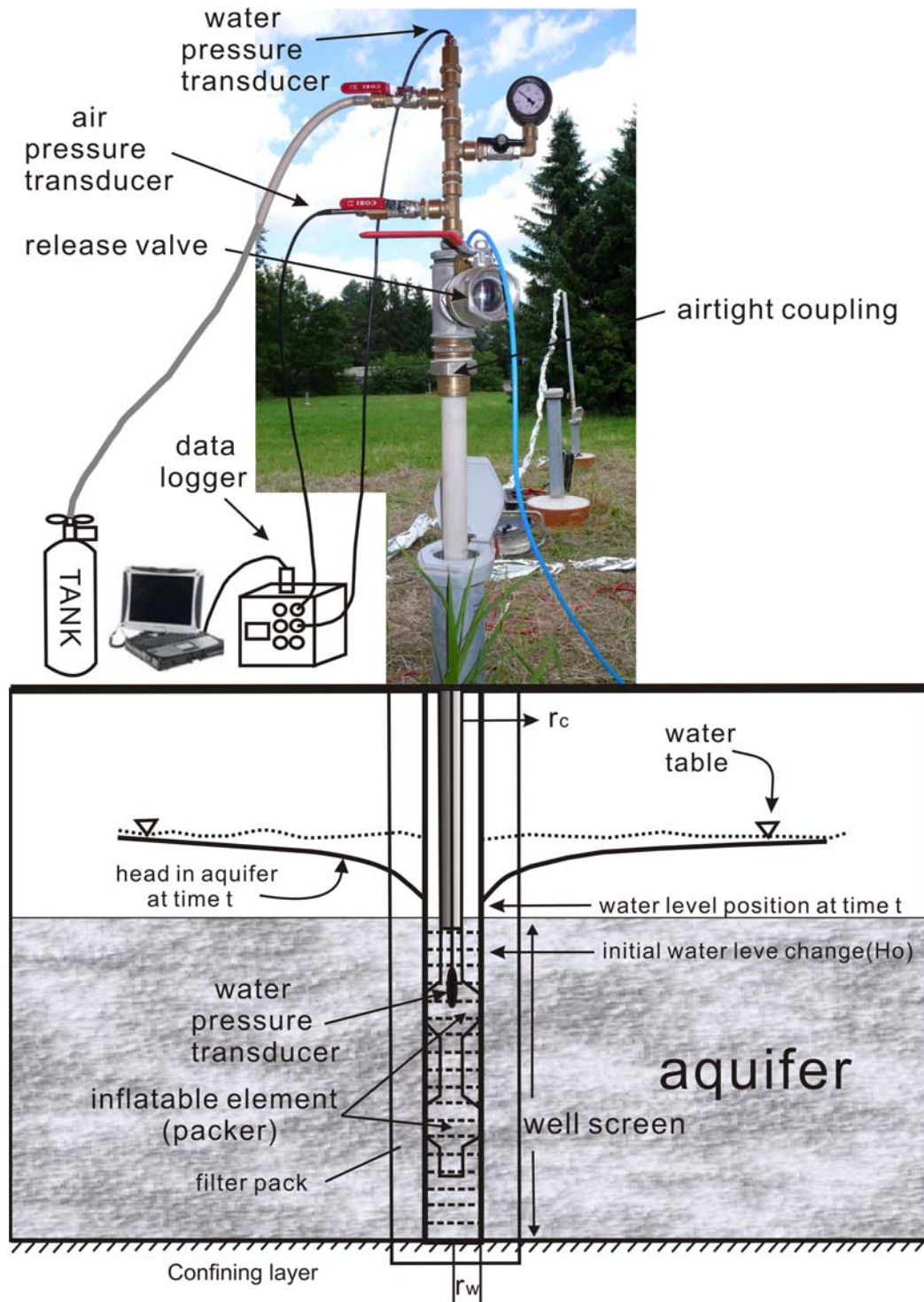
Figure 4.10: Schematic of test initiation set-up of a multi-level single-well slug test with a hypothetical cross-section displaying a well in which the pneumatic method is being used. A double packer system is used to separate a specific depth-section of the aquifer for testing. Modified from Butler (1998).

The response data of the pneumatic slug tests were recorded with an acquisition rate of 10 Hz through the data logger and then were normalized using the initial displacement measured by the pressure transducer installed in the air column. In Figure 4.11, the estimated hydraulic conductivity values against depth are displayed for all

71

wells within the five-point star area. In each well seven tests were performed in order to characterize the whole thickness of the aquifer, whereby the different slugged intervals were isolated by a double packer system with a screened opening of 0.25 m. The analysis of the response curves were based on the analytical solution of Butler (1998). For the application of the solution the following assumptions were made: the aquifer is confined, isotropic, non-bounded; the test well is partially penetrating and no well skin is present. Following the field guidelines for slug tests in highly permeable aquifers recommended by Butler et al. (2003), multi-stress level tests were performed using different initial displacements (0.1~0.2 m) and the results indicate no stress dependence.
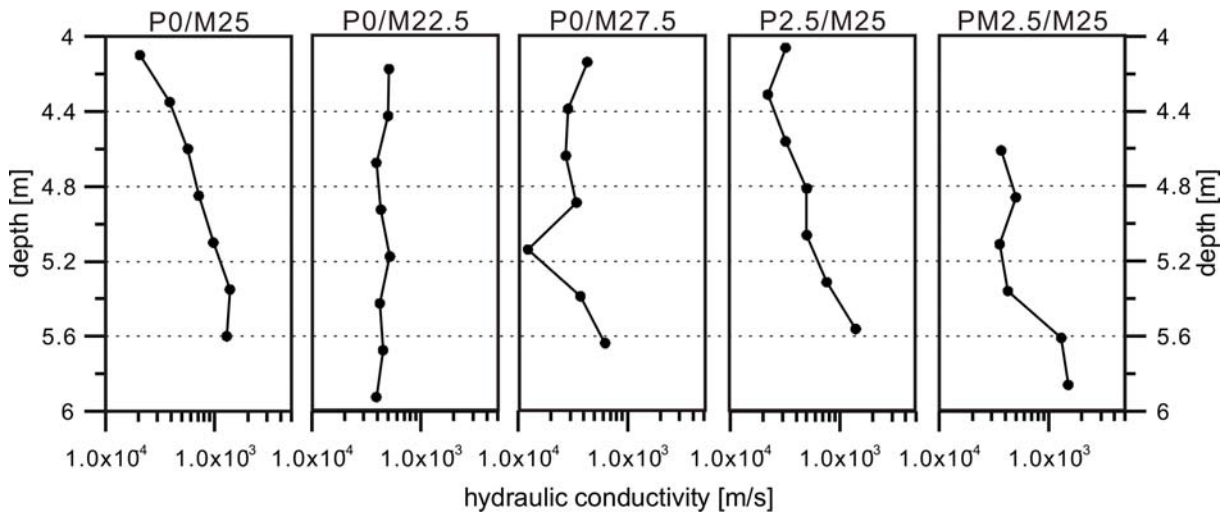
Figure 4.11: Hydraulic conductivity estimates based on multi-level single-well slug tests within the five-point star area (modified from Brauchler et al., 2010).

Four of the five profiles show that the lower 0.5 meters of the aquifer is characterized by a high conductivity layer. Above this layer the values for hydraulic conductivity continuously decrease. The difference between the highest value at the bottom and the lowest values at the top of the aquifer is approximately one order of magnitude. These results are in accordance with the geological interpretation based on soil core data (Hu, 2007), which show that the upper part of the aquifer material is characterized by a larger silt component than the lower part. Only the hydraulic conductivity profile of well P0/M22.5 shows a homogeneous hydraulic conductivity distribution.

Table 4.6: Statistical data of *K* values (m/s) obtained from slug tests within five-point star area.

	Minimum	Maximum	Mean	Variance [(m/s)^2]
P0/M25	2.07×10^{-04}	1.37×10^{-03}	7.86×10^{-04}	1.96×10^{-07}
P0/M22.5	3.90×10^{-04}	5.20×10^{-04}	4.51×10^{-04}	2.78×10^{-09}
P0/M27.5	1.23×10^{-04}	6.27×10^{-04}	3.51×10^{-04}	2.41×10^{-08}
P2.5/M25	2.20×10^{-04}	1.40×10^{-03}	5.74×10^{-04}	1.64×10^{-07}
PM2.5/M25	3.55×10^{-04}	1.50×10^{-03}	7.41×10^{-04}	2.68×10^{-07}

With the same slug test procedure the multi-level single-well slug tests were also carried out in the wells PM5.4/M15.5 and P5.4/M15.5. The results are shown in the following figure.
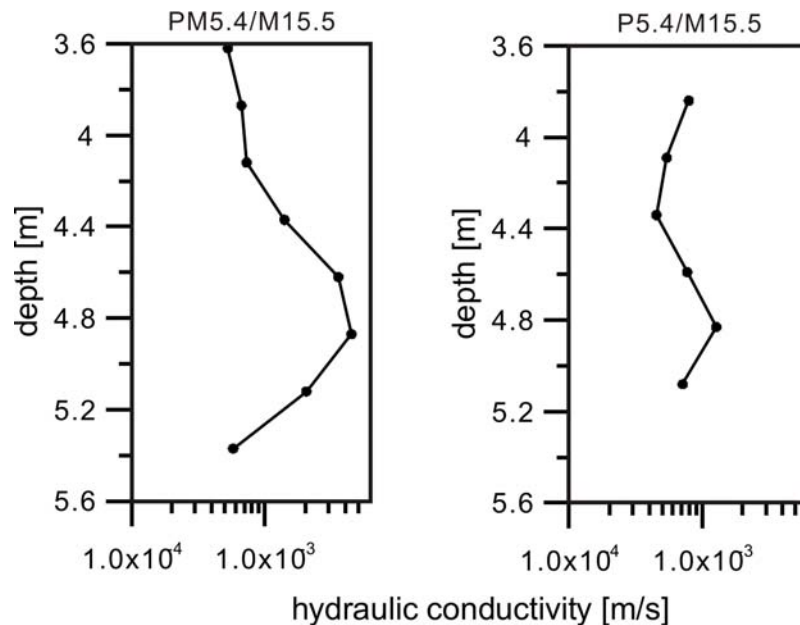
Figure 4.12: *K* estimates based on multi-level single-well slug tests at wells PM5.4/M15.5 and P5.4/M15.5.

For a general view of the hydraulic conductivity within the whole test site, the statistical data of other multi-level single-well slug tests, which were performed at other wells from Hu (2007) and Vogt (2007) are introduced with the following table.

Table 4.7: Statistical data of the *K* values (m/s) obtained from slug tests at other wells of the whole test site.

Well	N	Minimum	Maximum	Mean	Variance $[(m/s)^2]$
P0/0	4	1.57×10^{-04}	4.40×10^{-04}	2.44×10^{-04}	1.75×10^{-08}
P25/25	1	1.42×10^{-04}	1.42×10^{-04}	1.42×10^{-04}	-
PM25/0	4	1.02×10^{-06}	1.82×10^{-04}	1.12×10^{-04}	6.37×10^{-09}
PM25/M25	4	4.10×10^{-05}	7.76×10^{-05}	5.81×10^{-05}	2.25×10^{-10}
P25/0	4	2.55×10^{-05}	8.58×10^{-05}	5.56×10^{-05}	1.07×10^{-09}
P58/35	1	1.10×10^{-04}	1.10×10^{-04}	1.10×10^{-04}	-
PM50/0	1	1.56×10^{-03}	1.56×10^{-03}	1.56×10^{-03}	-
P42.5/4.5	1	3.79×10^{-04}	3.79×10^{-04}	3.79×10^{-04}	-
P0/25	1	1.85×10^{-04}	1.85×10^{-04}	1.85×10^{-04}	-
P0/M50	3	1.01×10^{-04}	2.10×10^{-04}	1.46×10^{-04}	3.26×10^{-09}
P25/M25	4	1.51×10^{-04}	2.91×10^{-04}	2.05×10^{-04}	4.10×10^{-09}
Sum/Mean	28	2.59×10^{-04}	3.33×10^{-04}	2.90×10^{-04}	5.42×10^{-09}

According to the mean values estimated from different wells, the hydraulic conductivity values vary from 5.56×10^{-5} to 1.56×10^{-3} m/s with an average of 2.9×10^{-4} m/s.

In order to display the variation of *K* values in the vertical direction, all *K* values estimated through the multi-level single-well slug test were plotted against depth in the following figure. Note that due to the changing topography in the test site, the *K* values are plotted against the absolute height above sea level.
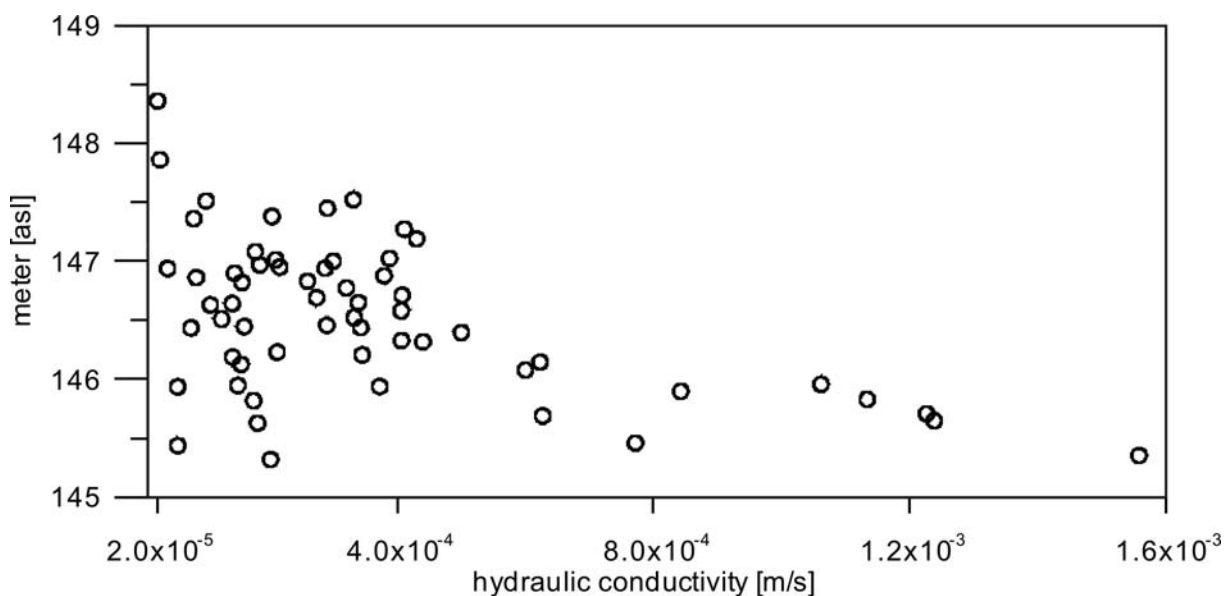
Figure 4.13: All *K* values evaluated through multi-level single-well slug tests at the test site Stegemühle.

This statistical data, based on a multitude of slug tests, indicates that within the test site, the bottom part of the aquifer has higher hydraulic conductivity than the upper part of the aquifer.

Multi-level cross-well slug interference tests

Investigations have shown that the additional evaluation of the pressure response in the observation well next to the pressure response in the test well, yields information about well-bore skin and anisotropy and improves the exact determination of specific storage (e.g. Butler, 1998; Brauchler et al., 2010). In order to characterize the spatial distribution of hydraulic parameters K and S_s, the potential of cross-well slug interference test was assessed.

A series of cross-well slug tests were first performed within the five-point star area, of which both the pressure heads in the test and observation wells were recorded. This series of tests comprise four profiles between every outer well and the central well P0M25. For each test, the central well was the test well and the outer wells served as the observation wells. Each of the four profiles consists of seven slugged intervals and seven observation points isolated with a double packer system, meaning that each profile consists of 49 transient pressure curves.

Slug tests of this series of tests were evaluated analytically. Slugged interval (source) and the observation interval (receiver) were at the same depth (Figure 4.15(a)), which is similar to the configuration of the analytical evaluation for the cross-well pumping tests. For the type curve matching of the pressure response curves, either the solution developed by Hyder et al. (1994) or the solution from Butler and Zhan (2004) were applied. Both solutions enable the evaluation of water-level response at the test and observation wells in a confined aquifer for fully and partially penetrating wells. The Butler and Zhan (2004) solution additionally enables the evaluation of underdamped responses typical for high K-aquifer sections and accounts for frictional losses in small-diameter wells and inertial effects in the test and observation wells. For the application of the solutions, the following assumptions were made: the aquifer is confined, isotropic, and of infinite extent; test and observation wells are partially penetrating and there is no well skin. The evaluated hydraulic parameters K and S_s at the positions of the four outer wells are illustrated in Figure 4.14.
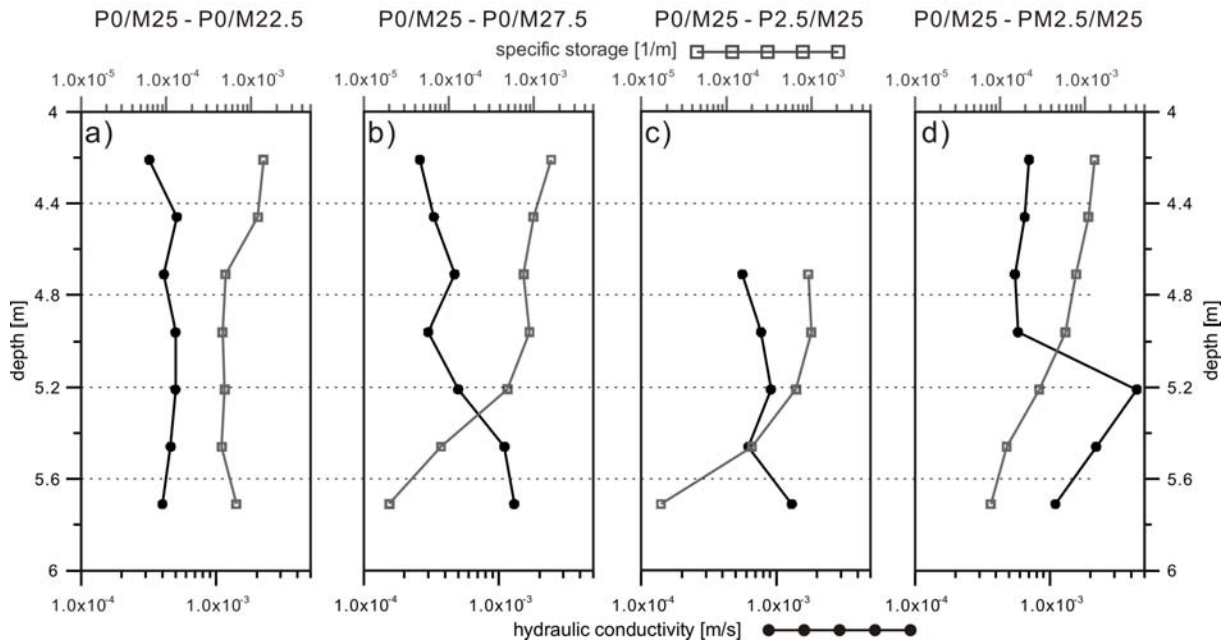
Figure 4.14: Analytically evaluated *K* and *S$_s$* values through multi-level cross-well slug tests. Note the depths refer to the center of the double packer system. (modified from Brauchler et al., 2011)

The profiles illustrated in Figure 4.14 (b)-(c) show similar parameter characteristics with increasing depth: *K* values increase and *S$_s$* values decrease. The *K* values are approximately 10^{-3} m/s close to the bottom and decrease to approximately 10^{-4} m/s at the top of the aquifer. The *S$_s$* distribution shows an opposite trend. They are approximately 10^{-5} m^{-1} close to the bottom of the aquifer to approximately 10^{-3} m^{-1} at the top of the aquifer. The profile P0/M25-P0/M22.5 shows no significant variation with depth (Figure 4.14(a)), which is in accordance with the results of single-well slug tests at the well P0/M22.5 (Figure 4.11).
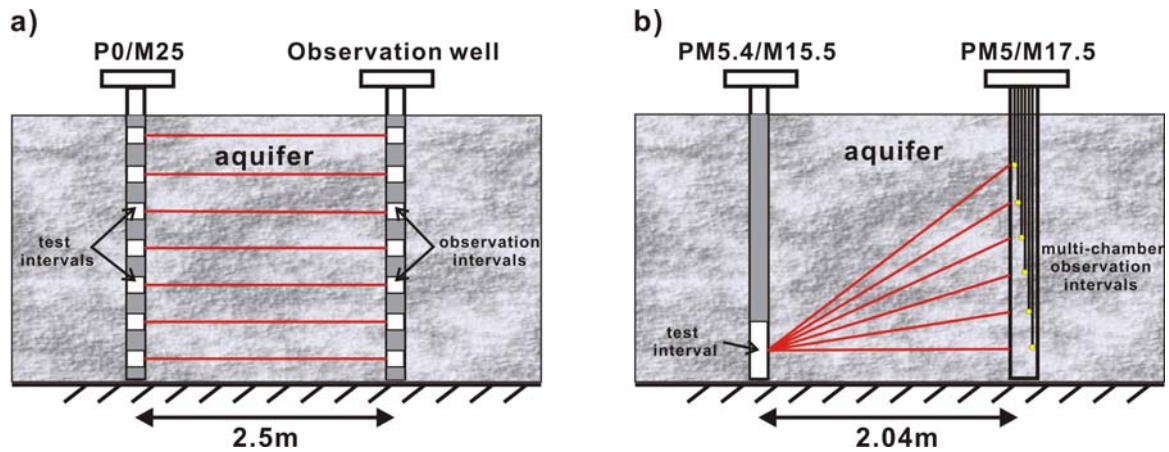
Figure 4.15: Schematic of the analytically evaluated cross-well slug tests. (a) The tests between the well P0/M25 and its outer wells; (b) The tests between wells PM5.4/M15.5 and PM5/M17.5. Note that the red trajectories do not represent the real flow paths, but only the connections between the middle point of the slug intervals (white boxes) and the observation intervals.

In order to get the hydraulic properties in the vicinity of well PM5/M17.5, another six cross-well slug test series (Figure 4.15(b)) were performed. During these tests, the well PM5.4/M15.5 (ID = 0.031 m) was the test well and the well PM5/M17.5 (multi-chamber well) served as the observation well. For each test, a screened interval of 0.5 m at the bottom of the test well was isolated with a packer system and the pressure responses were recorded in every chamber of the observation well. Being the same as for the evaluation of the cross-well slug tests in Figure 4.15(a), the response curves in the observation well were evaluated with the solution from Butler and Zhan (2004).

Table 4.8: The K and S_s values obtained from the cross-well slug tests between wells PM5.4/M15.5 and PM5/M17.5.

Chamber	K [m/s]	S_s [m^{-1}]
1	9.19×10^{-4}	1.00×10^{-4}
2	1.00×10^{-3}	7.25×10^{-5}
3	1.19×10^{-3}	2.86×10^{-5}
4	1.29×10^{-3}	3.48×10^{-5}
5	1.81×10^{-3}	2.24×10^{-5}
6	1.81×10^{-3}	9.49×10^{-6}

Similar to the results displayed in Figure 4.14, the S_s values increase from the aquifer bottom to the aquifer top and vary over one magnitude. The estimated K values are more uniform and reflect the hydraulic properties of the highly permeable zones

at the bottom of the aquifer, similar to the results from the type curve analyses of the multi-level pumping tests.

4.2.5 Tracer test

In order to assess the competence of the aquifer characterization methods briefly described above and to "trace" the path of flowing groundwater, a tracer test was performed. It is well known that the spatial structure and the connectivity of the hydraulic conductivity field dominate solute transport in heterogeneous porous aquifers (e.g. Dagan, 1990). For groundwater remediation purposes such as small- to medium-scale contaminant transport predictions, integrated parameter estimates over a large area are of little significance. This is due to the fact that interconnected highly conductive zones form preferential flow paths, which dominate the flow field and consequently result also in the restriction of the contaminant plume to these flow paths (Ptak and Teutsch, 1994).

The tracer experiment at the test site Stegemühle was conducted under the natural gradient with a non-reactive fluorescent dye tracer of uranine as a line-source injection. During the tracer experiment, both single- and multi-level groundwater samples were collected and analyzed (Figure 4.16).
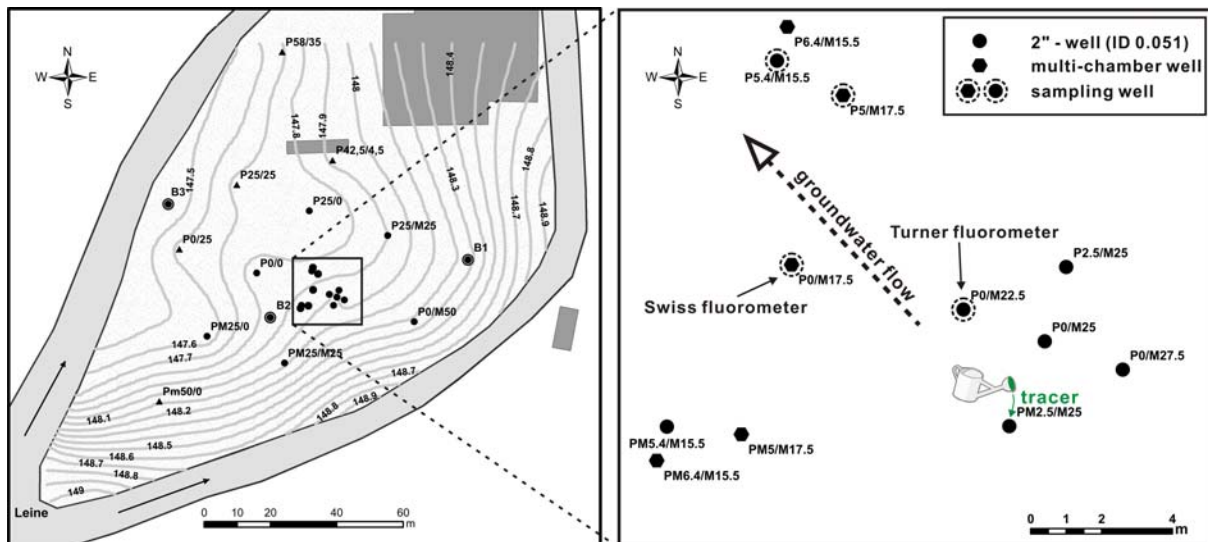
Figure 4.16: The position of the tracer injection and monitoring wells.

Because the wells downstream from the group of multi-level sampling wells (multi-chamber wells) have limited infiltration capability, the experiment was conducted under the natural hydraulic gradient and does not involve pumping of these wells. The natural hydraulic gradient within the area of the tracer test was approximately 5% and

remained relatively constant, according to the long-term water table monitoring. A disadvantage of natural gradient tracer tests is their longer duration as compared with forced gradient tracer tests. Thus they require long-term monitoring with a less predictable duration. Throughout the whole duration of the test, the measurements may possibly have been affected by the changes of the hydrological conditions, which may have caused fluctuations in the groundwater flow direction. To avoid this problem, such as the fluctuation in groundwater table, the experiment was performed in the autumn, i.e. in September, 2010.

The dissolved fluorescent tracer was injected with a small suction pump into the well PM2.5/M25. The tracer mass mixed with the water in the well by the turbulence inside the well casing and was then distributed across the entire length of the water column within the well using a mixing pumping and hypothetically instantaneously across the entire saturated aquifer thickness (Figure 4.17).
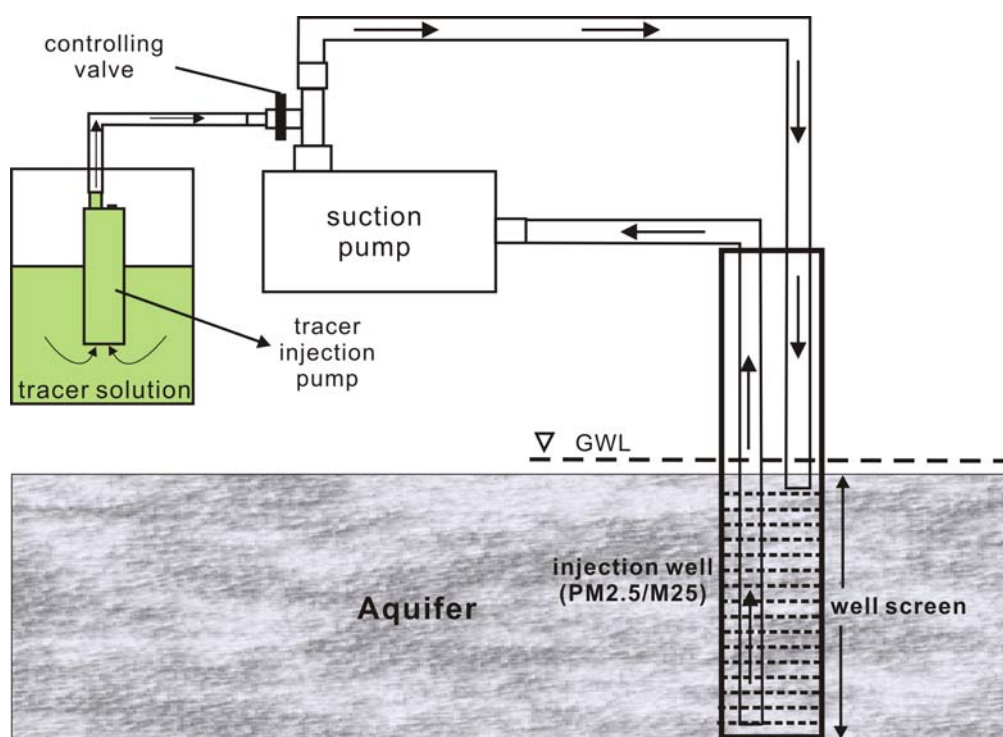
Figure 4.17: Schematic setup of the tracer injection.

For the tracer injection, 20 grams of fluoresceine uranine were dissolved in 20 liters of water and 40 liters of water were used for flushing the tracer container with the following assumption: the uranine solution of this concentration does not significantly change groundwater density and the dissolved constituents behave conservatively, meaning no mass is lost due to retardation or reaction. The only solute transport

processes affecting a conservative tracer are advection and dispersion. Advection is the movement of the solute (dissolved tracer) due to groundwater flow and can be predicted using the mean pore-water velocity. As the pore-water velocities within the groundwater system are not uniform, some solute will move slower and other solute will move faster, compared with the mean velocity. The resulting dispersion of the solute causes a broadening of the solute plume and a decrease in the concentration.

The concentration of tracer was subsequently monitored in-situ at the well P0/M22.5 (Turner fluorometer) and P0/M17.5 (Swiss Fluorometer) and water samples were taken from the sampling wells, which are indicated in Figure 4.16. Figure 4.18 shows the schematic of the setup of the multi-level sampling at the multi-chamber well P0/M17.5.
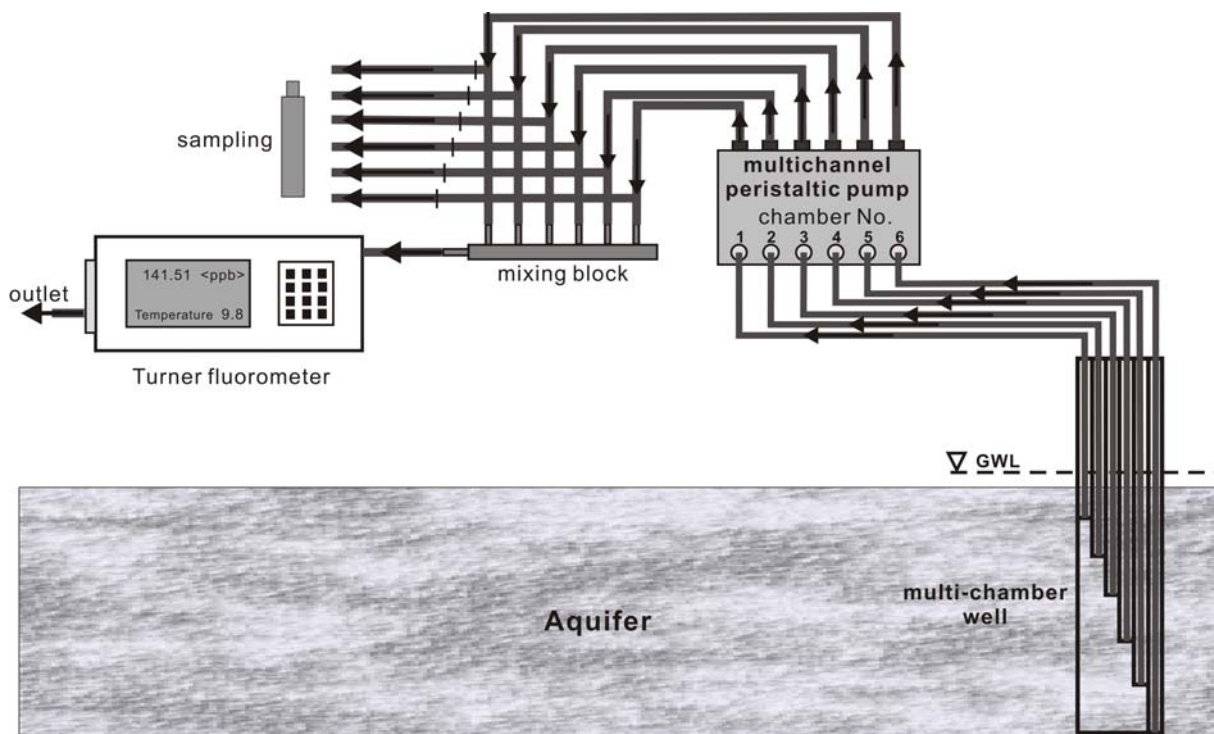
Figure 4.18: Schematic setup of the concentration monitoring and sampling system of the tracer test at the well P0/M17.5.

For the analysis of the experiment, parameters such as transport velocities and longitudinal macro-dispersivities were obtained by fitting one-dimensional analytical models to individual breakthrough curves with different characteristics, e.g. different measured peak concentrations, arrival times of peak concentrations, and the resulting peak velocities. This approach allows to identify, especially in the case of multi-

level breakthrough curves, the individual flow paths within a perfectly layered aquifer system.

A one-dimensional approach is certainly not sufficient to describe the mass transport in the heterogeneous aquifer investigated. However, the aim of this approach is not to find the spatial distribution of the absolute hydraulic parameters values for the heterogeneous system, but rather to demonstrate the general pattern of the aquifer heterogeneity and compare it with the results from other aquifer characterization methods. Transport parameters calculated from each measured breakthrough curve can individually be used for the relative comparison, providing a relative measure of the subsurface heterogeneity (Ptak and Teutsch, 1994).

The analytical evaluation of the breakthrough curve is based on Sauty (1980). In the following, the governing equations are briefly introduced. For further details of this method, the readers are referred to the work of Sauty (1980).

After the simplification of the equation of mass transfer (e.g. Bear, 1972), Sauty (1980) summarized the one-dimensional convection-dispersion equilibrium equation for nonreactive solute transport in a homogeneous soil as the following:

$$\frac{\partial c}{\partial t} = D_c \frac{\partial^2 c}{\partial x^2} - v_p \frac{\partial c}{\partial x}.$$

Eq. 4.3

This governing equation can be written in dimensionless form as:

$$\frac{1}{x_R} \frac{\partial C}{\partial t_R} = \frac{\partial^2 C}{\partial x_R^2} - \frac{\partial C}{\partial x_R},$$

Eq. 4.4

where $x_R = x / \alpha_L$ and $t_R = v_p t / x$. For a given distance X and given boundary conditions, the dimensionless distance fixes the breakthrough curve. This number is the Peclet number $P = \frac{X}{\alpha} = \frac{v_p}{D_c} = x_R$, where X is the reference length.

Assuming that a slug of tracer is instantaneously injected into a system governed by one-dimensional flow, the solution of Equation 4.3 can be written as:

$$C(t_R, P) = \frac{K}{(t_R)^{1/2}} \exp[-\frac{P}{4t_R}(1-t_R)^2],$$

with

Eq. 4.5

$$K = t_{R\max}^{1/2} \exp[\frac{P}{4t_R}(1-t_{R\max})^2],$$

Eq. 4.6

where

$$t_{R\max} = (1 + P^{-2})^{1/2} - P^{-1}.$$

Eq. 4.7

C	concentration of a substance transported by water
t	elapsed time since tracer injection
t_R	dimensionless time variable
v_p	effective velocity (mean pore velocity)
D_c	longitudinal dispersion coefficient
x	component of distance from injection well to observation point
x_R	dimensionless longitudinal distance
P	Peclet number
α, α_L	longitudinal dispersivity

At the multi-chamber wells P0/M17.5 and P5/M17.5, the concentration of uranine in groundwater was measured individually at different depths of the aquifer. The analytical solution Eq.4.5 is used to fit the measured breakthrough curves. Two typical fits of the analytical solution to measured breakthrough curves are shown in Figure 4.19 and Figure 4.20.

Chamber	v (m/d)	D (m²/d)	α_L (m)
1	1.72	0.25	0.15
2	1.73	0.23	0.13
3	1.83	0.21	0.11
4	1.83	0.15	0.08
5	1.88	0.12	0.06
6	1.89	0.10	0.05
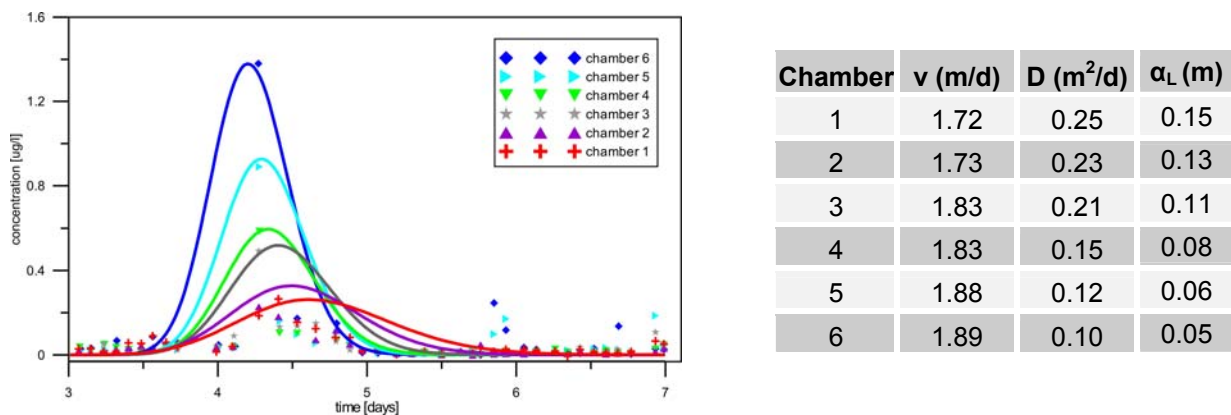
Figure 4.19: The observed concentration (points) at well P0/M17.5 with the fitted breakthrough curves (lines); right are the analyzed transport velocities, longitudinal dispersion coefficients and dispersivity values.
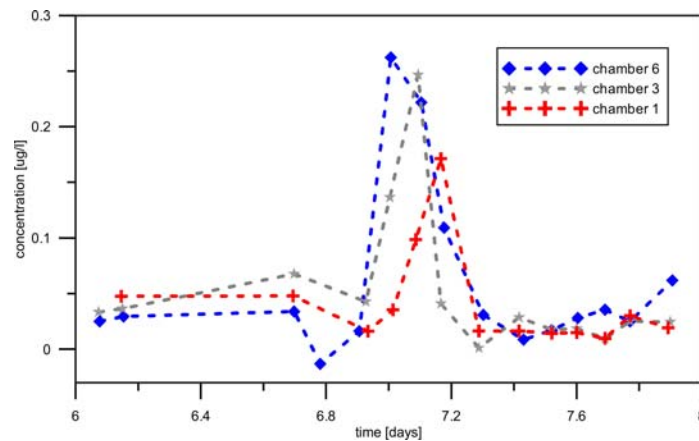
Figure 4.20: The observed concentration (points) at the well P5/M17.5 with the fitted breakthrough curves (lines) and the analyzed transport velocities and the dispersion coefficients.

At different depths of well P5/M17.5, the breakthrough curves with faster arrival times have higher peak concentration values Figure 4.20. This supports the concept of preferential flow paths within highly conductive zones: early arriving concentrations are less dispersed. Figure 4.19 displays a relative uniform arrival time with different peak concentrations at the different depths of well P0/M17.5. Due to the insufficient groundwater sampling rate, the time axis has insufficient resolution. Nevertheless, the increasing peak concentrations with depth indicate the faster transport paths at the aquifer bottom. These results completely consist with the previous results from other the aquifer characterization methods.

4.2.6 Comparison between grain size analysis, slug tests and pumping tests

Through different methods, the hydraulic conductivity values of the aquifer are estimated on three different scales:

(a) Small scale by grain size analysis;

(b) Large scale by pumping tests;

(c) Intermediate scale by slug tests.

To show the differences of the estimated K values with an example, the results of the different investigation methods used within the five-point star area and at the well PM5.4/M15.5 are plotted together against depth in Figure 4.21. Note that in the Figure for PM5.4/M15.5, the K value from pumping test is derived from the mean value of the evaluated K values from the multi-level pumping test at well PM6.4/M15.4, which is one meter away from the well PM5.4/M15.5.

83
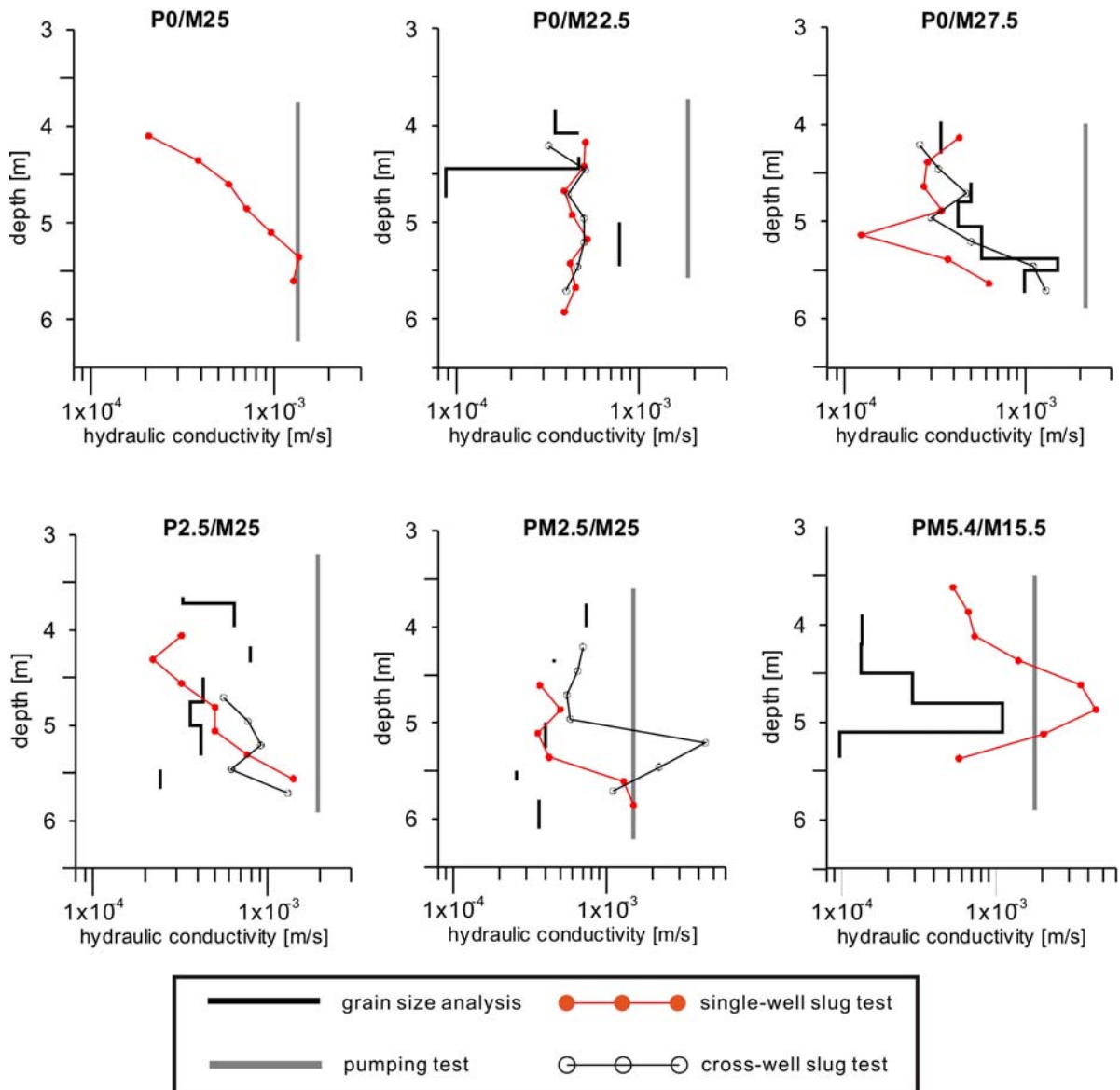
Figure 4.21: Comparison of *K* values derived from grain size analyses, slug tests, and pumping tests.

Figure 4.21 shows a general agreement of the results of the grain size analyses and slug tests. Four wells from the five-point star area show the following similar trend: the hydraulic conductivity increases with depth and varies from approximately 1×10^{-4} to 1×10^{-3} m/s. According to the grain size analyses and multi-level single-well slug tests, the *K* value reaches its maximum in the middle of the aquifer at well PM5.4/M15.5. This feature is also indicated by the result of cross-well slug tests at well PM2.5/M25.

The hydraulic conductivity values determined through pumping tests are generally larger than the values evaluated from grain size analysis and slug tests. Pumping tests determine the hydraulic parameters of the aquifer (*K* and S_s), integrated over a much larger volume in contrast to the grain size analysis and slug test. According to

Ptak et al. (1996), the parameters determined by pumping tests represent not a mathematical mean, but a physical average of the radial flow process in the total saturated aquifer thickness and reflect mainly the hydraulic properties of the highly permeable zones (Diem et al., 2010).

Hu (2007) and Vogt (2007) made a statistic comparison of 101 grain size analyses, 23 pumping tests, and 61 slug tests in this test site. The statistical comparison (Table 4.9) of the natural logarithm of the K values, estimated from different methods, can contribute to an improvement of the data analysis and interpretation.

Table 4.9: Statistical data of ln$K$ determined through different investigation methods.

	Grain size analysis		Pumping tests		Slug tests	
Parameter	K [m/s]	ln$K$	K [m/s]	ln$K$	K [m/s]	ln$K$
N	101	101	23	23	61	61
Minimum	4.60×10^{-05}	-9.99	7.82×10^{-04}	-7.15	1.02×10^{-06}	-13.80
Maximum	3.08×10^{-03}	-5.78	3.10×10^{-03}	-5.78	1.56×10^{-03}	-6.46
Mean	3.98×10^{-04}	-7.83	8.67×10^{-04}	-7.05	2.25×10^{-04}	-8.40
Variance	-	0.58	-	0.02	-	1.29
Skewness	-	-0.56	-	-0.20	-	-1.84

The K values of the pumping tests show the highest average hydraulic conductivity. Their mean values are approximately 2 times higher than the results of sieve analysis and 4 times higher than the slug test results. The differences between the mean values of the slug tests and grain size analyses results are relatively small. The ln$K$ distributions of the slug tests are the most skewed (-1.84), whereas the distribution of ln$K$ of the pumping tests is significantly less skewed (-0.201). Due to the large scale of investigation and the integrating effect, pumping test results show the lowest variance. The variance of the K values from grain size analysis and slug tests are higher because they parameterize smaller volumes of the aquifer, which enhances the possibility that local heterogeneities are being significantly represented.

A significant conclusion on geometry and the properties of complex subsurface geological structures, using the information from grain size analyses, is difficult to make because estimated K values are only representative of positions where soil samples were obtained from. Another consideration is that results from a grain size analysis can be inaccurate due to incomplete sampling through the drilling process. Multi-level slug tests can provide detailed information about vertical variations in horizontal K, however the radius of investigation is not likely to exceed several times the

well radius (Taylor et al., 1990). These two methods are point measurements and are hence insufficient to provide a spatial hydraulic parameter distribution over a larger area, which is required to determine the important transport paths or barriers for a groundwater transport model (Wu et al., 2005; Bohling et al., 2007).

4.3 Aquifer characterization with hydraulic tomography

In order to reconstruct the spatial distribution of hydraulic parameters in the aquifer, hydraulic tomography was applied to the test site. For this approach, multi-level cross-well short term pumping tests with a tomographic configuration were performed for the determination of hydraulic travel time, hydraulic attenuation steady shape inversions.

4.3.1 Hydraulic travel time/attenuation inversion based on pumping tests

D and Ss estimates

The cross-well multi-level pumping tests described in Chapter 4.2.3 (Figure 4.7), which were performed in a tomographic array between a pumping well (P0/M25) and two observation wells (PM6.4/M15.5 and PM5/M17.5), all three wells being positioned along a straight line, were used to create an inversion database. This database consists of 30 pressure responses for a two-dimensional profile between each pumping well and observation well. Due to the absence of extra pumping wells and observation wells, a three-dimensional configuration for the cross well pumping tests was not possible.

Based on the finding of Vasco et al. (2000), which shows that the pressure response of a Heaviside source can be transformed into a pressure response of an impulsive source (Dirac source) by differentiation of the transient head data, the inversion scheme are applied to the pressure responses of constant rate pumping tests. According to the introduced theory in Chapter 2.1.1 (Figure 2.1) and the application of the synthetic data in Chapter 3, the slope of drawdown was calculated by differentiating both the pumping well and observation well field data.

For the reconstruction of a diffusivity distribution, different travel times from these 30 pressure responses were simultaneously inverted. The presented results of the travel time inversion are based on the inversion of the travel time diagnostics t-50%, which was a compromise between obtaining high data quality (avoiding early time noise at t-10% from the field head data) and the findings of Brauchler et al. (2007)

and Cheng et al. (2009), that showed early travel time diagnostics to be more suited to resolve hydraulic heterogeneity. Due to the geometry of the aquifer within the investigation area (Figure 4.7), which has the dimensions of 2m (thickness) × 11.5m or 9m (distance between pumping well and observation well), all the source-receiver combinations had an angle of |α| smaller than 13°. Hence the inversion strategy based on a data subset, which is introduced in the analogue study, was not necessary in this case.

For the attenuation inversion, the developed approach introduced in Chapter 2.2 is applied. As described in Vasco (2000) (Figure 2.1), the peak amplitude of the drawdown slope ($h(x_2)$ in Equation 2.25) recorded in the observation well was divided by peak amplitude in the pumping well that initiated the test (H_0) to obtain the attenuation of the pressure response signal traveling between test and observation interval. After manipulation of the normalized attenuation, according to Equation 2.25, the spatial distribution of the specific storage was able to be reconstructed. Note that during the pumping test with the pumping interval at the bottom of the aquifer, the head data recorded in the pumping well has more noise at earlier times. Hence the H_0 of this test is not available for the attenuation inversion, which leads to a smaller thickness covered by the source-receiver configuration. Therefore, the hydraulic attenuation inversion could only reconstruct a smaller thickness of the aquifer than the travel time inversion. Due to the variation in ground surface height of the investigation area along the 11.5 meters, the inversions were processed using the absolute height above sea level instead of depth under surface.
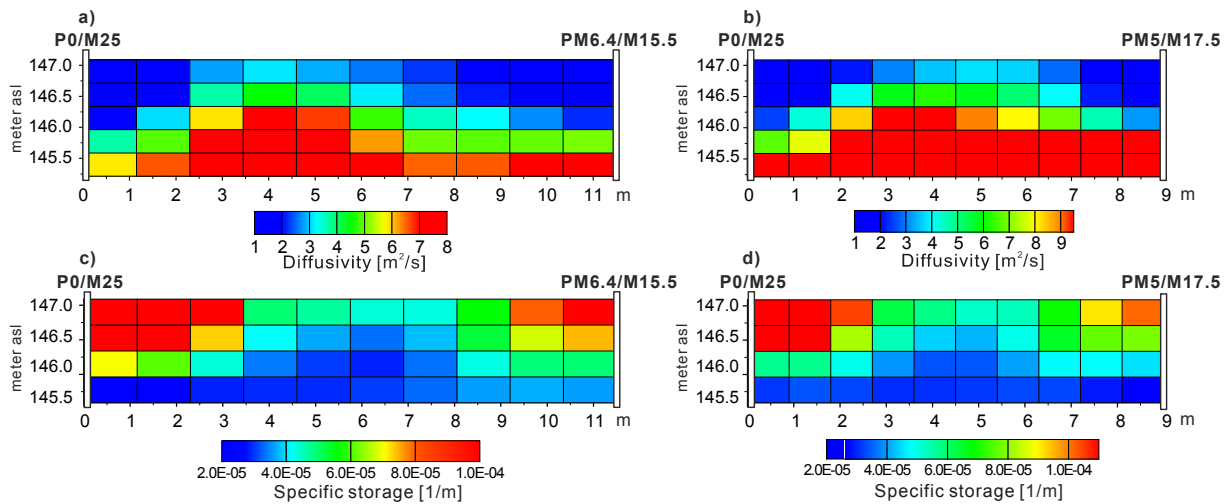
Figure 4.22: Tomograms gained from the data set from the short term pumping tests. (a)-(b) Reconstructed diffusivity tomograms; (c)-(d) Reconstructed specific storage tomograms.

The computing time for the inversion takes less than 20 seconds on a PC equipped with a 3.2 GHz CPU. In Figure 4.22, the reconstructed diffusivity tomogram shows that between the pumping well P0/M25 and observation well PM6.4/M15.5, the diffusivity values vary over an order of magnitude. The lowest values of up to 3 m^2/s are measured at the top of the aquifer. With increasing depth, the diffusivity increases up to 30 m^2/s. This distribution is consistent with the vertical variation of hydraulic conductivity, which is determined through other tests introduced in Chapter 4.2.

The diffusivity values calculated based on the values of hydraulic conductivity and specific storage ($D = K / S_s$), which were determined using the Cooper-Jacob straight line method (1946) in Chapter 4.2.3 (Figure 4.9 (a) and (b)), vary between 5.3 m^2/s and 14.4 m^2/s. These values agree with the values that were reconstructed with the travel time inversion at the lower part of the aquifer. This means that the values determined by analytical methods are dominated by the highly permeable zone at the bottom of the aquifer. This conclusion agrees with the observations of Diem et al. (2010), which have been confirmed in studies for an alluvial gravel aquifer: the pumping test results reflect the hydraulic properties of the highly permeable zones.

The specific storage tomograms show a very similar spatial distribution to the diffusivity tomograms with respect to horizontally layered structures, but with an opposite trend. This means that the lowest specific storage values (approx. 2×10^{-5} m^{-1}) are close to the bottom of the aquifer and increase to the top of the aquifer (approx. 2

$\times\ 10^{-4}\ m^{-1}$). This general pattern agrees with the distribution derived from the type curve analysis illustrated in Figure 4.14.

With the same test set-up, another series of 30 short pumping tests were also carried out between well P0/M25 and two other observation wells P5/M17.5 and P6.4/M15.5. The diffusivity and specific storage were inverted in the same way and the tomograms (Figure 4.23) show the similar pattern and parameter range as in Figure 4.22.
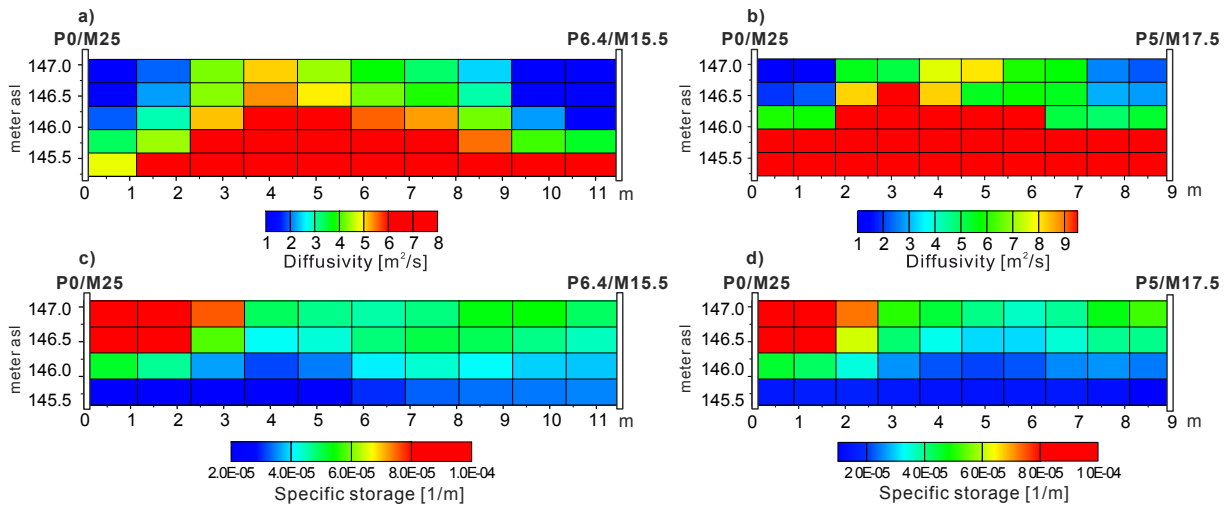
Figure 4.23: Tomograms gained from the data set from the second series of short term pumping tests. (a)-(b) Reconstructed diffusivity tomograms; (c)-(d) Reconstructed specific storage tomograms.

Due to the longer distance between the pumping well and observation wells, the response data of well PM6.4/M15.5 and P6.4/M15.5 have a lower signal-to-noise ratio than data of wells PM5/M17.5 and P5/M17.5. Therefore, the tomograms of 9 m length are slightly different from the tomograms with 11.5 m length. For the calculations of the constant D and S_s zones, the mean value of each corresponding zone from all tomograms was used. In cases where the tomograms are ambiguous, the values from the tomograms with 9 m length are considered to be more reliable.

Nevertheless, the similarity between the tomograms in two directions (Figure 4.22 and 4.23) strongly supports the results of the two inversion procedures and indicates that the aquifer in this investigation area of the test site has an even distribution of hydraulic parameters.

4.3.2 Zonation and Steady shape inversion

In order to estimate the K values with steady shape inversion, zones of constant diffusivity values were generated with the zonation (cluster) strategy described in the

numerical study (Chapter 3.2.3). Based on the tomograms in Figure 4.22(a) and 4.23(a), four clusters of equal hydraulic conductivity were identified to interpret the diffusivity tomograms (Figure 4.24).
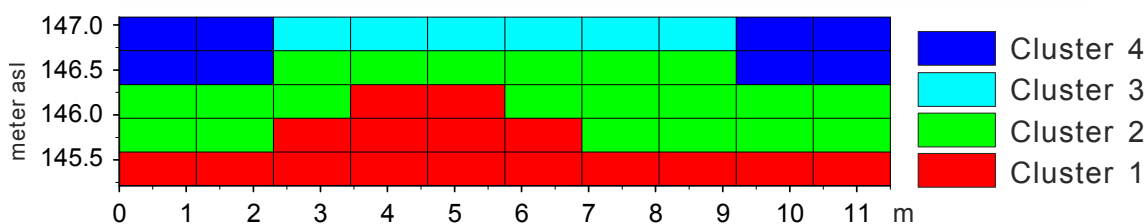
Figure 4.24: The zonation of hydraulic conductivity values, derived from the diffusivity tomograms.

The four clusters are characterized in the following table:

Table 4.10: Characteristics of the zones, derived from the diffusivity tomograms.

Clusters	Characteristics
1	Highest permeable zones at the bottom of the diffusivity tomogram.
2	Transition zone between the high-D and low-D zones.
3	Transition zone between the low-D zones.
4	Lowest permeable area at the top of the diffusivity tomogram.

The steady shape inversion was then performed with a steady state flow model from MODFLOW-96 (Harbaugh and McDonald, 1996). The model domain was separated into two parts. The central part represents the pumping test area, displayed in Figure 4.7 and the aquifer is discretized by voxels with an edge length of 0.5 m × 0.05 m × 0.3 m. The model edges are constant head boundaries. Based on the consistency of the zonation pattern between the profile P0/M25-PM6.4/M15.5 and P0/M25-P6.4/M15.5, the 2D-zonation is used to represent the 3D-zonation, which means: the central WE-profile of this model has the K-zonation from Figure 4.24 and this zonation is extended in both south and north direction within the investigation area. Outside the investigation area, the mesh is telescopically coarsened with increasing cell sizes, ranging from 5 cm at the central domain of interest to 10 m at the model boundaries (Figure 4.25).
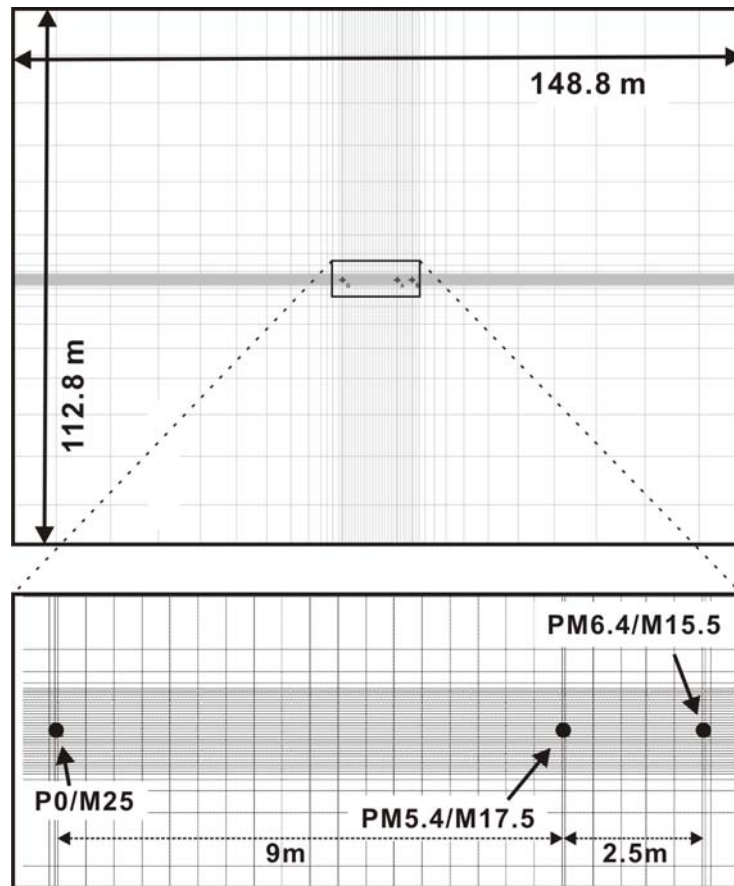
Figure 4.25: Model domain (top view) used for the steady shape inversion with a zoomed-in section of investigation area.

Using this model, pumping tests with the same configurations as in the field (Figure 4.7) were simulated. The calculated steady shape head differences between two observation points were recorded and compared with the observed head differences in the field. Same as in the numerical study, the automatic parameter estimator PEST (Doherty, 2003) was used to calibrate the model with an optimized K-distribution.

For parameter estimation, 30 (5×6) recorded head differences from a series of five simulated short-term pumping tests were used. Consistent with the pumping test setup in the field, the pumping well is screened every 0.25 m during each pumping test. The head differences generated by each pumping test were recorded at 6 different depths between the wells PM5.4/M17.5 and PM6.4/M15.5, which is the same as for the field tests shown in Figure 4.7.

Outside of the central investigation area of the model, a constant K value of 5.0 × 10^{-4} m/s (mean value of K from other tests) for the surrounding aquifer is assigned. Table 4.11 summarizes the starting values and the upper and lower bounds used for the steady shape inversion. The parameter estimation procedure required 80 model runs on a PC with a 3.33 GHz CPU, and each run of the steady shape model took

91

about 25 seconds. The minimized root mean squared error (RMSE) from the calculated and observed head difference is 0.097 mm and the mean value of the residuals between calculated and observed head differences is 0.045 mm.

Table 4.11: Initial parameters and value bounds used for the steady shape inversion.

	Diffusivity	Hydraulic conductivity [m/s]		
Cluster	[m^2/s]	starting value	lower bound	upper bound
1	>8	1×10^{-3}	1×10^{-6}	1
2	4~8	1×10^{-3}	1×10^{-6}	1
3	1~4	1×10^{-3}	1×10^{-6}	1
4	<1	1×10^{-3}	1×10^{-6}	1

The correlation coefficient R for the calculated and measured head differences from the calibrated model is 0.88, which is considered acceptable considering the coarse resolution of the tomograms. Table 4.12 lists the estimated K values as well as the respective specific storage values for the clusters. The specific storage values are calculated as the quotient of hydraulic conductivity over diffusivity ($S_s = K / D$).

Table 4.12: The estimated hydraulic conductivity, specific storage, and diffusivity values for the three clusters.

Cluster	K [m/s]	D [m^2/s]	S_s [m^{-1}]
1	1.0×10^{-3}	25.8	3.9×10^{-5}
2	3.0×10^{-4}	5.84	5.1×10^{-5}
3	2.1×10^{-4}	2.83	7.2×10^{-5}
4	1.0×10^{-4}	0.68	1.5×10^{-4}

For all of the four clusters, the K values derived from the steady shape inversion show a good agreement with the values from other tests from the field. At the aquifer bottom, the highest K value is 1.0×10^{-3} m/s and decreases to 1.0×10^{-4} closer the aquifer top.

4.4 Comparison and discussion

4.4.1 Hydraulic tomography based on short term pumping tests

Through short term pumping tests, the field aquifer characterization with hydraulic tomography in this study is based on three inversion procedures: hydraulic travel time, hydraulic attenuation and steady shape inversion. These three inversion approaches are naturally complementary, through which the D, S_s and K distributions can be directly and independently reconstructed. Besides that, with the D value serving as a bridge, which connects the K and S_s values, the K values can be calculated as $K = D \times S_s$ based on the travel time and attenuation inversion. Whereas the S_s values can be calculated as $S_s = K / D$ based on the travel time and steady shape inversion. Hence the K and S_s can be estimated additionally through an indirect way. In Table 4.13, the comparison of the estimation results based on different inversions are listed.

Table 4.13: Comparison of the estimated hydraulic parameters derived from three inversion procedures.

	attenuation		travel time	steady shape	
Cluster	S_s [m^{-1}]	K [m/s] = D × S_s	D [m^2/s]	K [m/s]	S_s [m^{-1}] = K / D
1	3.0×10^{-5}	7.6×10^{-4}	25.8	1.0×10^{-3}	3.9×10^{-5}
2	4.9×10^{-5}	2.9×10^{-4}	5.8	3.0×10^{-4}	5.1×10^{-5}
3	6.1×10^{-5}	1.7×10^{-4}	2.8	2.1×10^{-4}	7.2×10^{-5}
4	1.5×10^{-4}	1.0×10^{-4}	0.68	1.0×10^{-4}	1.5×10^{-4}

The estimated hydraulic parameters show in general a strong agreement among different combinations of inversion approaches. The calculated K values through hydraulic travel time and attenuation inversions have a smaller range than the values estimated through steady shape inversion. As introduced in Chapter 2, both travel time and attenuation inversions were developed using an asymptotic approach. Hence, the K values calculated based on the results, which derived from these two inversions, represent also an approximate solution.

Nevertheless, the agreement of the hydraulic parameter values and their distribution pattern derived from different inversions, strongly support the plausibility of the individual inversion procedure. Compared with the K estimates from other aquifer characterization methods introduced in Chapter 4.3 and the S_s estimates from cross well slug tests (Table 4.8), the estimated parameters all vary in the same range and the pattern of the parameter distribution is confirmed again: the K and D values are

higher at the bottom and decrease towards the top of the aquifer. The S_s distribution shows an opposite trend. They are smaller at the bottom and increase towards the top of the aquifer.

4.4.2 Hydraulic tomography and tracer test

The multi-chamber well P0/M17.5 is located (Figure 4.3) in between the two profiles P0/m25-PM6.4/M15.5 (Figure 4.22) and P0/M25-P6.4/M15.5 (Figure 4.23). The results of the tracer test breakthrough curve analyses at this well can provide important complementary information to the aquifer characterization in this area and validate the aquifer reconstruction results based on hydraulic tomography.

In the following figure (Figure 4.26), the peak concentrations of the breakthrough curves, which were observed at different depths of well P0/M17.5, as well as the evaluated dispersivity values are plotted, and compared to the results of hydraulic tomography.
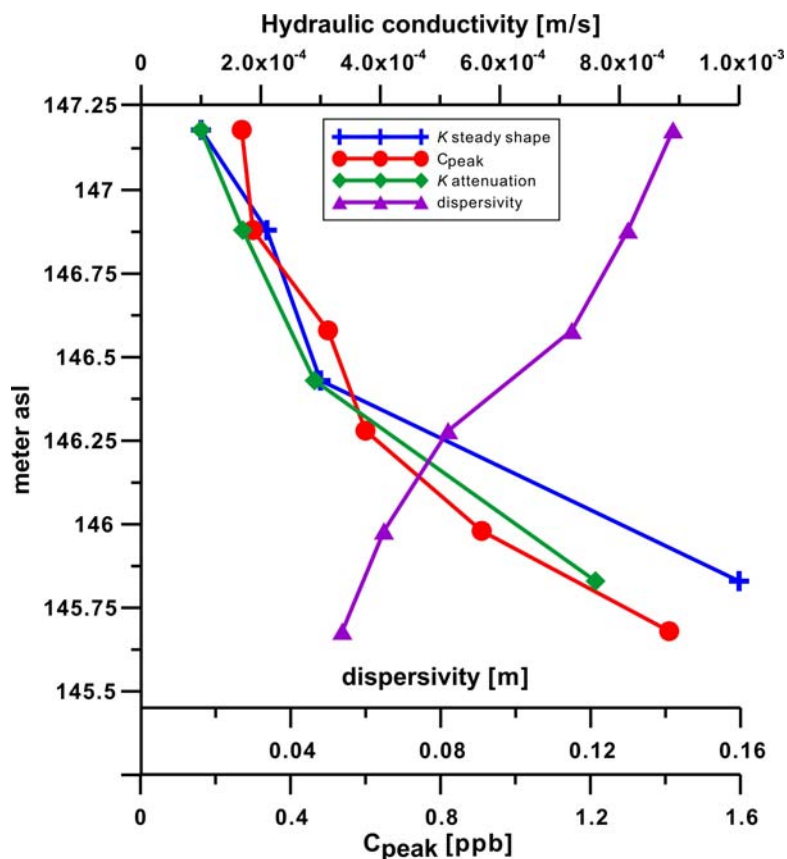
Figure 4.26: Results of the tracer test breakthrough curve analyses at well P0/M17.5, in comparison with the results of hydraulic tomography.

Figure 4.26 shows higher peak concentration and smaller dispersivity values at the bottom of the aquifer, which indicate that the transport velocity (see also Figure 4.19) increases with depth. Both the K-estimates from the hydraulic tomography and

the result of the breakthrough curve analyses strongly support the reconstruction of the highly conductive zones at the aquifer bottom, forming preferential flow paths for groundwater.

4.4.3 Hydraulic tomography based on slug tests

In order to validate the spatial distribution of the hydraulic parameters estimated through the short term pumping tests, I shortly introduced the 3-D inversion results from hydraulic tomography based on multi-level cross-well slug tests from Brauchler et al. (2011). These slug tests are carried out within the five-point star area and the 3-D reconstruction is based on hydraulic travel time and attenuation inversions.
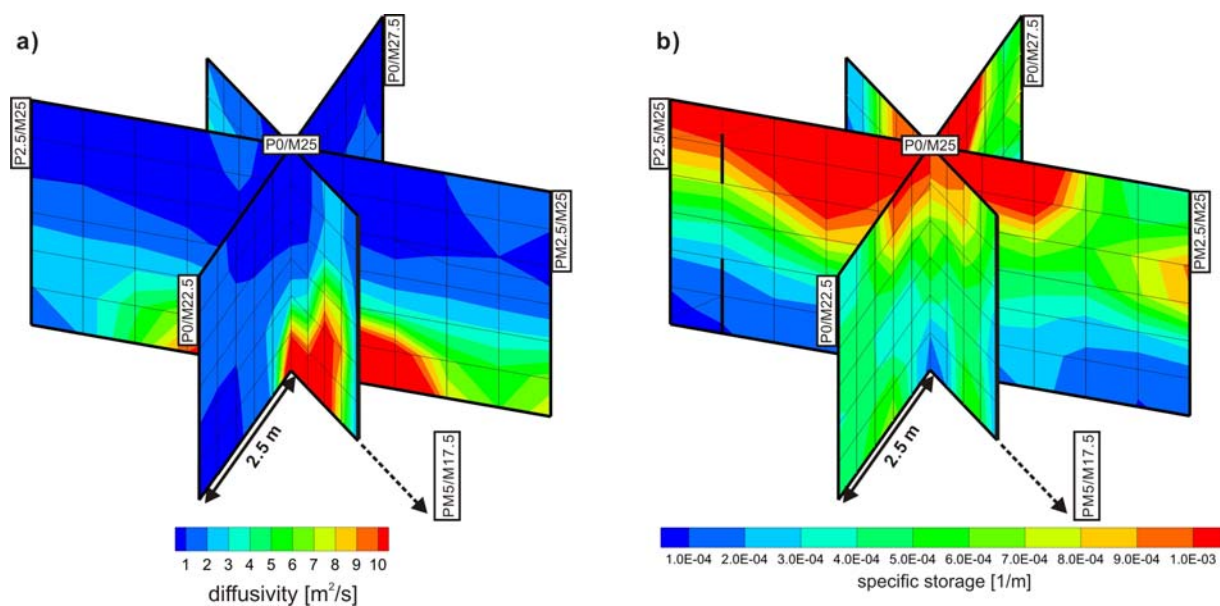
Figure 4.27: (a) Fence diagram of the three-dimensional diffusivity tomogram; (b) fence diagram of the three-dimensional storage tomogram. (modified from Brauchler et al., 2011)

In order to compare the 3-D results of Brauchler et al. (2011) with the two-dimensional inversion results from the short term pumping tests, a profile is extracted, starting from well P0/M25 and leading toward well PM5/M17.5. It is easy to recognize the low-D / high-S_s zone at the aquifer top and the high-D / low-S_s zone at the aquifer bottom. This general pattern, especially the expanding area of the high-D zone from the bottom to the middle of the aquifer, agrees with the inversion results based on short-term pumping tests (Figure 4.22).

During the pumping tests, the pressure pulses in fact propagate in three dimensions and the 2-D inversion has difficulty in reflecting 3-D processes. Thus the 2-D inversion results based on the pumping tests may lead to ambiguous results. Unfor-

tunately with the current pumping well and observation wells, a three-dimensional configuration for the cross well pumping tests is not possible. In further investigations with 3-D test configurations and a larger number of source/receiver points, the inversions are supposed to produce a more accurate aquifer reconstruction with higher spatial resolution.

5   SUMMARY AND OUTLOOK

In this study, the potential of a coupled hydraulic tomographic inversion approach was first investigated with an aquifer analogue outcrop model. With the aquifer analogue outcrop model, appraisal of the potential of the coupled tomographic inversion approach by numerical methods, taking into account realistic aquifer heterogeneity, is possible. The proposed coupled hydraulic tomographic inversion approach consists of two complementary and fast inversion techniques: hydraulic travel time and steady shape inversions. The hydraulic travel time based tomography approach is utilized to determine clusters of the analogue of constant diffusivity, and the steady shape inversion allowed the reconstruction of an average hydraulic conductivity estimate for each cluster. Finally, a specific storage estimate could be calculated for each cluster based on the diffusivity and hydraulic conductivity estimates for each cluster.

The comparison with the aquifer analogue data shows that the coupled inversion approach allows reliable estimation of hydraulic conductivity. The travel time inversion, however, does not resolve the diffusivity distribution of one cluster that represents a highly heterogeneous part of the analogue. Hence the interpreted specific storage for this cluster is too high. The reason for the underestimation is the resolution of hydraulic travel time tomography. The hydraulic travel time based inversion is based on the transformation of the transient groundwater flow equation into the eikonal equation using an asymptotic approach. The transformation is only valid for media that vary smoothly with respect to the spatial wavelength of the propagation of the pressure pulse. Beyond this, the voxel size has to be adapted to the number of available measurements in order to avoid an ill posed inverse problem. Therefore, the small clusters of stone rich gravel characterized by high diffusivity values cannot be reconstructed. Nevertheless the most significant hydraulic features can be easily reconstructed by the travel time based inversion approach.

Having realized the potential of the hydraulic tomographic approach for aquifer characterization, assessing this approach at a field test site was the next logical step.

In the field work of this study, traditional aquifer characterization methods, such as grain size analyses as well as type curve analyses of slug tests and pumping tests were first performed. These methods show a strong agreement in their results. The K values are approx. 10^{-3} m/s close to the bottom and decrease to approx. 10^{-4} m/s at the top of the aquifer. The mean value of hydraulic conductivity of this test site is $5 \times$

10^{-4} m/s, based on pumping tests and grain size analyses. The S_s distribution shows an opposite trend as that of K. At different positions in the field, S_s values vary from approx. 10^{-5} m^{-1} close to the bottom of the aquifer to approx. 10^{-3} m^{-1} at the top of the aquifer. Besides these tests, a tracer test with multi-level sampling was performed. The analyses of the breakthrough curves from this tracer test indicate that the fastest transport paths are at the aquifer bottom and the lowest transport paths are closer to the aquifer top.

Traditional pumping tests provide estimations of average K and S_s for relatively large areas. The parameter estimates are therefore integrated estimates. Besides that, S_s estimates from pumping tests are very often problematic, since the variation in S_s is often produced by the large impact of spatial variations in K of the aquifer material between the pumping well and the observation well. As shown in this work, a near-constant K but large variations in S_s are obtained from analyses of drawdown at different observation wells. Hence, for a small investigation area, the representative S_s estimated through pumping tests should be cautiously considered.

The parameters gained from grain size analysis and slug tests represent smaller volumes of the aquifer. Thus they can provide significant results for detecting local heterogeneities. However, the K estimates through grain size analyses are only meaningful for the positions where the soil samples are taken from. Besides that, results from grain size analysis can be inaccurate due to incomplete sampling through the drilling process. Multi-level slug tests can provide detailed information about vertical variations in horizontal K and S_s, however the radius of investigation is not likely to exceed several times that of the well radius. These two methods are point measurements and are hence insufficient to provide a spatial hydraulic parameter distribution over a larger area.

In order to reconstruct the aquifer both in vertical and lateral direction with a larger investigation area, the approach of hydraulic tomography based on short term pumping tests is applied. From the cross-well multi-level pumping tests, which are performed in a tomographic array between the pumping well and observation wells, a database for the hydraulic travel time, attenuation and steady shape inversions is created.

The direct results of the inversions confirm the same distribution pattern and range of hydraulic parameters as estimated through traditional methods. The results of hydraulic travel time inversion show that the lowest D values of up to 3 m^2/s are at

the top of the aquifer. With increasing depth, the diffusivity increases up to 30 m^2/s at the bottom of the aquifer. This distribution is consistent with the vertical variation of hydraulic conductivity, which was determined through the traditional methods. In addition to this information, a high-D zone at the aquifer bottom with increasing thickness in the middle of the investigation area was also detected. This shows exactly the advantage of the inversion approach in the aquifer reconstruction with respect to the lateral variation of hydraulic parameters.

Derived from the hydraulic attenuation inversions, the S_s tomograms show very similar spatial distribution as the D tomograms, but with an opposite trend. The lowest S_s values (approx. 2×10^{-5} m^{-1}) are close to the bottom of the aquifer and increase to the top of the aquifer (approx 2×10^{-4} m^{-1}). This general pattern agrees with the distribution derived from the type curve analyses for the multi-level cross-well slug tests.

The results of K estimates through steady shape inversion show the same trend of variation as the D values estimated through travel time inversion: They vary from ca. 1×10^{-4} m/s at the aquifer bottom to ca. 1×10^{-3} m/s at the aquifer top. This result is also consistent with the evaluation of the response curves through multi-level cross-well slug tests.

Beside the direct inversions described above, both for the K and S_s values, there are alternative ways to achieve their distribution: (1) calculation for the K values based upon the relationship of $K = D \times S_s$, where the D values are derived from the travel time and the S_s values from attenuation inversions; (2) calculation for the S_s values based upon the relationship of $S_s = K / D$, where the K values are gained from the steady shape inversion and the D values from travel time inversion. Hence, with the D values serving as an interconnection, there are two methods to reconstruct both the K and S_s distributions. Naturally, the D values derived from the travel time inversion can also be verified by the relationship of $D = K / S_s$.

The results with both methods show the same trend of the variation: the K values increase from the aquifer top to the bottom and the S_s values increase from the aquifer bottom to the top. However, the ranges of variation of the K values are slightly different from these two methods. As introduced in Chapter 2, both travel time and attenuation inversions are developed using an asymptotic approach. Hence, the K values calculated based on these two inversions' results, represent also an approximate solution. Besides that, according to the hydraulic parameter values from the litera-

tures (e.g. in Table 3.1), hydrofacies with different K values might have the same specific storage values. This means that the distribution of K values might not be exactly the same as the distribution of S_s values at some cases. This could lead to an inaccurate zonation of D and S_s values at some positions, which of course as a consequence, could have influence on the estimate based on method (1).

An important feature of this field study is that a large amount of information is collected in the field from different independent methods. This allows us to appraise the quality and reliability of the reconstructed tomograms. For example the D values calculated based on the K and S_s values ($D = K / S_s$), which are determined analytically from 227 response curves of pumping tests and slug tests, have a mean value of 4.5 m^2/s. Among these response curves, 11 response curves are from pumping tests. The derived D values from the pumping tests vary between 5.3 m^2/s and 14.4 m^2/s and have a mean value of 9.7 m^2/s. 216 response curves are from slug tests and the calculated mean value of D is 3.9 m^2/s. These values agree with the values that are reconstructed with the travel time inversion at the middle and lower part of the aquifer. This means that for this alluvial gravel aquifer, the values determined by analytical methods are dominated by the highly permeable zone at the bottom of the aquifer. The agreement between D and S_s tomograms and the results of the pumping and slug tests based on type curve analysis proves again the reliability of the travel time based inversion approach by the reconstruction of both vertical and lateral changes in hydraulic properties with higher spatial resolution.

With the current pumping well and observation wells in the investigation area, a three-dimensional configuration for the cross well pumping tests is not available. In order to validate the inversion results, the results of three-dimensional inversions from Brauchler et al. (2011) are introduced. These results are based on the multi-level cross-well slug tests within the five-point star area. Compared with the two-dimensional inversion, the advantage of the three-dimensional inversion is that the spatial distribution of the parameter can be reconstructed for different directions. This gives us the possibility to find the potential horizontal anisotropy of the subsurface. For example at the interface of the tomograms in Figure 4.27 at the vicinity of well P0/M25, two perpendicular profiles do not exactly have the same pattern. The reconstructed tomograms in this work show the same pattern of parameter distribution as the tomograms from Brauchler et al. (2011), but the parameter ranges are slightly different. These could be the horizontal anisotropy within sedimentary architectural

elements due to complex sedimentation processes. Besides that, since the pressure pulses through short pumping tests in fact propagate in three dimensions, the 2-D inversion in this study has difficulty in reflecting 3-D processes and thus can lead to ambiguous results. As a consequence, the steady shape inversion fulfilled through a 3-D steady state model might have integrated-type estimates. Since the zonation of this model is based on the 2-D representation of four diffusivity tomograms, the aquifer is assumed to have the same K zonations along the North-South direction. Hence, the K estimates for the potential extreme heterogeneous parts of the aquifer, which locate outside or between the estimated diffusivities' profiles, were not considered.

In addition to the above-mentioned limitation of the 2-D inversions, some problems during data acquisition in the field also occurred. These problems prevented the attainment of the planned amount of data that are required for high resolution inversions. For example, due to the problem of well development, the well is sometimes not completely connected to the aquifer at some multi-chamber opening ports. This results in some response data with more noise, which cannot be used for the inversion. Besides that, due to the current pumping rate controlling system, a constant-rate pumping test cannot be performed with a very small and stable pumping rate. Hence, it is hard to prevent the pumping well from drying out or to keep the aquifer under a confined situation throughout the test. This is especially problematic during the pumping test with pumping intervals near the aquifer top and the groundwater level, where the hydraulic conductivity is much smaller. These problems largely reduce the available amount of source-receiver combinations for the inversions. Therefore the inversions have a smaller length in the vertical direction for the reconstruction and the resolution of the aquifer reconstruction is lower than expected.

Nevertheless, the approach of hydraulic tomography based on short term pumping tests has shown its great potential for aquifer characterization with impressive efficiency and accuracy. With the combination of hydraulic travel time, attenuation and steady shape inversions, which are naturally complementary, the spatial distribution of the three important hydraulic parameters K, S_s and D can be directly reconstructed. With further test site implementation and development in the future, there is enough room for the improvement of data acquisition for the inversions. Since the resolution limit of the aquifer reconstruction is strongly dependent on the amount of source-receiver combinations, more hydraulic tests between wells can be performed for the inversions. Through each test, the source/receiver interval (e.g. pumping interval) can

be changed to that of a much smaller scale. To perform and analyze these tests will be quite time-consuming, but it provides us at least the possibility by the achievement of the inversion result with a much more reliable and higher resolution. Therefore it is supposed that through the investigation with a three-dimensional test configuration and a much larger number of source/receiver points, the inversions can produce a more accurate aquifer reconstruction with higher spatial resolution.

The zonations derived from the proposed inversions can serve as a starting model for further investigations with the goal to resolve the multi scale heterogeneity. A promising approach in unconsolidated sediments is e.g. the coupling with high resolution direct-push profiling (Butler et al., 2007, Dietrich et al., 2008; Liu et al., 2009). Coupling this approach will help overcome the problem of non-uniqueness and uncertainty caused by the limits of hydraulic tomography.

6 REFERENCES

Barker, J.A., 1988. A generalized radial flow model for hydraulic tests in fractured rock. Water Resour. Res., Vol. 24, NO. 10, pp. 1796-1804, Oct. 1988.

Bayer P., 1999. Aquifer-Analog-Studie in grobklastischen braided river Ablagerungen: Sedimentäre/hydrogeologische Wandkartierung und Kalibrierung von Georadarmessungen, Diplomkartierung, Universität Tübingen.

Bear, J., 1972. Dynamics of Fluids in Porous Media, Dover, Mineola, N.Y.,

Becht, A., Tronicke, J., Appel, E., Dietrch, P., 2004. Inversion strategy in crosshole radar tomography using information of data subsets, Geophysics, 69, 220-230.

Beckie, R. and Harvey, C.F., 2002. What does a slug test measure: An investigation of instrument response and the effects of heterogeneity. Water Resour. Res., VOL. 38, NO. 12, 1290, doi:10.1029/2001WR001072, 2002.

Béland-Pelletier, C., Fraser, M., Barker, J., Ptak, T., 2010. Estimating contaminant mass discharge: a field comparison of the multilevel point measurement and the integral pumping investigation approaches and their uncertainties. Journal of Contaminant Hydrology. doi:10.1016/j.jconhyd. 2010.11.004.

Bohling, G.C., 1993. Hydraulic tomography in two-dimensional, steady-state groundwater flow, Eos Trans. AGU, 74, 141, 1993.

Bohling, G.C., Zhan, X., Butler, J.J., Jr., Zheng, L., 2002. Steady shape analysis of tomographic pumping tests for characterization of aquifer heterogenous. Water Resour. Res., (3812): 1324.

Bohling, G.C., Butler, J.J., Jr., Zhan, X., Knoll, M.D., 2007. A field assessment of the value of steady shape hydraulic tomography for characterization of aquifer heterogeneities. Water Resour. Res., 43, W05430, p. 21.

Bohling, G.C., 2009. Sensitivity and resolution of tomographic pumping tests in an alluvial aquifer, Water Resour. Res., 45, W02420, doi:10.1029/2008WR007249.

Bohling, G.C. and Butler, J.J., Jr., 2010. A Potential-Based Inversion of Unconfined Steady-State Hydraulic Tomography. Ground Water, Vol. 48, No. 3, May-June 2010. DOI: 10.1111/j.1745-6584.2010.00685_1.x.

Bohling, G.C. and Butler, J.J., Jr., 2010. Inherent Limitations of Hydraulic Tomography. Ground Water, doi: 10.1111/j.1745-6584.2010.00757.x.

Bois, S., La Porte, M., Lavergne, M., Thomas, G., 1972. .Well to well seismic measurements, Geophysics, 3, 471-483, 1972.

Boman, G.K., Molz, F.J., Boone, K.D, 1997. Borehole flowmeter application in fluvial sediments: Methodology, results, and assessment. Ground Water, 35(3), 443-450,1997.

Brauchler, R., Liedl, R., Dietrich, P, 2003. A travel time based hydraulic tomographic approach. Water Resources Res., VOL. 39, NO. 12, 1370, doi:10.1029/ 2003WR002262, 2003.

Brauchler, R., Cheng, J., Everett, M., Johnson, B., Dietrich, P., Liedl, R., Sauter, M., 2007. An inversion strategy for hydraulic tomography: Coupling travel time and amplitude inversion. Journal of Hydrology 345, 184– 198, doi:10.1016/j.jhydrol.2007.08.011.

Brauchler, R., Hu, R., Vogt, T., Halbouni, D., Heinrichs, T., Ptak, T., Sauter, M., 2010. Cross-well interference slug tests: An efficient tool for high resolution characterization of hydraulic heterogeneity. Journal of Hydrology 384, 33-45, doi:10.1016/j.jhydrol.2010.01.004.

Brauchler, R., Hu, R., Dietrich, P., Sauter, M., 2011. A field assessment of high resolution aquifer characterization based on hydraulic travel time and hydraulic attenuation tomography. Water Resour. Res., doi:10.1029/2010WR009635, 2011

Burger, R.L., and Belitz, K., 1997. Measurement of anisotropic hydraulic conductivity in unconsolidated sands: A case study from a shoreface deposit, Oyster, Virginia, Water Resour. Res., 33(6), 1515-1522.

Butler, J.J. Jr., 1988. Pumping tests in nonuniform aquifers – the radially symmetric case. Journal of Hydruology, 101 (1988) 15-30.

Butler, J.J., Jr., 1990. The role of pumping tests in site characterization: Some theoretical considerations, Ground Water, 28(3), 394-402.

Butler, J.J. Jr., Bohling, G.C., Hyder, Z., McElwee, C.D, 1994. The use of slug tests to describe vertical variations in hydraulic conductivity. J. Hydrol. 156, 1994.

Butler Jr., J.J., Elwee, C.D., 1996. Well-testing methodologies for characterizing heterogeneities in alluvial-aquifer systems: final technical report. Project Report to USGS Water Resour. Res. Program, US Department of Interior, 320 pp. (also Ks. Geol. Survey Open –File Rept. 95-75).

Butler, J.J., Jr., 1998. The Design, Performance, and Analysis of Slug Tests, Lewis Pub., 252 pp.

Butler, J.J. Jr., and Healey, J.M., 1998. Relationship between pumping-test and slug-test parameters: scale effect or artifact? Vol. 36, No.2, Ground Water, March-April 1998.

Butler, J.J. Jr., McElwee, C.D., Bohling G.C., 1999. Pumping tests in networks of multilevel sampling wells: Motivation and methodology. Water Resour. Res., 35(11), 3553-3560, 1999.

Butler, J.J. Jr., Garnett, E.J., Healey, J.M., 2003. Analysis of slug tests in formations of high hydraulic conductivity, Ground Water, v. 41, no. 5, pp. 620-630, 2003.

Butler, J.J., Jr. and Zhan, X., 2004. Hydraulic tests in highly permeable aquifers. Water Resources Res., v. 40, W12402, doi:10.1029/2003WR002998.

Butler, J.J. Jr. and Dietrich, P., 2004. New methods for high-resolution characterization of spatialy variations in hydraulic conductivity. Proceedings of International Symposium on Hydrogeological Investigation and Remedial Technology, Nov. 15 – 16, 2004, National Central University, Jhongli, Taiwan, pp.42 – 55.

Butler, J.J., Jr., 2005. Hydrogeological methods for estimation of hydraulic conductivity, in Hydrogeophysics, edited by Y. Rubin and S. Hubbard, Kluwer, in press, 2005.

Butler, J.J. Jr., Dietrich, P., Wittig, V., Christy, T., 2007. Characterizing Hydraulic Conductivity with the Direct-Push Permeameter. Vol. 45, No. 4 Ground Water, 409–419, 2007.

Butler, J.J. Jr., 2008. Pumping tests for aquifer evaluation - time for a change? Technical Commentary, Groundwater, Vol. 47, No. 5, September-October 2008, doi: 10.1111/j.1745-6584.2008.00488.x.

Cardiff, M., Barrash, W., Kitanidis, P.K., Malama, B., Revil, A., Straface, S., Rizzo, E., 2009. A potential-based inversion of unconfined steady-state hydraulic tomography. Ground Water 47(2): 259-270, DOI: 10.1111/j.1745-6584.2008.00541.x.

Cardwell, Jr., W.T., Parsons, R.L., 1945. Average permeabilities of heterogeneous oil sands. Trans Am Inst Min Metall Pet Eng 160:34–42.

Cheng, J.T., Brauchler, R., Everett, M.E., 2009. Comparison of early and late travel times of pressure pulses induced by multilevel slug tests. Engineering Applications of Computational Fluid Mechanics Vol. 3, No. 4, pp. 514-529.

Christy, C.D., Christy T.M., Wittig, V., 1994. A percussion probing tool for the direct sensing of soil conductivity. In Proceedings of the 8th National Outdoor Action Conference, Westerville, Ohio: National Ground Water Association, 381-394.

Clemo, T., Michaels, P., Lehman, R.M., 2003. Transmissivity resolution obtained from the inversion of transient and pseudo-steady drawdown measurements, in Proceedings of MODFLOW and More 2003 Understanding Through Modeling, pp. 629 – 633, Int. Ground Water Model. Cent., Golden Colo.

Cooley, R.L, and Naff, R.L., 1990. Techniques of water-resources investigations of the United States geological survey. Chapter B4: Regression modeling of ground-water flow. Book 3, Applications of hydraulics. USGS.

Cooper, H. H., Jr. and Jacob, C. E., 1946. A generalized graphical method for evaluating formation constants and summarizing well field history. Trans. AGU, 27: 526-534.

Dagan, G., 1990. Transport in heterogeneuous porous formations: spatial moments, ergodicity, and effective dispersion. Water Resour. Res., Vol. 26, pp 1281-1290, June 1990.

Danielson, R.E. and Sutherland, P.L., 1986. Porosity, In: Methods of Soil Analysis, Part 1. Physical and Mineralogical Methods, ed. by A. Klute Agronomy Monograph 9, American Soc. of Agronomy, 443-461 (1986)

Datta-Gupta, A., Kulkarni, K.N., Yoon, S., Vasco, D.W., 2001. Streamlines ray tracing and production tomography: Generalization to compressible flow, Petroleum Geosciences, 7, 75-86, 2001.

Davis, J. L. and Annan, A.P., 1989. Ground penetrating radar for high-resolution mapping of soil and rock stratigraphy, Geophysical Prospecting, 37(5), 531-551, 1989.

de Marsity, G ., 1986. Quantitative Hydrogeology. Academic, San Diego, Calif.,

Diem S, Vogt T., Hoehn E., 2010. Räumliche Charakterisierung der hydraulischen Leitfähigkeit in alluvialen Schotter-Grundwasserleitern: Ein Methodenvergleich. Grundwasser, 15, 241-251, DOI 10.1007/s00767-010-0153-6.

Dietrich, P., Fechner, T., Teutsch, G., 1995. Einsatz tomographischer Verfahren zur Erkundung von Aquiferparametern.- Z. Dt. Geol. Ges., 146(1), 161-166, 1995.

Dietrich, P., Fechner, T., Whittaker J., Teutsch, G., 1998. An Integrated Hydrogeophysical Approach to Subsurface Characterization.- In: Herbert M., Kovar K. (Eds.): Groundwater Quality: Remediation and Protection, IAHS Publication No. 250, ISSN 0144-7815: 513-520, 1998.

Dietrich, P., Fechner, T., Whittaker, J., 1999. Anmerkungen zur Interpretation tomographischer Messungen. - Mitteilungen der Deutschen Geophysikalischen Gesellschaft, Sonderband II/1999: 13-21, 1999.

Dietrich, P., Helmig, R., Hötzl, H., Köngeter, J., Sauter, M., G. Teutsch, 2005. Flow and Transport in Porous Fractured Media Springer, Berlin, ISBN 3-540-23270-2, 447 pp.

Dietrich, P., Leven, C., 2006. Direct push technologies. In Groundwater Geophysics, ed. R. Kirsch, 321–340. Berlin, Heidelberg, Germany: Springer.

Dietrich, P., Butler, J.J., Jr., Faiß, K., 2008. A Rapid Method for Hydraulic Profiling in Unconsolidated Formations. Ground Water, Vol. 46, No. 2, March–April 2008, 323–328.

Doherty, J., 2003. Version 5 of PEST Manual. Watermark Numerical Computing, Brisbane Australia, 2003.

Domenico, P.A. and Mifflin, M.D., 1965. Water from low-permeability sediments and land subsidence. Water Resour. Res. VOL. 1. NO. 4, Fouth quarter 1965.

DVWK Technische Regel Arbeitsblatt W 111 „Planung, Durchführung und Auswertung von Pumpversuchen bei der Wassererschließung" (März, 1997, Deutsche Vereinigung des Gas und Wasserfaches e.V. Technisch-wissenschaftlicher Verein) Bonn.

Einarson, M.D., and J.A. Cherry, 2002, A new multilevel groundwater monitoring system using multichannel tubing, Ground Water Monit. Rem., 22(a), 52-65 (2002)

Farrell, D.A., Woodbury, A.D., Sudicky, E.A., 1994. The 1978 Borden tracer experiment: analysis of the spatial moments. Water Resour. Res., VOL. 30, NO. 11, PP 3213-3223, Nov. 1994.

Fatemi, E., Engquist, B., Osher, S., 1995. Numerical solution of the high frequency asymptotic expansion for the scalar wave equation. J. Comput. Phys., 120, 145-155, 1995.

Fienen, M.N., Clemo, T., Kitanidis, P.K., 2008. An interactive Bayesian geostatistical inverse protocol for hydraulic tomography, Water Resour. Res., 44, W00B01, doi:10.1029/2007WR006730.

Flint, S.S., Bryant, I.D., 1993. The Geological Modelling of Hydrocarbon Reservoirs and Outcrop Analogues. Special Publication of the International Association of Sedimentologists, 15. Oxford: Blackwell Scientific Publications

Freyberg, D.L., 1986. A natural gradient experiment on solute transport in a sand aquifer. 2. spatial moments and advection and dispersion of nonreactive racers. Water Resour. Res., VOL. 22, NO. 13, pp 2031-2046, Dec. 1986.

Gee, G.W. and Bauder, J.W., 1986. Particle-size analysis. In: Methods of Soil Analysis, Part 1., Physical and Mineralogical Methods, ed. By A. Klute Agronomy Monograph 9, American Soc. of Agronomy, 383-411,1986.

Gelbke, Ch., Felslabor Grimsel C., 1988. Seismische Durchschallungs-Tomographie, NAGRA   NTB, 88-106, 1988.

Gelhar, L.W. and C.L. Axness, 1983. Three-dimensional stochastic analysis of macrodispersion in aquifers. Water Resour. Res., VOL. 19, NO. 1, PP. 161-180, Feb. 1983.

Gilbert, P., 1972. Iterative methods for the three-dimensional reconstruction of an object from projections. Journal of Theoretical Biology. Volume 36, Issue 1, July 1972, Pages 105-117 doi:10.1016/0022-5193(72)90180-4.

Gottlieb, J. and Dietrich, P., 1995. Identification of the permeability distribution in soil by hydraulic tomography. Inverse Problems 11: 353-360.

Häfner, F., Sames, D., Voigt, H.-D., 1992. Wärme- und Stofftransport, Mathematische Methoden, Springer-Verlag, New York, 626 pp.

Han, D., A. Nur, and D. Morgan, Effect of porosity and clay content on wave velocity in sandstones, Geophysics, 51, 2093-2107, 1986.

Hantush, M.S., 1964. Hydraulic of Wells. in Advances in Hydroscience, edited by Ven Te Chow, Academic Press, New York, 281-442,1964.

Hao, Y., Yeh, T.-C. J., Xiang, J., Illman, W. A., Ando, K., Hsu, K.-C., Lee, C.-H., 2008. Hydraulic tomography for detecting fracture zone connectivity. Ground Water 46(2): 183-192, doi: 10.1111/j.1745-6584.2007.00388.x.

Harbaugh, A.W. and McDonald, M.G., 1996. User's documentation for MOD- FLOW-96, an update to the U.S. Geological Survey modular finite-difference ground-water flow model. U.S. Geological Survey Open-File Report 96-485.

Harris, J.M., Lazaratos, S., Michelena, R., 1990. Tomographic string inversion, paper presented at the 60th Annual International Meeting and Exposition of the Society of Exploration Geophysicists: Exploration in Difficult Areas, San Francisco, Calif., Sept. 23-27, 1990. SEG Expanded Abstracts 9,

82 (1990); doi:10.1190/1.1890353

Hazen, A., 1893. Some physical properties of sands and gravels: with special reference to their use in filtration.- Am. Rep. Mass. State Bd. Health, 24, Boston: pp. 541 - 556.

He, Z., Datta-Gupta, A., Vasco, D.W., 2006. Rapid inverse modeling of pressure interference tests using trajectory based traveltime and amplitude sensitivities, Water Resour. Res., 42, W03419, doi:10.1029/2004WR003783.

Hofmann, B., Kobus, H., Ptak, T., Schad, H., Teutsch, G., 1991. Schadstofftransport im Untergrund, Erkundungs- und Überwachungsmethoden. Abschlußbericht 1. Projektphase, KfK-PWAB 9, PWAB (Hrsg.), Kernforschungszentrum Karlsruhe.

Hu, R., 2007. Einrichtung eines Naturmessfelds, hydraulische und hydrogeochemische Untersuchungen, Transportmodellierung. Unpublished diploma thesis, Georg-August-University of Göttingen.

Hubbard, S.S., Rubin, Y., Majer, E., 1999. Spatial correlation structure estimation using geophysical and hydrogeological data. Water Resour. Res., Vol. 35, No. 6, p. 1809-1825.

Huggenberger, P. and Aigner, T., 1999. Introduction to the special issue an Aquifer-sedimentology: problems, perspectives and modern approaches. Sediment Geol 129(3-4):179-186.

Hughson, D.L., and Yeh, T.-C.J., 1998. A geostatistically based inverse model for three-dimensional variably saturated flow, Stochastic Hydrol. Hydraul., 12(5), 285– 298, 1998.

Huntley, D. 1986, Relations between permeability and electrical resistivity in granular aquifers. Ground Water. V. 24, no. 4, p. 466.

Hyder, Z., Butler Jr., J.J., McElwee, C.D., Liu, W., 1994. Slug test in partially penetrating wells, Water Resour. Res., 30(8), 2945-2957.

Hyndman, D.W., Harris, J.M., Gorelick, S.M., 1993. Coupled seismic and tracer test inversion for aquifer property characterization, STP Volume 3, No.5, April 1993.

Hyndman, D. and Tronicke, J., 2005. Hydrogeophysical case studies at the local scale: the saturated zone. In: Rubin, Y., Hubbard, S. (Eds.), Hydrogeophysics. Springer, Berlin, ISBN 1-4020-3101-7, p. 522.

Illman, W. A., Liu, X., Craig, A. J., 2007. Steady-state hydraulic tomography in a laboratory aquifer with deterministic heterogeneity: multi-method and multiscale validation of hydraulic conductivity tomograms. Journal of Hydrology 341: 222-234.

Illman, W.A., Craig, A.J., Liu, X., 2008. Practical issues in imaging hydraulic conductivity through hydraulic tomography. Ground Water 46(1): 120-132.

Illman, W.A., Liu, X., Takeuchi, S., Yeh, T.-C. J., Ando, K., Saegusa, H., 2009. Hydraulic tomography in fractured granite: Mizunami Underground Research site, Japan. Water Resour. Res. 45: W01406, doi:10.1029/2007WR006715.

Illman, W. A., Berg, S. J., Liu, X., Massi, A., 2010a. Hydraulic/partitioning tracer tomography for DNAPL source zone characterization: Small-scale sandbox experiments. Environmental Science and Technology 44(22): 8609-8614, doi:10.1021/es101654j.

Illman, W.A., Zhu, J., Craig, A.J., Yin, D., 2010b. Comparison of aquifer characterization approaches through steady state groundwater model validation: A controlled laboratory sandbox study. Water Resour. Res. 46: W04502, doi:10.1029/2009WR007745.

ISO 13320-1. 1999-11-01. Particle Size Analysis – Laser diffraction methods.

Jackson, M.J., Tweeton, D.R., 1996. 3DTOM: Three-dimensional geophysical tomography: U.S. Department of the Interior, Report of Investigations 9617, p. 84.

Jacob, C.E., 1963. Determining the permeability of water-table aquifers, in Methods of Determining Permeability, Transmissibility, and Drawdown, compiled by R. Bentall, U.S. Geol. Surv. Water Supply Pap., 1536-I, 245–271, 1963.

Kabala, Z.J., 1993. The dipole flow test: A new single-borehole test for aquifer characterization, Water Resour. Res., 29(1), 99-107.

Kabala, Z.J., and Xiang, J., 1992, Skin effect and its elimination for single-borehole aquifer tests, in T.F. Russell et al. (eds.), Computational Methods in Water Resources IX, Vol. 1, Elsevier, New York, 467-474.

Klute, A., and Dirksen. C., 1986. Hydraulic conductivity and diffusivity: Laboratory methods, In: Methods of Soil Analysis, Part 1., Physical Mineralogical Methods, ed. by A. Klute, Agronomy Monograph 9, American Soc. of Agronomy, 687-734.

Kohn, R. and Vogelius, M., 1984. Determining conductivity by boundary measurements, Commun. Pure Applied Math. 37, 113-123, 1984.

Kohn, R., Shen H., Vogelius, M., Weinstein, M.I., 2008. Cloaking via change of variables in electric impedance Tomography, IOP publishing, Inverse Problems 24 (2008) 015016 (21pp)

Kruseman, G.P. and de Ridder, N.A., 1990. Analysis and Evaluation of Pumping Test Data, ILRI Publ. 47, 377 pp., Int. Inst. for Land Reclam. and Impr., Wageningen, Netherlands.

Kruseman, G.P. and de Ridder, N.A., 1994. Analysis and Evaluation of Pumping Test Data (2nd ed.) ILRI publication 47, Wageningen, The Netherlands: p. 377.

Kulkarni, K.N., Datta-Gupta, A., Vasco, D.W., 2001. A Streamline Approach to Integrating Transient Pressure Data into High Resolution Reservoir Models. SPE Journal, 6(3): 273-282.

Kwader, T., 1985. Estimatin aquifer permeability from formation resistivity factors. Ground Water. V. 23, no.6, p. 762

Lambare, G., Virieux, J., Madariaga, R., Jin, S., 1992. Iterative asymptotic inversion: applications for one parameter, Geophysics, 57, 1138-1 154.

Lessoff, S.C., Schneidewind, U., Leven, C., Blum, P., Dietrich, P., Dagan, G., 2010. Spatial characterization of the hydraulic conductivity using direct-push injection logging. Water Resour. Res., 46, W12502, doi:10.1029/2009WR008949.

Li, W., Nowak, W., Cirpka, O.A., 2005. Geostatistical inverse modeling of transient pumping tests using temporal moments of drawdown. Water Resour. Res. 41(W08403): 1-13, doi:10.1029/2004WR003874.

Li, W., Englert, A., Cirpka, O.A., Vanderborght, J., Vereecken, H., 2007. Two-dimensional characterization of hydraulic heterogeneity by multiple pumping tests. Water Resour. Res. 43(W04433).

Li, W., Englert, A., Cirpka, O.A., Vereecken, H., 2008. Three-dimensional geostatistical inversion of flowmeter and pumping test data. Ground Water 46(2): 193-201.

Liedl, R. and Ptak, T., 2003. Modelling of diffusion-limited retardation of contaminants in hydraulically and lithologically nonuniform media. Journal of Contaminant Hydrology, 66 (2003) 239– 259, doi:10.1016/S0169-7722(03)00028-7

Liu, G., Zheng, C., Gorelick, S.M., 2004. Limits of applicability of the advection-dispersion model in aquifers containing connected high-conductivity channels. Water Resour. Res. 40, W08308, doi:10.1029/2003WR002735.

Liu, G., Butler, J.J. Jr., Bohling, G.C., Reboulet, E., Knobbe, S., Hyndman, D.W., 2009. A new method for high-resolution characterization of hydraulic conductivity. Water Resour. Res., Vol. 45, W08202, doi:10.1029/2009WR008319, 2009

108

Liu, S., Yeh, T.-C.J., Gardner, R., 2000, Effectiveness of Tomography: Sandbox experiments, Water Resourc. Res., 38(4), 9pp.

Liu, S., Yeh, J. T.-C. Gardiner, R., 2002. Effectiveness of Hydraulic Tomography: Sandbox Experiments. Water Resour. Res. 38(4): 10.1029/2001WR000338.

Liu, X., Illman, W.A., Craig, A.J., Zhu, J., Yeh, T.-C. J. , 2007. Laboratory sandbox validation of transient hydraulic tomography. Water Resour. Res. 43(5): W05404.

Liu, X. and Kitanidis, P.K., 2011. Large-scale inverse modeling with an application in hydraulic tomograpy. Water Resour. Res.. VOL. 47, W02501, doi:10.1029/2010WR009144, 2011.

Maji, R., Sudicky, E.A., 2008. Influence of mass transfer characteristics for DNAPL source depletion and contaminant flux in a highly characterized glaciofluvial aquifer, Journal of Contaminant Hydrology Volume 102, Issues 1-2, 14 November 2008, Pages 105-119.

Marion, D., A. Nur, H. Yin, and D. Han, 1992, Compressional velocity and porosity in sand-clay mixtures, Geophysics, 57(4), 554-563.

Marquardt, D.W., 1963. An Algorithm for Least-Squares Estimation of Nonlinear Parameters. Journal of the Society for Industrial and Applied Mathematics. Vol. 11, No. 2 (Jun., 1963), pp. 431-441

Mazac, O., Kelly, W.E., Landa, I., 1985, A hydrogeophysical model for relations between electrical and hydraulic properties of aquifers. J. of Hydrology. V. 79, pp. 1-19.

McDermott, C., Sauter, M., Liedl, R., 2003. New experimental techniques for pneumatic tomographical determination of the flow and transport parameters of highly fractured porous rock samples, Journal of Hydrology 278, pp. 51–63.

Melville, J.G., Molz, F.J., Guven, O., Widdowson, M.A., 1991. Multilevel slug tests with comparison to tracer data. Ground Water, 29(6), 897-907, 1991.

Menke, W., 1984, The resolving power of cross-borehole tomography: Geophysical Research Letters, 11, 105–108.

Möck, C., 2009. Characterization of spatial variability of hydraulic subsurface parameters: hydraulic field testing and numerical modeling. Unpublished master thesis, Georg-August-University of Göttingen.

Molz, F.J., Young, S.C., 1993. Development and application of borehole flowmeters for environmental assessment, The Log Analyst, 34(1), 13-23.

Molz, F.J., Morin, R.H., Hess, A.E., Melville, J.G., Guven, O., 1989. The impeller meter for measuring aquifer permeability variations: Evaluation and comparison with other tests, Water Resour. Res., 25(7), 1677-1683, 1989.

Peursem, D.V., Zlotnik, V.A., Ledder, G., 1999. Groundwater flow near vertical recirculatory wells: Effect of skin on flow geometry and travel times with implications for aquifer remediations, Jour. Hydrology, 222, 109-122.

Poeter, E.P., and Mckenna, S.K., 1995. Reducing uncertainty Associated with ground-water flow and transport predictions. Ground Water, Vol. 33, No. 6, p.899-904, November-December 1995.

Ptak, T. and Teutsch, G., 1994. A comparison of investigation methods for the prediction of flow and transport in highly heterogeneous formations.- International Symposium on Transport and Reactive Processes in Aquifers, April 11-15, 1994; ETH Zürich, Switzerland.

Ptak, T., Schad, H., Hofmann, B., Teutsch, G.., Kobus, H., 1996. Methoden zur Erkundung und zur Simulation von Strömung und Transport in heterogenen Aquiferen. Untersuchungen im Testfeld Horkheimer Insel; Projekt Wasser-Abfall-Boden im Forschungszentrum Karlsruhe: pp.152.

Ptak, T., Piepenbrink, M., Martac, E., 2004. Tracer tests for the investigation of heterogeneous porous media and stochastic modeling of flow and transport-areview of some recent developments. J. of Hydrology 294 (2004) 122-163, doi:10.1016/j.jhydrol.2004.01.020.

Ramirez, A.L., Daily, W., Binley, A., LaBrecque, D., 1999. Electrical Impedance tomography of known targets, Jour. of Environm. and Engineer. Geophysics, 4(1), 11-26.

Renard, Ph. and de Marsily, G., 1997. Calculating equivalent permeability: a review. Advances in Water Resources, Vol. 20, Nos 5-6, pp. 253-278, 1997.

Rovey, C.W., II, 1998. Discussion of Relationship between pumping-test and slug-test parameters: Scale effects or artifact? Ground Water, 36(6), 866-867,1998.

Sánchez-Vila, X., Meier, P.M., and J. Carrera, 1999. Pumping tests in heterogeneous aquifers: An analytical study of what can be obtained from their interpretation using Jacob's method, Water Resour. Res., 35(4), 943-952.

Sauty, J.P., 1980. An analysis of hydrodispersive transfer in aquifers. Water Resour. Res., Vol. 16, NO. 1, PP. 145-158, Feb. 1980.

Schad, H. and Teutsch, G., 1994. Effects of the Investigation Scale on Pumping Test Results in Heterogeneous Porous Aquifers.- Journal of Hydrology, 159: pp. 61-77.

Schlie, P., 1989. Hydrogeologie des Grundwasserwerkes Stegemühle in Göttingen. – Göttinger Arb. Geol. Paläot., 43 : 4-11; Göttingen

Schulmeister, M.K., Butler, J.J., Jr., Healey, J.M., Zheng, L., Wysocki, D.A., McCall, W., 2003. Direct-push electrical conductivity logging for high-resolution hydrostratigraphic characterization. Ground Water Monitoring and Remediation, 23(3), 52-62.

Shepley, M.G. and Taylor, A., 2003. Exploration of aquifer management options using a groundwater model. Water and Environment Journal, Vol. 17, Issue 3, pages 176–180, August 2003.

Snodgrass, M.F. and Kitanidis, P.K., 1998. Transmissivity identification through multi-directional aquifer stimulation. Stochastic Hydrology and Hydraulics 12(5): 299-316.

Straface, S., Yeh, T.-C.J., Zhu, J., Troisi, S., Lee, C.H., 2007. Sequential aquifer tests at a well field, Montalto Uffugo Scalo, Italy, Water Resour. Res., 43, W07432, doi:10.1029/2006WR005287.

Sudicky, E.A., 1986. A natrual gradient experiment on solute transport in a sand aquifer: spatial variability of hydraulic conductivity and its role in the dispersion process. Water Resour. Res., VOL. 22, NO. 13, PP 2069-2082, Dec. 1986.

Tarantola, A. 2005. Inverse Problem Theory and Methods for Model Parameter Estimation. Society for Industrial and Applied Mathematics, Philadelphia, 342 pp.

Taylor, K., Molz, F., Hayworth, J., 1988. A single well electrical tracer test for the determination of hydraulic conductivity and porosity as a function of depth. Proceedings of the 2nd Annual outdoor Action Conference on Aquifer Restoration, Groundwater Monitoring and Geophysical Methods. V. 2, p. 925.

Taylor, K.C., Wheatcraft, S.W., Hess, J., Hayworth, J., Molz, F., 1990. Evaluation of methods for determining the vertical distribution of hydraulic conductivity. Ground Water, 28(2):88-98.

Teutsch, G., Glingbeil, R., Kleineidam, R., 1998. Groundwater quality : remediation and protection, Numerical modeling of reactive transport using aquifer analogue data. GQ'98 : Groundwater quality conference, Tübingen , 1998,n250,pp.381-390[Note(s) : XII, 598 p.,](16 ref.)ISBN1-901502-55-4.

Theis, C.V., 1935: The relation between the lowering of the piezometric surface and the rate and duration of discharge of a well using groundwater storage.- Am. Geophys. Union Trans., vol. 16: pp. 519-524.

110

Thiem, G., 1906. Hydrologische Methoden (The hydrogeologic method). Gebhardt, Leipzig, 56 pp.

Urish, D.W., 1981. Electrical resistivity-hydraulic conductivity relationships in glacial outwash aquifers. Water Resour. Res.. V. 17, no. 5, pp. 1401-1408.

Vasco D.W. and Datta-Gupta A., 1999. Asymptotic solutions for solute transport: A formalism for tracer tomography, Water Resour. Res. 35(1), 1-16, 1999.

Vasco D.W., Yoon, S., Datta-Gupta, A., 1999. Integrating dynamic data into high resolution reservoir models using streamline based analytic sensitivity coefficients, SPEJ Soc. Pet. Eng. J., 1-11, 1999.

Vasco, D.W. and Karasaki, K., 2006. Interpretation and inversion of low-frequency head observations. Water Resour. Res. 42: W05408, doi:10.1029/2005WR004445.

Vasco, D.W., Keers, H., Karasaki, K., 2000. Estimation of reservoir properties using transient pressure data: An asymptotic approach, Water Resour. Res., 36(12), 3447-3465.

Vasco, D.W., Peterson, J.E., Jr., Majer, E.L., 1996. Nonuniqueness in traveltime tomography: Ensemble inference and cluster analysis: Geophysics, 61, 1209–1227.

Vesnaver, A. and Böhm, G., 2000: Staggered or adapted grids for seismic tomography? The Leading Edge, 9, 944-950.

Vesselinov, V.V., Neuman, S.P., Illman, W.A., 2001a. Three-dimensional numerical inversion of pneumatic cross-hole tests in unsaturated fractured tuff, 1. Methodology, Water Resourc. Res. 37(12), 3001-3017.

Vesselinov, V.V., Neuman, S.P., Illman, W.A., 2001b. Three-dimensional numerical inversion of pneumatic cross-hole tests in unsaturated fractured tuff: 2. Equivalent parameters, high-resolution stochastic imaging and scale effects, Water Resour. Res., 37(12), 3019-3041.

Virieux J., Flores-Luna C., Gibert, D., 1994. Asymptotic theory for diffusive electromagnetic imaging Geophys. J. Int., 119, 857-868, 1994.

Vogt, T., 2007. Implementation of an experimental field site - hydraulic and borehole geophysical measurements, numerical groundwater flow modelling. Unpublished diploma thesis, Georg-August-University of Göttingen.

Wu, C.-M., Yeh, T.-C.J., Zhu, J., Lee, T.H., Hsu, N.-S., Chen, C.-H., Folch Sancho, A., 2005. Traditional analysis of aquifer tests: Comparing apples to oranges? Water Resour. Res. 41, no. 9:W09402, doi: 10.1029/2004WR003717.

Yeh, T.-C. J., Mas-Pla, J., Williams, T.M., McCarthy, J.F., 1995. Observation and three-dimensional simulation of chloride plumes in a sandy aquifer under forced-gradient conditions, Water Resour. Res., 31(9), 2141-2157.

Yeh, T.-C. J. and Liu, S., 2000. Hydraulic tomography: Development of a new aquifer test method, Water Resour. Res. 36 (8), 2095-2105.

Yin, D. and Illman, W.A., 2009. Hydraulic tomography using temporal moments of drawdown recovery data: A laboratory sandbox study. Water Resour. Res. 45: W01502, doi:10.1029/2007WR006623.

Yorkey T. J., Webster, J.G., Tompkins W.J., 1987, Comparing reconstruction algorithms for electrical impedance tomograpy. IEEE Trans. On Biomedical Eng. BME-34, 843-852.

Young, S.C., and Pearson H.S., 1995. The electromagnetic borehole flowmeter: Description and application. Ground Water Monit. and Remed., 15(2), 138-146 1995.

Zheng, C. and Gorelick, S.M., 2003. Analysis of solute transport in flow fields influenced by preferential flow paths at the decimeter scale, Ground Water, 41(2), 142–155, doi:10.1111/j.1745-6584.2003.tb02578.x.

Zhu, J. and Yeh, J. T.-C., 2005. Characterization of aquifer heterogeneity using transient hydraulic tomography. Water Resour. Res. 41(W07028): doi:10.1029/2004WR003790, doi:10.1029/2004WR003790.

Zhu, J. and Yeh, T.-C. J., 2006. Analysis of hydraulic tomography using temporal moments of drawdown recovery data. Water Resour. Res. 42: W02403, doi:10.1029/2005WR004309.

Zlotnik, V.A. and Ledder, G., 1996. Theory of dipole flow in uniform anisotropic aquifers, Water Resour. Res., 32(4), 1119-1128.

Zlotnik, V.A. and Zurbuchen, B.R. 1998. Dipole probe: Design and field applications of a single-borehole device for measurements of small-scale variations of hydraulic conductivity, Ground Water, 36(6), 884-893.

7 APPENDIX

7.1 List of symbols

[L]: length   [M]: mass   [T]: time   [°]: angle (degree)

$A_0(x)$	[L]	amplitude used for the zero-order term of the solution
$A_n(x)$	[L]	real functions that relate to the amplitude of the wave
B	[L]	aquifer thickness
c	[M/L^3]	resident concentration
C	[-]	normalized dimensionless concentration variables
d_{10}	[L]	effective grain size
$d_{cal(j)}$	[L]	calculated head difference for the j'th observation pair
$d_{ob(j)}$	[L]	observed head difference of the j'th observation pair
D	[L/T^2]	diffusivity
D_c	[L^2/T]	dispersion coefficient
f_α	[-]	transformation factor
$h_d(r,t)$	[L]	hydraulic head in dependence of time and space
$h(x,t)$	[L]	hydraulic head in dependence of time and space
$h(r,t_{peak})$	[L]	hydraulic head at peak response and position r
H_0	[L]	initial displacement
$H(x,\omega)$	[L]	head H in dependence of frequency ω and space x
J	[-]	object function
$K(x)$	[L/T]	hydraulic conductivity
K_h	[L/T]	horizontal hydraulic conductivity
K_v	[L/T]	vertical hydraulic conductivity
L	[L]	characteristic length
m	[L]	mean value of observations
m_o	[L]	mean value of model-generated counterparts to observation values
P	[-]	Peclet number
Q	[L^3/T]	pumping rate
R	[L]	radial distance from the circular section to the well
r_c	[L]	casing radius
S_s	[L^{-1}]	specific storage
$S(x)$	[-]	storage
t	[T]	time
t_R	[-]	dimensionless time variable
t_α	[-]	travel time diagnostic

t_{peak}	[T]	travel time of the peak of a Dirac signal
t_i^e	[T]	estimated travel time for the i'th measurement
t_i^m	[T]	measured travel time for the i'th measurement
T	[L^2/T]	transmissivity
v	[L/T]	velocity
v_p	[L/T]	mean pore velocity
U	[-]	non-uniform degree
$W(\ )$	[-]	Lambert's *W function*.
w_i	[-]	weight associated with the i'th observation value
x	[L]	space variable
x_1	[L]	coordinate of the source
x2	[L]	coordinate of the receiver
x_R	[-]	dimensionless longitudinal distance
α, α_L	[L]	longitudinal dispersivity
$|\alpha|$	[°]	angle between the horizontal and a straight line which connects the source and receiver
α_d	[-]	head ratio
$\Delta(x)$	[T^2/L]	inverse of the diffusivity.
$\tau(x)$	[-]	phase of a propagating wave

Indices

d	subscript stands for a Dirac source
m	with respect to measured data
e	with respect to estimated data
ob	with respect to observed data
cal	with respect to calculated data

7.2 List of publications and award

Publications authored or co-authored by me and related to the present work

Journals (Peer-reviewed)

Brauchler, R., **HU, R.**, Hu, L., Ptak, T. – Bestimmung von hydraulischen Parametern in Lockergesteinen: Ein Vergleich unterschiedlicher Feldmethoden. (Investigation of hydraulic parameters in unconsolidated sediments: A comparison of methods.) Submitted to Grundwasser,2011.

HU, R., Zhao, W., Brauchler, R. – (2010) An aquifer analogue study of high resolution aquifer characterization based on hydraulic tomography (Geoenvironmental Engineering and Geotechnics, GSP 204/231-238/ 2010, American Society of Civil Engineers).

HU, R., Brauchler, R., Herold, M., Bayer, P. - Hydraulic tomography analogue study: Coupling travel time and steady shape inversion. In review by Journal of Hydrology.

Brauchler, R., **HU, R.**, Dietrich, P., Sauter, M. – (2011) A field assessment of high resolution aquifer characterization based on hydraulic travel time and hydraulic attenuation tomography. , Water Resour. Res., 47, W03503, doi:10.1029/2010WR009635.

Brauchler, R., **HU, R.**, Vogt, T., Halbouni, D., Heinrichs, T., Ptak, T., Sauter, M. – (2010) Cross-well slug tests: An efficient tool for high resolution characterization of hydraulic heterogeneity. Journal of Hydrology, Volume 384, Issues 1-2, 15 April 2010, Pages 33-45.

In preparation

Hu, R., Brauchler, R., Hu, L., Ptak, P. - High-resolution aquifer characterization based on hydraulic tomography coupling multi-level slug-test, pumping test and tracer test data.

Conference papers / Abstracts

Brauchler, R., **HU, R.**, Hu, L., Ptak, T. – A field assessment of high resolution aquifer characterization: A combination of three different hydraulic tomographic inversion techniques. Submitted to MODFLOW and More 2011: Integrated Hydrologic Modeling. International Ground Water Modeling Center, Colorado, USA.

HU, R., Brauchler, R., Herold, M., Bayer, P., Zhao, W., Sauter, M. – (2010) Untersuchungen zur hydraulischen Tomographie basierend auf hydraulischer Laufzeit- und „Steady-Shape"-Inversion (Analysis of hydraulic tomography based on an hydraulic travel time and steady shape inversions) FHDGG 2010 (German Groundwater Association).

Brauchler, R., Möck, C., **HU, R.**, Ptak T. – (2010) Hydraulische Tomographie: Eine innovative Erkundungsmethode zur Bestimmung der räumlichen Variabilität von transportrelevanten hydraulischen Parametern. FHDGG 2010 (German Groundwater Association).

Brauchler, R., **HU, R.**, Dietrich, P., Sauter, M.– (2009) A field assessment of high resolution aquifer characterization: Coupling of hydraulic travel time and hydraulic attenuation tomography, AGU Fall Meeting 2009, San Francisco.

HU, R., Brauchler, R., Herold, M., Bayer, P., Zhao, W., Sauter, M. – (2009) Hydraulic tomography: An innovation for groundwater modeling and field investigation, International Sympo-

sium on Hydaulic Physical Modeling and Field Investigation (ISHPF 2010).

Brauchler R., **HU, R.**, Dietrich, P., Sauter, M.– (2009) High resolution aquifer characterization: An integrated approach coupling hydraulic and seismic tomography, Assembly of the European Geosciences Union (EGU), Vienna.

HU, R., Zhao, W., Brauchler, R. – (2010) An aquifer analogue study of high resolution aquifer characterization based on hydraulic tomography, Geo-Shanghai 2010.

HU, R., Brauchler, R., Herold, M., Bayer, P., Sauter, M. – (2009) A hydraulic tomography approach coupling travel time inversion with steady shape analysis based on aquifer analogue study in coarsely clastic fluvial glacial deposit. Geophysical Research Abstracts, Vol. 11, EGU2009-4243, EGU General Assembly 2009.

Brauchler, R., **HU, R.**, Al-Halbouni, D., Wahle, M., Fechner, T., Dietrich, P. – (2008) A field assessment of high resolution aquifer characterization based on an integrated approach combining hydraulic and seismic travel time tomography, AGU Fall Meeting 2008, San Francisco.

HU, R., Brauchler, R., Herold, M., Bayer, P. – (2008) Untersuchungen zur hydraulischen Tomographie basierend auf einer Aquifer-Analog-Studie in grobklastischen fluvio-glazialen Ablagerungen (Analysis of hydraulic tomography based on an aquifer-analogue-study in the river glacial coarsely clastic sediment) FHDGG 2008 (German Groundwater Association).

Brauchler, R., **HU, R.**, Vogt, T., Butler, J.J. Jr., Ptak, T., Sauter, M. – (2007) A field assessment of high resolution aquifer characterization based on hydraulic tomography with cross-hole slug tests, AGU (American Geosciences Union) Fall Meeting 2007, San Francisco.

Brauchler, R., **HU, R.**, Vogt, T., Butler, J.J. Jr., Ptak, T., Sauter, M. – (2007) In-situ determination of the spatial variability of hydraulic properties using hydraulic tomography with cross-hole slug tests at the test site Stegemühle, Germany, Assembly of EGU (European Geosciences Union), Vienna, Austria.

Award

Chinese Government Award for Outstanding Self-financed Students Abroad 2010

This award was set up in 2003 to recognize the achievements of non-government funded students abroad and by 2011 the prize has been awarded to around 2400 Chinese students world-wide. The selection process is fiercely competitive and begins when the education divisions of the Chinese embassies recommend PhD students of the highest academic caliber, who are then shortlisted and considered by a panel of experts in China. In 2011, 36 students in Germany are selected for this award.

Rui Hu

Date of birth	December 13th, 1979
Place of birth	Nanjing, China
Nationality	China

EDUCATION

Since May 2007	**Georg-August-Universität Göttingen** Geosciences Center, Applied Geology *Ph.D. student*
Oct. 2003 - May 2007	**Georg-August-Universität Göttingen** *Dipl.-Geow. (MSc Geoscience)*
Sept. 1998 - July 2002	**Nanjing University** *BSc Engineering Geoscience*

RELEVANT WORK EXPERIENCE

Since May 2007	Research and teaching assistant at Geosciences Center, Applied Geology, University of Göttingen. (supported by German Research Foundation (Deutsche Forschungsgesellschaft) within the project "High resolution aquifer characterization based on direct-push technology: An integrated approach coupling hydraulic and seismic tomography", grant no. BR3379/1-2.)
May 2008 – Aug. 2008	Applied Geohydrology Summer Research Assistantship Kansas Geological Survey / University of Kansas, USA
Nov. 2004 - May 2007	Student assistant at the University of Göttingen

MEMBERSHIPS

AGU	member of American Geophysical Union
FH-DGG	member of Hydrogeology Division of German Society for Geosciences (Fachsektion Hydrogeologie in der Deutschen Gesellschaft für Geowissenschaften)
EGU	member of European Geosciences Union
AstA Uni-Göttingen	member of students' union executive committee
NJUAA Germany e.V.	Vice President of Nanjing University Alumni Association Germany
CSV Göttingen	Chairperson of Chinese Sports Club Göttingen (Chinesischer Sportverein Göttingen)

AWARD

Chinese Government Award for Outstanding Self-financed Students Abroad 2010